Journal of Medicinal Chemistry

pubs.acs.org/jmc Article

Fungal-Selective Resorcylate Aminopyrazole Hsp90 Inhibitors: Optimization of Whole-Cell Anticryptococcal Activity and Insights into the Structural Origins of Cryptococcal Selectivity

Paul T. Marcyk, Emmanuelle V. LeBlanc, Douglas A. Kuntz, Alice Xue, Francisco Ortiz, Richard Trilles, Stephen Bengtson, Tristan M. G. Kenney, David S. Huang, Nicole Robbins, Noelle S. Williams, Damian J. Krysan, Gilbert G. Privé,* Luke Whitesell,* Leah E. Cowen,* and Lauren E. Brown*

Cite This: *J. Med. Chem.* 2021, 64, 1139–1169 Read Online

ACCESS | Metrics & More | Article Recommendations | Supporting Information

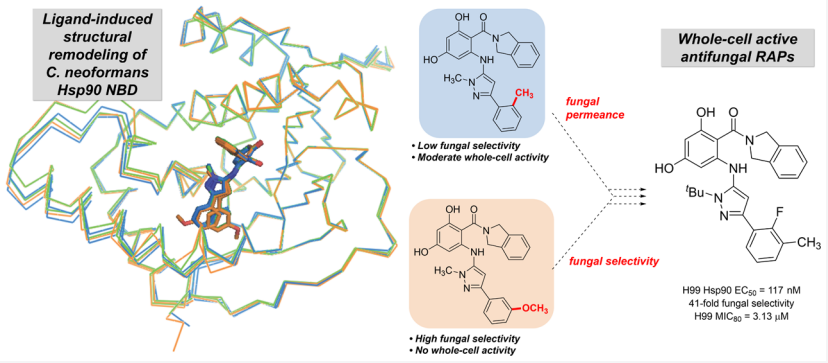

ABSTRACT: The essential eukaryotic chaperone Hsp90 regulates the form and function of diverse client proteins, many of which govern thermotolerance, virulence, and drug resistance in fungal species. However, use of Hsp90 inhibitors as antifungal therapeutics has been precluded by human host toxicities and suppression of immune responses. We recently described resorcylate aminopyrazoles (RAPs) as the first class of Hsp90 inhibitors capable of discriminating between fungal (*Cryptococcus neoformans*, *Candida albicans*) and human isoforms of Hsp90 in biochemical assays. Here, we report an iterative structure−property optimization toward RAPs capable of inhibiting *C. neoformans* growth in culture. In addition, we report the first X-ray crystal structures of *C. neoformans* Hsp90 nucleotide binding domain (NBD), as the apoprotein and in complexes with the non-species-selective Hsp90 inhibitor NVP-AUY922 and three RAPs revealing unique ligand-induced conformational rearrangements, which reaffirm the hypothesis that intrinsic differences in protein flexibility can confer selective inhibition of fungal versus human Hsp90 isoforms.

INTRODUCTION

Invasive fungal diseases impose a major economic and public health burden worldwide, killing over 1.5 million each year.[1−3] Approximately 90% of deaths due to fungal infection are caused by *Candida*, *Aspergillus*, and *Cryptococcus* species.[4] Of these, *Cryptococcus* is now recognized as one of the most significant fungal threats to human health, with incidence increasing in both immunocompromised and immunocompetent hosts.[1,5] Recent data from the WHO place the annual global burden of cryptococcal meningitis, the major clinical manifestation of the disease, in excess of 223 000 cases annually, causing more than 150 000 attributable mortalities and approximately 30% of all AIDS-associated deaths.[6,7] Cryptococcal meningitis has a 100% mortality rate if left untreated, and mortality rates remain high at 30% in resource-rich and 70% in resource-poor contexts.[8] Of the meager four drug classes approved for treatment of systemic fungal infections, only three are effective against *Cryptococcus*. Azoles and polyenes, which can each be used as single agents, both act *via* distinct mechanisms to deplete ergosterol, the major component of fungal membranes.[9,10] Resistance to each class has emerged, particularly for the azoles, with fungal infections becoming increasingly difficult to cure. A third class, antimetabolite pyrimidines, are only used in combination with other antifungals due to rapid emergence of resistance.[11] The fourth antifungal class, the cell wall-targeting echinocandins, have limited activity against *Cryptococcus* and no CNS penetration.[12−15] Given the limited array of antifungal drug classes and targets and the dramatically increasing incidence of

Received: October 20, 2020
Published: January 14, 2021

https://dx.doi.org/10.1021/acs.jmedchem.0c01777
J. Med. Chem. 2021, 64, 1139−1169

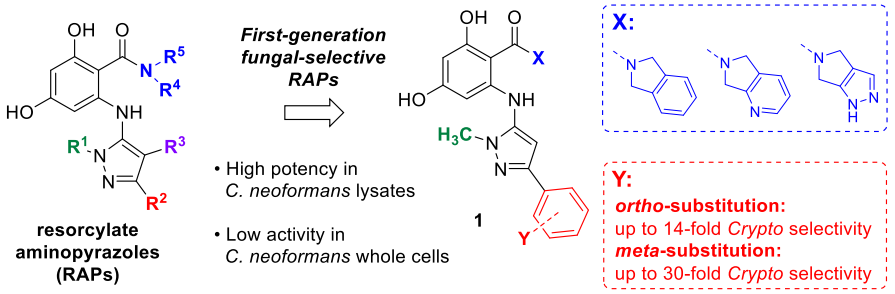

Figure 1. Generic structure of resorcylate aminopyrazoles (RAPs, left) and summary of activity and selectivity profile for previously reported first-generation cryptococcal-selective RAP series of type **1**, which are *N*-methylated at R^1 and bear a monosubstituted phenyl ring at R^2 to increase fungal selectivity.

resistance to current agents, the discovery of new chemotypes that act in ways that are mechanistically distinct from the available armamentarium is desperately needed.

Targeting core hubs of stress response circuitry is a powerful, yet unexploited strategy to cripple fungal pathogens. A prime example is the eukaryotic molecular chaperone Hsp90.[16−19] Hsp90 is essential in all fungi, and in addition to enabling survival, Hsp90 client proteins are also critical to virulence and drug resistance mechanisms.[20] Although profound compromise of Hsp90 expression or function is lethal to fungi, more modest compromise *via* chemical inhibitors or genetic reduction prevents and reverses resistance to antifungals in culture.[21−23] In *Cryptococcus neoformans*, recent studies have implicated Hsp90 in its thermotolerance, capsule assembly, and sensitivity to antifungals, strongly influencing its virulence in a nematode model.[24,25] Beyond an intrinsic potential for broad-spectrum single-agent antifungal activity, the unique effects on fungal biology inherent to Hsp90 inhibitors also render them strong candidates for the development of combination treatment regimens that would actively impede mechanisms of drug resistance.

Due in large part to its prominent role in supporting the function of numerous oncoproteins, Hsp90 has been studied extensively as an anticancer target.[26] Unfortunately, all Hsp90 inhibitors currently being developed as anticancer drugs exert mammalian host toxicities, especially suppression of innate and acquired immune mechanisms, that preclude their use as antifungals.[27] In fact, although numerous drug candidates have progressed into clinical trials over the past decade, none have been approved due to limited anticancer efficacy at their maximally tolerated doses.[28] One approach to reducing toxicity and improving therapeutic index for cancer and other indications has been the pursuit of paralog-selective inhibitors across the four Hsp90 family members in humans: Hsp90α, Hsp90β, Trap1, and Grp94.[29,30] The resorcylate scaffold, one of several privileged Hsp90-inhibitory chemotypes, has been modified to confer human paralog selectivity with applications in oncology and glaucoma.[31−38] In addition, selective purine mimetics, such as TAS-116[39] and modified analogues of BIIB021 selectively targeting Trap1,[30] have been described. Paralog selectivity has also been reported for modified benzamides resembling SNX-2112.[40,41]

We previously described efforts to develop Hsp90 inhibitors that are selective for fungal isoforms, initially templated from the resorcylic acid macrolactone natural products radicicol and monocillin.[42] Building on successes in achieving *Candida albicans* selectivity with semisynthetic radicicol and monocillin oximes, as well as the strong preclinical track record of nonmacrocyclic resorcylate drug candidates such as AT13387 (onalespib),[43−46] NVP-AUY922 (luminespib),[47−52] and STA-9090 (ganetespib),[53−61] we more recently disclosed the design, synthesis, and characterization of resorcylate aminopyrazoles (RAPs). RAPs are the first class of inhibitors capable of selectively inhibiting fungal isoforms of Hsp90 (specifically, *C. neoformans* and *C. albicans*) over their human orthologues Hsp90α/β, TRAP1, and Grp94.[62] Our development of increasingly potent and fungal-selective RAPs, as well as structure−activity relationships (SARs) for 112 early members of the series against *C. neoformans* and *C. albicans* culminated in our first generation of fungal-selective lead RAPs (**1**, Figure 1), which were all *N*-methylated at R^1 and *C*-arylated at R^2. Interestingly, species-specific divergences in potency and fungal selectivity (FS) occurred with ortho/para positioning of R^2 aryl-ring substituents, while activity and selectivity generally converged with meta-substituents. However, despite this interesting biochemical activity profile, whole-cell permeance of RAPs was an unsolved problem; of the 94 compounds from this study that showed potent cryptococcal Hsp90 binding ($EC_{50} \leq 1$ μM in fungal lysate), only six had whole-cell minimal inhibitory concentrations (MICs) ≤ 25 μM and only one of these six fit the desired profile of high biochemical potency and high fungal selectivity.

In fungi, the cell wall presents an inherent impediment to passive small-molecule permeability that is not present in mammalian cells and other microorganisms, which lack this strong protective barrier.[63] As a key virulence factor, *C. neoformans* also elaborates a dense polysaccharide capsule, which in addition to the plasma membrane and semipermeable fibrillary network of the cell wall contributes to limiting the accumulation of passively permeable compounds within this organism.[64−66] In *C. neoformans* as in other fungi, a network of efflux pumps also prevents accumulation of many xenobiotics.[67] In this report, we thus designate "permeant" molecules as having the combined features of active or passive cell penetration and evasion of efflux in *C. neoformans* so as to accumulate within the fungus and engage the target.[67]

Among the six cryptococcal-permeant analogues in our first-generation RAP library, we identified unique structural features that appeared to distinguish these compounds from non-permeant near-neighbors. Here, we now report significant achievements toward improving whole-cell anticryptococcal activity *via* a rational structure−property approach. In addition, we describe the first X-ray structures of the *C. neoformans* Hsp90 nucleotide binding domain (NBD), crystallized as the apoprotein and in co-complexes with three fungal-selective RAPs. Together, these new developments define the binding

https://dx.doi.org/10.1021/acs.jmedchem.0c01777
J. Med. Chem. 2021, 64, 1139−1169

mode of this novel Hsp90 inhibitor class, providing insights into the most plausible chemostructural origins of their observed fungal selectivity. Equally important from the therapeutic perspective, they advance our understanding of the structure−activity and structure−property relationships critical to conferring selective, whole-cell anticryptococcal activity.

RESULTS AND DISCUSSION

Rational Optimization of RAPs toward the Combined Features of Potent, Fungal-Selective Hsp90 Inhibition and Improved Whole-Cell Activity. To arrive at rationally designed, second-generation RAPs with the combined qualities of fungal accumulation and fungal selectivity, we sought to merge the structural features found to confer biochemical selectivity for fungal Hsp90 with nascent features, which appeared to track with permeance. To enable efficient elaboration of new second-generation analogues, the RAP scaffold (Figure 1) was synthesized in a convergent manner using an alternate protecting group strategy from our published first-generation set,[62] allowing for modular variation of the aminopyrazole and amide portion of the molecule. By synthesizing bespoke 5-aminopyrazoles, various *N*-alkyl groups at R^1 as well as differential substitution patterns on the R^2 aromatic ring could be incorporated (Scheme 1). Starting from

Scheme 1. Preparation of Building Block Aminopyrazoles 4[a]

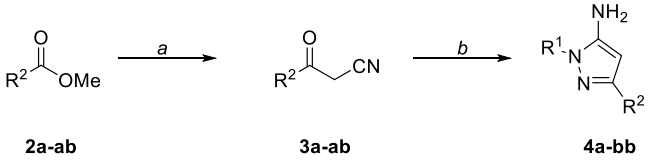

2a-ab 3a-ab 4a-bb

[a]Conditions: (a) MeCN, *n*-BuLi, tetrahydrofuran (THF), −78 °C to room temperature (rt); (b) $R^1NH\text{-}NH_2$, MeOH, 120 °C, microwave or $R^1NH\text{-}NH_2{\cdot}HCl$, NEt_3, MeOH, 120 °C, microwave.

commercially available mono- and disubstituted methyl benzoate derivatives (**2a−ab**), acylation of deprotonated acetonitrile afforded α-cyanoketone products **3a−ab**. Condensation of **3a−ab** with a variety of *N*-alkyl-hydrazines incorporated the R^1 alkyl group of the 5-aminopyrazole building blocks (**4a−bb**).

The resorcinol core was prepared by the formylation of 3,5-dimethoxybromobenzene (**5**) and subsequent demethylation with BBr_3 (Scheme 2). Bis-benzyl protection of **6** gave stable common intermediate (**7**), which could be elaborated with various amide groups. Pinnick oxidation of the aldehyde (**7**), followed by hexafluorophosphate azabenzotriazole tetramethyl uronium (HATU)-mediated amide coupling with isoindoline hydrochloride or substituted fluoroisoindoline derivatives, gave resorcylate amide bromides (**8a−c**). The synthesis was completed by the Buchwald−Hartwig cross-coupling of aryl bromides **8a−c** with 5-aminopyrazole (**4a−bb**) followed by global deprotection with palladium on carbon to give the targeted RAP compounds (**9a−bi**).

To determine target binding affinity, we used a fluorescence polarization (FP)-based competitive binding assay.[42,62] Use of whole-cell lysates enables assessment of binding to Hsp90 while complexed with relevant cochaperones and, in the case of human lysate, to the entire repertoire of Hsp90 family members expressed in human cells. Given these factors, FP in lysate is highly relevant to selectivity in the whole-cell context but can only provide relative quantification of binding affinity because the absolute concentration of the protein targets is unknown. In comparison, FP using purified NBD proteins allows for measurement of assay-independent ligand dissociation constants.[68] In our published first-generation set, the most potent and selective inhibitors were *meta*-methoxy-substituted RAPs **10−12** (Figure 2A), which disappointingly all failed to inhibit cryptococcal growth at concentrations of up to 25 μM. In addition to five nonselective whole-cell-active RAPs (**13−17**, Figure 2B), the only RAP exhibiting the combined features of >5-fold cryptococcal selectivity plus a cryptococcal MIC ≤ 25 μM was the R^2 *ortho*-tolyl-substituted compound **18**. This compound was one of only three examples of an RAP bearing an ortho-substituted R^2 aryl ring and was the single instance among these three with an isoindoline amide. Notably, despite a roughly equal proportion of isoindoline, pyridopyrrolidine, and pyrazolopyrrolidine amides within the early SAR set (Figure

Scheme 2. Convergent Synthesis of RAPs 9a−bi from Resorcylate Amides 8a−c and Aminopyrazoles 4a−bb[a]

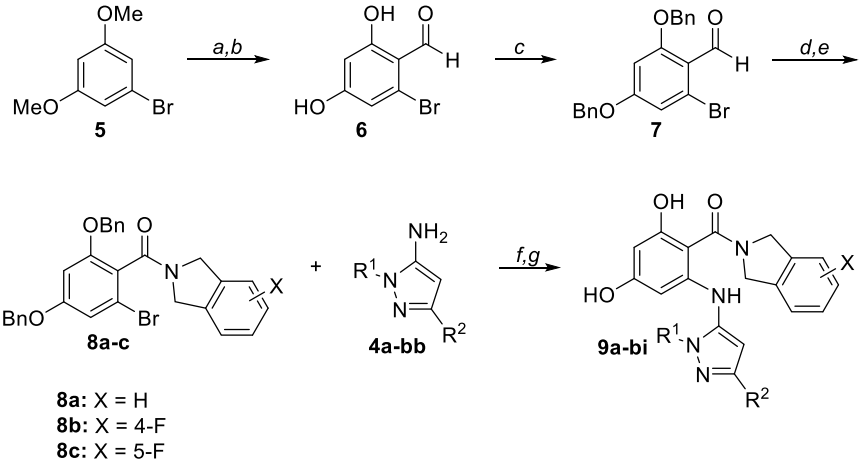

8a: X = H
8b: X = 4-F
8c: X = 5-F

[a]Conditions: (a) $POCl_3$, DMF, 0 °C to 100 °C; (b) BBr_3, CH_2Cl_2, 0 °C to rt; (c) BnBr, K_2CO_3, MeCN, reflux; (d) $NaOCl_2$, $NaH_2PO_4{\cdot}H_2O$, 2-methyl-2-butene, THF/*t*-BuOH/H_2O; (e) isoindoline·HCl (for **8a**), 4-fluoroisoindoline·HCl (for **8b**), or 5-fluoroisoindoline·HCl (for **8c**), HATU, Et_3N, THF/CH_2Cl_2; (f) $Pd(OAc)_2$ (10 mol %), Xantphos (20 mol %), Cs_2CO_3, toluene, 130 °C or $Pd_2(dba)_3$ (4 mol %), Xantphos (10 mol %), NaOPh, dioxane, 170 °C, microwave; (g) Pd/C (cat.), H_2, MeOH or $Pd(OH)_2$/C (cat.), H_2, EtOAc.

https://dx.doi.org/10.1021/acs.jmedchem.0c01777
J. Med. Chem. 2021, 64, 1139−1169

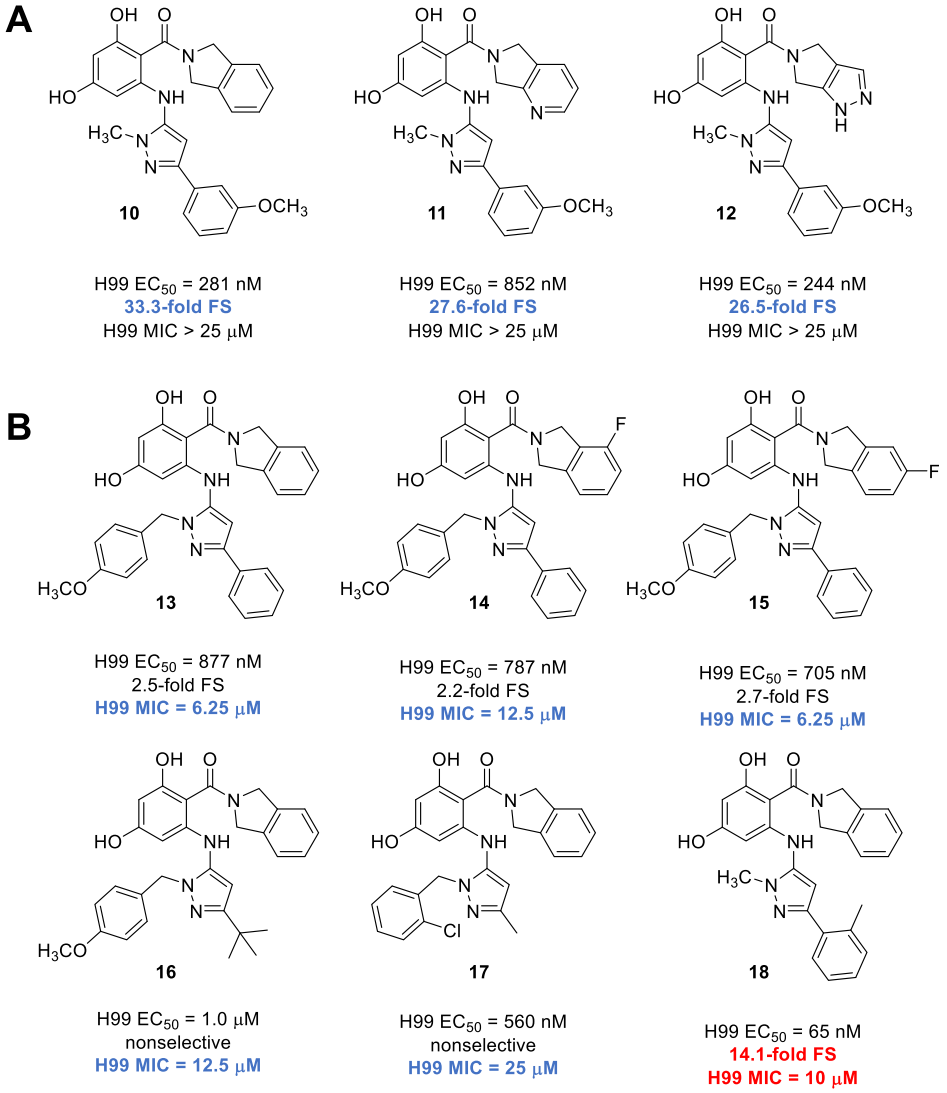

Figure 2. (A) RAPs with meta-substituted R^2 aryl rings exhibiting high fungal selectivity (FS) for cryptococcal Hsp90 over human isoforms. (B) Among 94 RAPs with fungal target affinity (H99 EC_{50}) $\leq$ 1 μM, only six demonstrate whole-cell antifungal activity (MIC $\leq$ 25 μM). Values for compounds with either fold-selectivity >5 **or** $MIC_{80} \leq 12.5$ μM are highlighted in **blue**. Values for compounds with both fold-selectivity >5 **and** $MIC_{80} \leq 12.5$ μM are highlighted in **red**.

1), whole-cell activity was limited solely to isoindoline or fluoroisoindolines at this site.

Based on these observations, we postulated that lipophilicity at the amide may be a key driver for permeance, and opted to explore other ortho-substituents in combination with isoindoline (Table 1, entries 1−3) to discern whether compound **18** represented an outlier or was suggestive of a potential structural trend. Gratifyingly, improved whole-cell activity was also observed in the biochemically potent *ortho*-fluorinated (**9a**), *ortho*-chlorinated (**9b**), and *ortho*-trifluoromethylated (**9c**) analogues. However, this improvement was offset by a disappointing drop in fungal selectivity for all three compounds.

Given the comparatively higher selectivity observed with the *ortho*-methylated parent compound, we next designed analogues in which this substituent was retained, and instead paired with other potentially permeance-enhancing features. Revisiting the cohort of permeant compounds in Figure 2B, another structural commonality that we deemed unique to these compounds compared to the larger set was the presence of relatively large, lipophilic groups at both R^1 and R^2, again in the presence of an isoindoline or fluoroisoindoline amide. Analogues **9d** and **9e** were prepared as examples of such features in combination with the *ortho*-tolyl group at R^2. The introduction of an *N*-*tert*-butyl group (**9d**) at R^1 was sufficient to retain both fungal selectivity (11.1-fold) and whole-cell activity (MIC 12.5 μM) that was comparable to the *N*-Me parent **18** (14.1-fold and MIC 10 μM, respectively). Isoindoline fluorination of **18**, however, was detrimental to both whole-cell activity and selectivity (compound **9e**).

In our prior study,[62] similar biochemical potencies and fungal selectivities were observed among compounds bearing a *meta*-tolyl or *meta*-methoxyphenyl group at R^2. In contrast, at the ortho site, we found that new compound **9f**, the methoxy analogue of **18**, showed a precipitous loss of selectivity and no measurable whole-cell activity, despite high binding affinity for Hsp90. Compounds **9g**−**9l** were next prepared to again test the strategy of increased bulk and lipophilicity at R^1 to improve permeance; for these analogues, whole-cell activities were again improved, but gains in fungal selectivity were only modest. Interestingly, converting the methoxy to trifluoromethoxy

https://dx.doi.org/10.1021/acs.jmedchem.0c01777
J. Med. Chem. 2021, 64, 1139−1169

Table 1. Early Exploration of the Impact of (1) Ortho-Substituents at the R^2 Aryl Ring and (2) Increased Aliphatic Bulk at R^1 on Biochemical Potency and Selectivity in Binding Cryptococcal Hsp90, and in Growth Inhibition of *C. neoformans* in Culture[c]

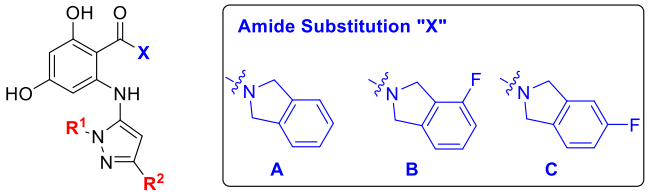

Entry	Compound	Amide ("X")	R^1	R^2	*C. neoformans* EC_{50}[a] (μM)	*C. neoformans* Fold-selectivity[b]	*C. neoformans* MIC_{80}[c] (μM)
1	**9a**	A	Me		0.180	2.0	<6
2	**9b**	A	Me		0.105	0.9	6.25
3	**9c**	A	Me		0.055	0.8	3.25
4	**9d**	A	^{t}Bu		0.421	11.1	12.5
5	**9e**	C	Me		0.199	5.0	<25
6	**9f**	A	Me		0.137	1.4	<25
7	**9g**	A	^{i}Pr		0.189	2.5	12.5
8	**9h**	A			0.655	2.1	6.25
9	**9i**	B	^{cy}Hex		0.248	4.3	12.5
10	**9j**	C			0.137	5.8	12.5
11	**9k**	A	^{cy}Pent		0.626	1.7	12.5
12	**9l**	A	^{i}Bu		0.431	3.5	12.5
13	**9m**	A	^{t}Bu		0.066	0.7	25
14	**9n**	A	Me		0.041	0.3	0.5
15	**9o**	A	^{t}Bu		0.107	6.8	1.8
16	**9p**	A	^{t}Bu		2.993	2.9	12.5
17	**9q**	A	^{t}Bu		4.206	>2.8	6.25
18	**9r**	A	^{t}Bu		10.000	0.8	6.25
19	**9s**	A	Me	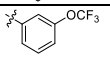	4.951	0.7	>25
20	**9t**	A	^{t}Bu		7.591	0.4	3.13
21	**9u**	A	Me		0.023	37.3	25
22	**9v**	A	^{t}Bu		0.782	10.5	12.5
23	**9w**	A	Me		1.001	8.0	25
24	**9x**	A	^{t}Bu		1.897	>6.3	25
25	**9y**	A	^{cy}Hex		0.976	2.3	12.5

[a]EC_{50} values were determined by fluorescence polarization (FP)-based equilibrium competition assay performed in 384-well format using whole-cell lysates prepared from *C. neoformans* and serial compound dilutions. All determinations were performed in duplicate. [b]To calculate fold-selectivity, the EC_{50} values determined by FP using human HepG2 cell lysate were divided by the EC_{50} value determined using *C. neoformans* lysate. The resulting ratio was then normalized by the ratio of values determined for the Hsp90 inhibitor geldanamycin using lysate of each cell type. Results for key selective compounds were confirmed by repeat assay in lysates, as well as by measuring ligand dissociation constants (K_i) using purified NBDs in FP assays (see Supporting Tables 1 and 2; Figures S1−S3). [c]Concentration of compound resulting in >80% inhibition of fungal cell growth compared to vehicle control. Values for compounds with either fold-selectivity >5 **or** $MIC_{80} \leq 12.5$ μM are highlighted in **blue**. Values for compounds with both fold-selectivity >5 **and** $MIC_{80} \leq 12.5$ μM are highlighted in **red**.

delivered mixed results, with the *N*-methylated compound **9n** exhibiting no selectivity and submicromolar whole-cell activity, while the *N*-*tert*-butyl compound **9o** showed modest 6.8-fold selectivity in combination with an impressive MIC of 1.8 μM.

With initial confirmation that the whole-cell activity of R^2-arylated RAPs could be improved *via* increased bulk and lipophilicity at R^1, we next sought to deploy this strategy on R^2 meta-substituted scaffolds, which had trended toward the highest cryptococcal Hsp90 selectivity in our previous study. Compounds **9p**, **9q**, and **9r** were each prepared as *N*-*tert*-butyl analogues of earlier *N*-methylated inhibitors, which had exhibited fungal selectivities ranging from low (e.g., *meta*-trifluoromethyl) to the highest observed in the study at 12- or 33-fold (*meta*-methyl or *meta*-methoxy). Unfortunately, although this modification was again successful in achieving sufficient permeance for whole-cell activity, biochemical potencies dropped to the low micromolar range and a concomitant drop in selectivity was also observed. Similar trends were also observed with *meta*-trifluoromethoxylated compounds **9s** and **9t**. In contrast, improved selectivity and potency were observed with *meta*-fluorination at R^2 (compounds **9u** and **9v**) with measurable, albeit high MIC values

https://dx.doi.org/10.1021/acs.jmedchem.0c01777
J. Med. Chem. 2021, 64, 1139−1169

Table 2. Efforts to Improve Whole-Cell Anticryptococcal Activities and Selectivities for Inhibitors *N*-Methylated at R^1, *via* a Paring of Ortho/Meta-Substituents on the R^2 Aryl Ring[c]

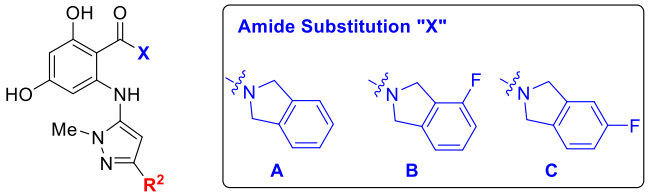

Entry	Compound	Amide ("X")	R^2	*C. neoformans* EC_{50}[a] (μM)	*C. neoformans* fold-selectivity[b]	*C. neoformans* MIC_{80}[c] (μM)
1	**9z**	A		0.227	**30.0**	>25
2	**9aa**	B		1.096	**9.6**	>25
3	**9ab**	C		0.020	**169.5**	25
4	**9ac**	A		0.034	**38.8**	**6.25**
5	**9ad**	B		0.017	**168.4**	**12.5**
6	**9ae**	C		0.267	**10.0**	14.1
7	**9af**	A		0.108	**29.5**	**12.5**
8	**9ag**	B		0.020	**233.9**	25
9	**9ah**	C		0.259	**11.5**	**12.5**
10	**9ai**	A		0.190	**9.6**	25
11	**9aj**	A		2.343	**5.0**	>25
12	**9ak**	A		0.406	**7.3**	**9.4**
13	**9al**	A		0.391	4.2	25
14	**9am**	A		0.115	**6.5**	**12.5**
15	**9an**	A		0.117	**25.4**	**6.3**
16	**9ao**	A		0.921	4.3	15.7
17	**9ap**	A		0.202	**10.4**	25
18	**9aq**	A		0.078	**18.1**	>25
19	**9ar**	A		0.334	**7.6**	**12.5**
20	**9as**	A		0.239	0.3	**12.5**
21	**9at**	A		0.468	3.2	18.8
22	**9au**	A		0.039	1.2	**9.4**

[a]EC_{50} values were determined by FP-based equilibrium competition assay performed in a 384-well format using whole-cell lysates prepared from *C. neoformans* and serial compound dilutions. All determinations were performed in duplicate. [b]To calculate fold-selectivity, the EC_{50} value determined in human HepG2 cell lysate was divided by the EC_{50} value determined in *C. neoformans* lysate. The resulting ratio was then normalized by the ratio of values determined for the Hsp90 inhibitor geldanamycin using lysate of each cell type. Results for key selective compounds were confirmed by repeat assay in lysates, as well as by measuring ligand dissociation constants (K_i) using purified NBDs in FP assays (see Supporting Tables 1 and 2). [c]Concentration of compound resulting in >80% inhibition of fungal cell growth compared to vehicle control. Values for compounds with either fold-selectivity >5 **or** $MIC_{80} \leq 12.5$ μM are highlighted in **blue**. Values for compounds with both fold-selectivity >5 **and** $MIC_{80} \leq 12.5$ μM are highlighted in **red**.

against whole cells. Replacement of the fluorine with chlorine in these analogues (**9w** and **9x**), plus an *N*-cyclohexyl variant (**9y**) reduced biochemical potencies from nanomolar to low micromolar range. Again, with these chlorinated analogues, there was an apparent trade-off between fungal selectivity >5-fold and whole-cell activity <25 μM, with no compounds espousing both features.

In sum, this initial cohort of second-generation RAPs confirmed our prior observations: while selectivity and permeance were most often orthogonal qualities, the combina-

https://dx.doi.org/10.1021/acs.jmedchem.0c01777
J. Med. Chem. 2021, 64, 1139−1169

Table 3. Strategic Merging of Bulky Aliphatic Moieties at R^1 and Optimal Disubstituted Aromatics at R^2 Result in Advanced Leads with Significantly Improved Activity Profiles[c]

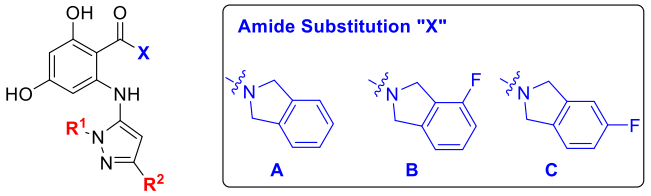

Entry	Compound	Amide ("X")	R^1	R^2	*C. neoformans* EC_{50}[a] (μM)	*C. neoformans* fold-selectivity[b]	*C. neoformans* MIC_{80} (μM)
1	**9av**	A	^{t}Bu		0.945	>12.7	25
2	**9aw**	A	^{i}Pr		0.337	18.7	25
3	**9ax**	A	^{t}Bu		0.634	13.0	12.5
4	**9ay**	A	^{cy}Pent		0.571	3.1	6.25
5	**9az**	A	^{cy}Hex		0.469	5.9	6.25
6	**9ba**	A	^{i}Pr		0.117	59.7	6.25
7	**9bb**	A	^{t}Bu		0.156	40.7	3.13
8	**9bc**	A	^{cy}Pent		0.316	10.8	6.25
9	**9bd**	A	^{cy}Hex		0.130	9.3	3.13
10	**9be**	A	^{i}Pr		0.234	23.5	6.25
11	**9bf**	A	^{t}Bu		0.347	20.2	3.13
12	**9bg**	B	^{t}Bu		1.150	>10.5	6.25
13	**9bh**	A	^{cy}Pent		0.533	3.9	6.25
14	**9bi**	A	^{cy}Hex		0.295	7.0	3.13

[a]EC_{50} values were determined by FP-based equilibrium competition assay performed in 384-well format using whole-cell lysates prepared from *C. neoformans* and serial compound dilutions. All determinations were performed in duplicate. [b]To calculate fold-selectivity, the EC_{50} value determined in human HepG2 cell lysate was divided by the EC_{50} value determined in *C. neoformans* lysate. The resulting ratio was then normalized to the ratio of values determined for the nonselective inhibitor geldanamycin using lysate of each cell type. Results for key selective compounds were confirmed by repeat assay in lysates, as well as by measuring ligand dissociation constants (K_i) using purified NBDs in FP assays (see Supporting Tables 1 and 2). [c]Concentration of compound resulting in >80% inhibition of fungal cell growth compared to vehicle control. Values for compounds with either fold-selectivity >5 **or** $MIC_{80} \leq 12.5$ μM are highlighted in **blue**. Values for compounds with both fold-selectivity >5 **and** $MIC_{80} \leq 12.5$ μM are highlighted in **red**.

tion of key structural features could in some cases (e.g., compounds **9d**, **9u**, **9v**) provide an inroad to optimized inhibitors.

Although the trend was not consistent across all analogues, we did note that in several instances, conversion of the R^1 *N*-methyl to *N*-*tert*-butyl dampened fungal selectivity in addition to improving whole-cell activity. In response, we next pursued an alternative method of pairing the apparent permeance-inducing ortho-substituent with a selectivity-inducing meta-substituent, on scaffolds that retained the R^1 *N*-methylation (Table 2). Here, we observed improved fungal selectivities with the 2,3-dimethyl series **9z**–**9ab**, but this R^2 group generally did not render the inhibitors permeant. Interestingly, this set also exhibited an extreme sensitivity to positioning of the isoindoline fluorine substituent with respect to biochemical potency. In contrast, we had significant success with R^2-fluorinated analogues. Compounds **9ac**–**9ae**, with an R^2 2,5-substitution pattern embodying one of two possible hybrids of monosubstituted compounds **18** and **9u**, showed dramatically improved potencies and selectivities, in concert with good whole-cell MICs ranging from 6.25 to 14.1 μM. Similarly, improved activity profiles were observed among 2-fluoro-3-methyl analogues **9af**–**9ah**. Inspired by these promising results, we next examined an array of disubstituted aryl rings at R^2, paired with isoindoline amide A (compounds **9ai**–**9au**). While selectivity and permeance sometimes diverged, we identified a number of ortho/meta pairings (again in both 2,3- and 2,5-relationships), which conferred high selectivity, and in select cases (**9ak**, **9am**, **9an**, and **9ar**) good concomitant whole-cell activity (MIC values 12.5 μM or lower). Of note, the *meta*-chlorination present in analogues **9ak** and **9ao** again appeared to dampen biochemical potency, as was observed in **9w**–**9y** (Table 1). This reduced cryptococcal potency in turn lowered fungal selectivity in comparison to other near-neighbor analogues. In contrast, *meta*-fluorination appeared to consistently yield biochemical potencies below 100 nM, fungal selectivities greater than 15-fold, and whole-cell activity at or below MIC 12.5 μM when paired with either a suitable ortho-substituent (**9ac**–**9ae**, **9am**, **9an**) or a bulky aliphatic group at R^1 (**9v**, Table 1). Compound **9as**, bearing two *ortho*-fluorine substituents in a 2,6 arrangement, exhibited moderate potency and whole-cell activity, but a complete loss of selectivity. Finally, ortho substitution (**9at**, **9au**) was also sufficient to achieve permeance in combination with additional para-substituents, but consistent with our previously published SAR, these para-substituted analogues were not found to confer any cryptococcal selectivity.

With two successful permeance-enhancing strategies identified, we next examined the combination of both approaches (Table 3). Gratifyingly, merging our optimal disubstitution patterns at R^2 with a variety of bulky aliphatic moieties at R^1 (*tert*-butyl, isopropyl, cyclopentyl, and cyclohexyl) afforded inhibitors **9av**–**9bi** with almost universally improved activity profiles. Notably, all compounds in this series had measurable MICs at or below 25 μM, with several compounds achieving the best cryptococcal whole-cell growth inhibition observed for fungal-selective RAPs to date at 3.13 μM (**9bb**, **9bd**, **9bf**, and **9bi**). Among this series, the strongest whole-cell potencies appeared to track to the *N*-*tert*-butyl and *N*-cyclohexyl

https://dx.doi.org/10.1021/acs.jmedchem.0c01777
J. Med. Chem. 2021, 64, 1139−1169

Table 4. Mammalian Cytotoxicity and Microsomal Stability Assessments for 24 Select RAPs, Including 22 RAPs with Biochemical FS >5 and *C. neoformans* MIC ≤ 12.5 μM[a]

Entry	Compound	*C. neoformans* fold-selectivity	*C. neoformans* MIC_{80} (μM)	HepG2 Cytotoxicity IC_{50} (μM)	NIH 3T3 cytotoxicity IC_{50} (μM)	NIH 3T3 Therapeutic Index (TI)	Microsomal stability $T_{1/2}$ (min)	Microsomal stability CL_{int} (μL/min/mg)
1	**9d**	11.1	12.5	5.9	8.0	0.6	**19.8**	**70.0**
2	**9j**	5.8	12.5	0.4	1.3	0.1	**21.7**	**63.8**
3	**9o**	6.8	1.8	0.7	5.7	**3.2**	**33.8**	**41.0**
4	**9v**	10.5	12.5	3.6	18.8	1.5	**40.8**	**34.0**
5	**9ac**	38.8	6.25	0.3	2.8	0.4	5.0	278.3
6	**9ad**	168.4	12.5	0.4	5.8	0.5	14.4	96.0
7	**9ae**	10.0	14.1	0.5	1.9	0.1	**24.5**	**56.6**
8	**9af**	29.5	12.5	0.1	5.8	0.5	**36.3**	**38.2**
9	**9ah**	11.5	12.5	0.1	1.4	0.1	**33.5**	**41.4**
10	**9ak**	7.3	9.4	0.5	4.4	0.5	**23.9**	**58.0**
11	**9am**	6.5	12.5	0.3	1.8	0.1	**22.4**	**61.8**
12	**9an**	25.4	6.3	0.56	2.9	0.5	17.6	78.6
13	**9ar**	7.6	12.5	0.7	1.8	0.1	**28.8**	**48.2**
14	**9av**	>12.7	25	9.9	>10	--	17.9	77.4
15	**9ax**	13.0	12.5	11.3	>10	--	5.7	243.2
16	**9az**	5.9	6.25	2.2	4.6	0.7	14.4	96.6
17	**9ba**	59.7	6.25	2.7	7.8	1.2	5.2	268.6
18	**9bb**	40.7	3.13	0.6	7.1	**2.3**	12.7	109.0
19	**9bc**	10.8	6.25	2.4	5.8	0.9	18.4	75.2
20	**9bd**	9.3	3.13	0.8	1.4	0.4	16.5	84.0
21	**9be**	23.5	6.25	1.9	3.1	0.5	**20.9**	**66.4**
22	**9bf**	20.2	3.13	1.2	4.0	1.3	**22.5**	**61.6**
23	**9bg**	>10.5	6.25	3.1	11.2	1.8	18.8	73.8
24	**9bi**	7.0	3.13	1.5	3.0	1.0	11.6	119.6

[a]All whole-cell testing results are representative of two independent experiments, each performed with technical triplicates. Compounds with NIH 3T3 therapeutic index >2 are highlighted in **green**. Compounds with intermediate microsomal stability (CL_{int} ~ 20−70 μL/min/mg)[69] are highlighted in **orange**.

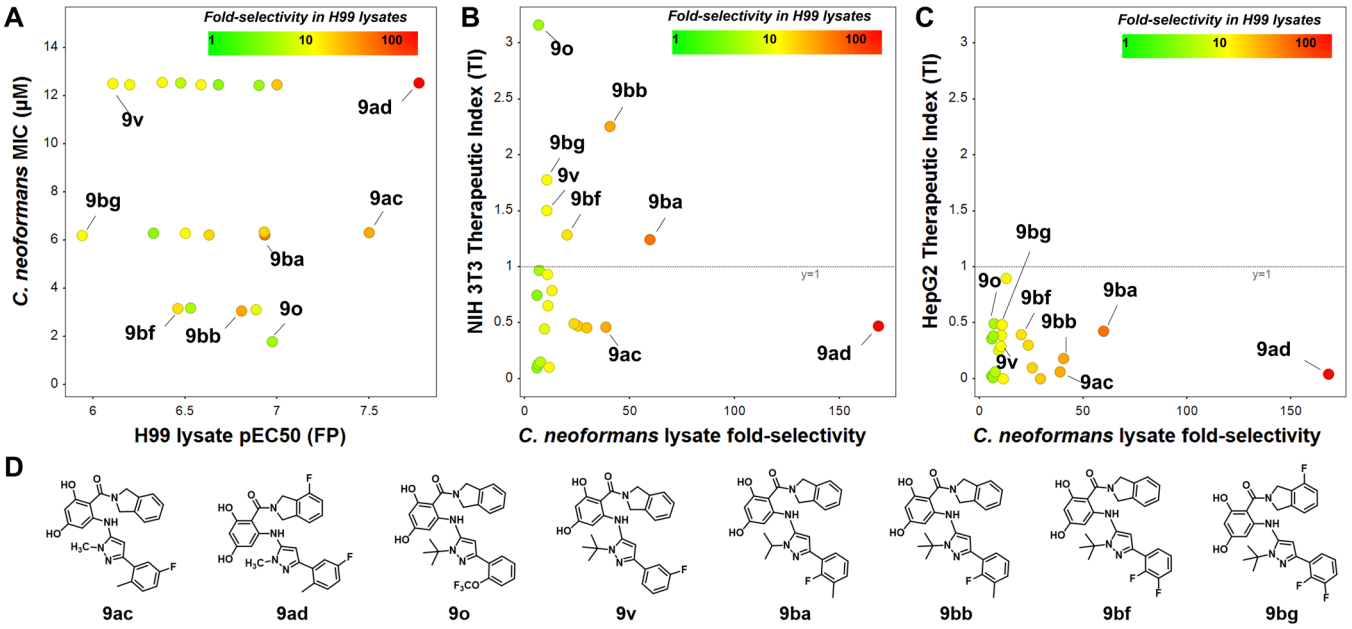

Figure 3. Scatter plots of the top 22 most fungal-selective, whole-cell-active RAPs showing that (A) biochemical potency (H99 lysate pEC50, *x*-axis) and whole-cell antifungal activity (*C. neoformans* MIC, μM, *y*-axis) are poorly correlated. Similarly, no correlation is seen between fungal selectivity and therapeutic index (TI, mammalian IC_{50} ÷ *C. neoformans* MIC) in (B) NIH 3T3 cells or (C) HepG2 cells. In (A−C), scatter points are colored based on relative H99 selectivity in cellular lysates. (D) Structures of key highlighted compounds.

substitutions at R^1, with the corresponding *N*-isopropyl (**9ba**, **9be**) and *N*-cyclopentyl (**9bc**, **9bh**) congeners espousing slightly higher MICs at 6.25 μM. Interestingly, while substitution of the isoindoline amide of **9bf** for 4-fluoroisoindoline (compound **9bg**) depressed potency to increase the lysate EC_{50} to the low micromolar range, this compound still exhibited selectivity and whole-cell activity comparable to near-neighbor analogues with lysate EC_{50}'s in the 100−400 nM range.

With a larger cohort of whole-cell-active, fungal-selective compounds in hand, we next sought to further evaluate these compounds for potential use in animals. In our prior study, poor metabolic stability was identified as a significant liability among

https://dx.doi.org/10.1021/acs.jmedchem.0c01777
J. Med. Chem. 2021, 64, 1139−1169

several of our most promising first-generation RAPs, with many compounds showing very high microsomal metabolism ($T_{1/2}$ < 10 min), and only one RAP with intermediate (CL_{int} ~ 20−70, $T_{1/2}$ 20−60 min) metabolic stability. In this study, we examined a wider array of RAPs from our second-generation set, including all of the most promising compounds summarized in Table 4, to better understand the metabolic liabilities present and attempt rational modifications to minimize them. Starting from first-generation RAP **18** ($T_{1/2}$ = 6 min), we found that a number of structural modifications conferred a net stabilizing effect, with microsomal half-lives for nearly half of the compounds (11 of 24) extended to >20 min. Such modifications include conversion of the R^1 methyl to *tert*-butyl (**9ax**) and cyclohexyl (**9az**), fluorination of the isoindoline at the 4- (**9ad**) and 5-position (**9ae**), and conversion of the R^2 *ortho*-methyl substituent to fluorine (**9am**) and chlorine (**9an**). However, matched-pair analysis for other members of the cohort (not shown) showed that these same types of single structural modifications impart divergent effects on microsomal stability, depending on the structure of the parent RAP. While it is difficult to discern clear structure−property relationships or pinpoint exact sites of metabolism from these data, we postulate that the observed trends are consistent with either metabolism that is largely occurring at the isoindoline with extreme sensitivity to CYP450 binding effects imparted by the entire aminopyrazole subunit, or more likely that several potential metabolic soft spots exist on the RAP scaffold, and that access to these potential hot spots by CYP450 enzymes is strongly governed by each site's positioning relative to other substituents exerting distal effects on CYP450 binding. While the extension of half-lives from the low to intermediate range represents a key advancement, there is clearly room for further optimization of metabolic stability.

Next, we examined the downstream translatability of potency and selectivity in lysates to the context of whole cells. Strikingly, a plot of biochemical vs whole-cell potency (Figure 3A) clearly shows that these values are noncorrelative. The lack of correlation suggests that although barriers to cryptococcal permeance have been lowered with this series, as-yet-undefined mechanisms still reduce compound accumulation in *Cryptococcus* and, as a result, dampen whole-cell potency to levels well below what would be expected based on biochemical target engagement. This point is perhaps best exemplified by direct comparison of compounds **9bg** and **9ac** (Figure 3A); despite a >30-fold difference in biochemical potency in cryptococcal H99 lysate (1.15 μM vs 34 nM, respectively), both compounds were equally effective in H99 whole cells (MIC 6.25 μM).

To investigate whether permeance limitations in *Cryptococcus* extended to mammalian cells, we proceeded to evaluate the cytotoxicity of our most promising compounds, again mainly focused on those with FS >5 and MIC ≤ 12.5 μM, in mammalian systems (Table 4). These RAPs were tested in nine-point dose response for cytotoxic activity against human liver cancer (HepG2) and mouse fibroblast (NIH 3T3) cell lines (Table 4, Supporting Tables 3 and 4; Figures S4 and S5). The disparity in these cell lines between whole-cell activity and biochemical potency for our RAPs was not as great as in *Cryptococcus*. As a result, we found that high fungal target selectivity in lysates did not translate to a useful therapeutic index (TI = mammalian IC_{50} ÷ *C. neoformans* MIC_{80}) in most cases. Using the noncancerous cell line NIH 3T3, known to be less sensitive to Hsp90 inhibition than cancer cells such as HepG2,[43] only a handful of compounds showed a modest therapeutic window (TI 1.5−3.1). Somewhat surprisingly, we observed a near-inverse relationship between cellular TI and lysate fold-selectivity; the most selective compound in mouse fibroblasts (**9o**) was among the least selective in lysates, whereas the RAP exhibiting the highest lysate selectivity (**9ad**) was among the least selective in NIH 3T3 cells (Figure 3B,D). In HepG2 cells, which due to their oncogenic nature are known to be hypersensitive to Hsp90 inhibition, none of the compounds exhibited cytotoxicity less than the minimum concentration required to suppress *C. neoformans* growth (all TIs < 1, Figure 3C,D). From these data, we conclude that although progress has been made, achieving adequate fungal permeance remains a challenge, a well-recognized hurdle for many small-molecule xenobiotics.[70]

Structural Insights into Fungal Selectivity of RAPs. In addition to pursuing a property-driven optimization of our RAP series, we performed structural studies to better understand the binding mode of these inhibitors and the basis of their selectivity. We determined the crystal structures (Supporting Tables 5 and 6) of the *C. neoformans* NBD domain in the apo state, in complex with the nonselective Hsp90 inhibitor NVP-AUY922 (luminespib)[71] and in complex with the fungal-selective RAPs **10**, **18** (Figure 2), and **19** (Figure 4).[62] These structures provide the first insights into the mode of RAP binding and also reveal a plausible structural rationale for their fungal selectivity.

Multiple copies of the protein were present in the asymmetric units of the crystals in all cases (three in apo, six in complex with

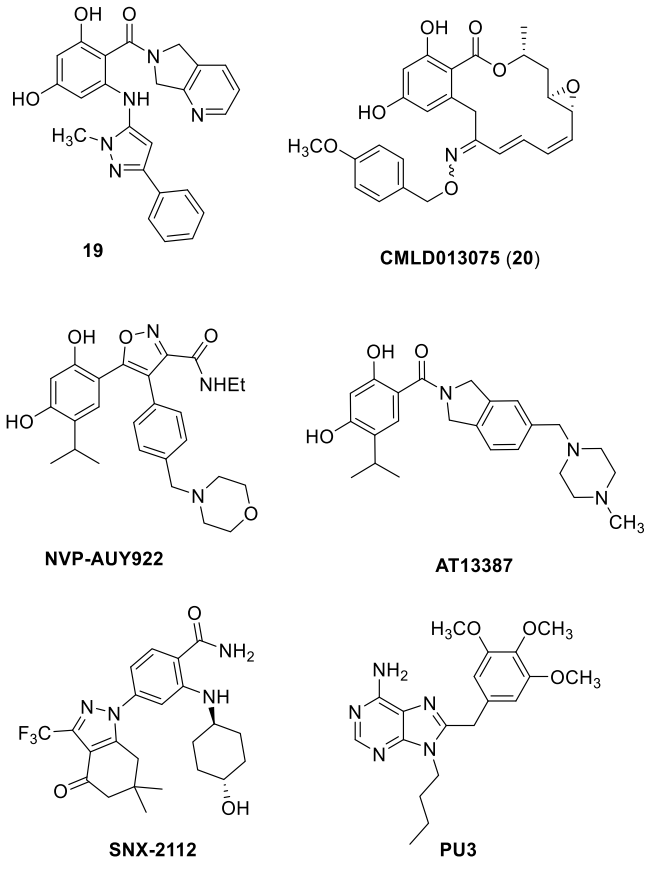

Figure 4. Chemical structures of ligands including RAP **19**;[62] previously reported *C. albicans*-selective inhibitor CMLD013075;[42] clinical inhibitors NVP-AUY922,[71] AT13387, and SNX-2112; and purine inhibitor PU3.[72]

https://dx.doi.org/10.1021/acs.jmedchem.0c01777
J. Med. Chem. 2021, 64, 1139−1169

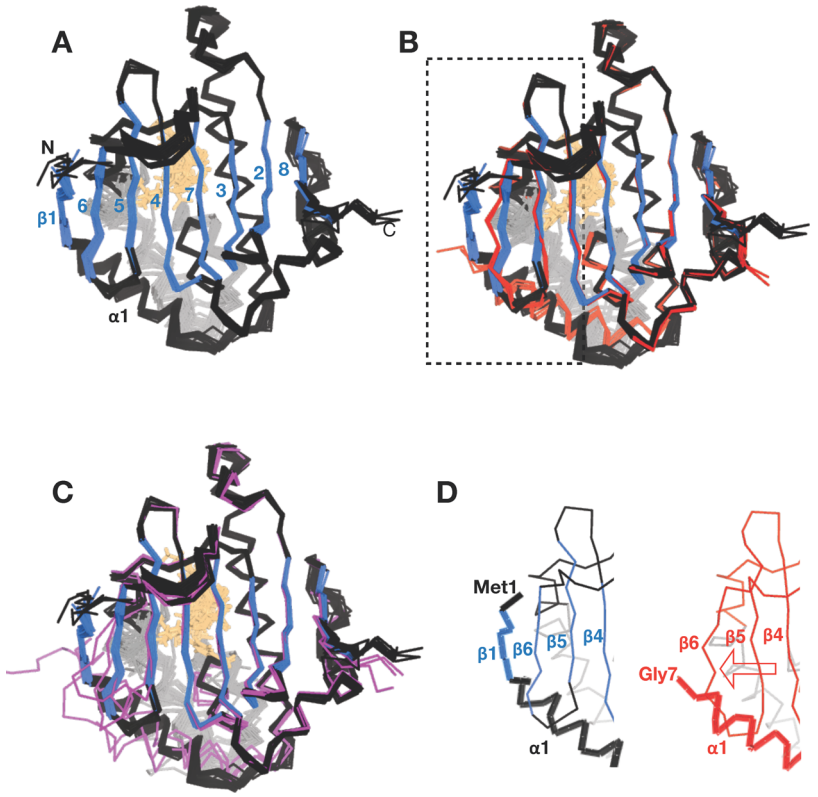

Figure 5. Overlay of human, *C. albicans*, and *C. neoformans* Hsp90 NBD structures, viewed from the "back" side of the domain. In this view, the ligand-binding pocket and lid helices $\alpha4-\alpha6$ are behind the protein, away from the viewer, and are deemphasized to accentuate the changes in the β-sheet and $\alpha1$. (A) Superposition of Cα traces from 21 structures that share a similar core. Traces are colored black, with β-strands in blue with blue labels. The lid is in light gray behind strands $\beta5$-$\beta4$-$\beta7$. Bound ligands in the nucleotide binding pocket are shown in pale orange behind strands $\beta4-\beta7$. The structures include the human protein in the apo state (PDB ID 1YER and 1YES, 2 chains) and in complex with radicicol (4EGK, 1 chain), SNX-2112 (4NH7, 2 chains), AUY922 (2VCI, 1 chain), AT13387 (2XJX, 1 chain), and PU3 (1UY6, 1 chain); *C. albicans* apo (6CJI, 1 chain) and in complex with ADP (6CJJ, 1 chain), radicicol (6CJL, 2 chains), and SNX-2112 (6CJR, 1 chain); and *C. neoformans* apo (7K9R, 3 chains) and in complex with AUY922 (7K9S, 6 chains). (B) Same as (A), but with the addition of structures from *C. neoformans* with compounds **10** (7K9W, 2 chains), **18** (7K9V, 2 chains), and **19** (7K9U, 2 chains), shown in red. This set shows consistent changes in $\beta5$, $\beta6$, and $\alpha1$ and a disordering of strand $\beta1$ (not modeled in the crystal structures). (C) Same as (A), but with the addition of chains from *C. albicans* in complex with AUY922 (6CJS, 1 chain) and CMLD013075 (**20**) (6CJP, 2 chain), shown in magenta. Changes in the core structure are seen in $\beta6$, $\beta1$, and $\alpha1$. (D) Individual structures from the box in (B) showing *C. neoformans* in complex with AUY922 (7K9S, left) and **18** (7K9V, right).

AUY922, and two with each of **10**, **18**, and **19**), providing independent views of the protein in different states (Supporting Figure S6). Excluding the flexible lid domain that spans residues 86−124 and includes helices $\alpha4-\alpha6$, the core backbone structure of the *C. neoformans* NBD in the apo state and in complex with AUY922 aligns well with the previously determined human and *C. albicans* structures (Figure 5A). The conservation of this core, which includes the entire β sheet and $\alpha1$, across three distantly related species in both apo and ligand-bound states demonstrates that this core is rigid and not easily deformed. In the more flexible lid domain, two of the three *C. neoformans* apo chains resemble the "closed" (catalytically active) state of the human structure (PDB: 1YER[73]), as defined by the inward positioning of the catalytic loop between helices $\alpha4$ and $\alpha5$, while the third chain adopts the "open" state, similar to that seen in the human structure (1YES[73]). In the apo and AUY922 structures, the lid adopts a range of conformational states and the catalytic loop between helices $\alpha4$ and $\alpha5$ ranges in length from two to eight residues. The lid regions in the six RAP structures, however, are similar to each other but differ from the previously described structures. Notably, helices $\alpha4$ and $\alpha5$ are fused into a single continuous helix from residues 86−110 that curves around the nucleotide binding site (Supporting Figure S6). The structure of this lid region is similar in all six RAP complex structures; however, there are minor differences in the conformation of the fused helix, including a bulge[74] at residue L93 in three of six cases. In addition, and in contrast to the *C. neoformans* apo and AUY922 structures, the six RAP structures show consistent changes in the conserved core of the domain. Notably, strand $\beta1$ could not be modeled due to disorder, while $\alpha1$ and the following loop connecting to $\alpha2$ are shifted relative to the canonical structure (Figure 5B). Similar N-terminal changes involving $\beta1$ and $\alpha1$ have been observed in structures of *C. albicans* with AUY922 and the *C. albicans*-selective Hsp90 inhibitor CMLD013075 (**20**, Figure 4), although the specific details differ (Figure 5C).[42]

Overall, five regions of the NBDs make contact with the ligands: residues from $\alpha2$; the loop that precedes $\alpha4$; the $\alpha4-\alpha5$ segment of the lid; helix $\alpha7$; and residues on the inward-facing strands of $\beta4$, $\beta5$, and $\beta7$ of the main sheet (Supporting Figure S7). With the exception of the lid, there is little structural variability in the backbone of these elements, and most of the side chains adopt similar rotamers irrespective of the species or bound ligand. As previously described, the vast majority of the Hsp90 residues in direct contact with ligands are identical between the three species, with the exception of positions S38/

https://dx.doi.org/10.1021/acs.jmedchem.0c01777
J. Med. Chem. 2021, 64, 1139−1169

A41/S52 on α2 and M173/L176/V186 on β7 (*C. neoformans*/*C. albicans*/human residue numbering). These side chains occupy similar volumes in all structures and are roughly isosteric, but they do make contributions to the surface of the pocket that accepts the resorcinol ring, among others. These positions may modulate ligand-binding affinity and thus may contribute to species specificity.

A comparison of the *C. neoformans* complex with **10** and the human complex with AT13387 shows excellent overlap between the common resorcinol and isoindoline rings (Figure 6A). In comparison to other liganded Hsp90 structures in the PDB, the RAP aminopyrazole ring is positioned in an induced pocket that is similar to, but slightly deeper than, the pocket induced by the indazole ring of nonselective inhibitor SNX-2112.[41,42] While originally designed to mimic the CMLD013075 oxime, the aminopyrazole instead sits in an orthogonal position, with a π-stacking interaction between the R^2 aryl ring and Hsp90 F124.

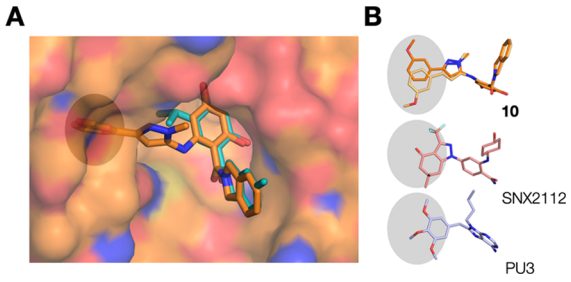

Figure 6. Comparison with previously reported complexes. (A) Overlay of the human Hsp90/AT13387 complex (2XJX, cyan carbon atoms) with the *C. neoformans*/**10** complex (7K9W, orange carbon atoms). The surface of the fungal protein is shown, and the AT13387 piperazine ring is omitted for clarity. (B) Staggered view of aligned ligands from four complexes: the two chains from the *C. neoformans*/**10** crystal structure (7K9W), human/SNX-2112 (4NH7), and human/PU3 (1UY6). The gray oval represents the deep hydrophobic pocket of Hsp90, indicated in the left part of (A).

The R^2 aryl rings in the RAP series introduce an important feature that distinguishes these compounds from previously reported inhibitors.[62] A comparison of the structures of the human and two fungal NBDs in complex with AUY922 reveal highly similar structures, with the exception of moderate shifts in the α4-α5 lid region (Figure 7A). However, in all six RAP structures, the lid is displaced outward in response to the R^2 rings (Figure 7B). Hydrophobic residues L93, F124, and W148 are in close contact in all of the apo and AUY922 complexes (Figure 7C,D) but are displaced in the RAP structures to accommodate the aryl rings (Figure 7E,F). The aromatic residues F124 and W148 in the NBD are on the relatively well-fixed α7 and β5 strand elements, while L93 is on the more malleable lid and is more easily displaced to accept the aryl ring. The disruption of this packing and outward displacement of L93 promotes the adoption of an α-helical conformation in the loop between α4 and α5, resulting in the formation of a continuous helix that spans the N-terminus of α4 to the C-terminus of α5 (residues 86−110) (Supporting Figure S6). Equivalent L93/F124/W148 packing is observed in the majority of apo and complex NBD structures from human and *C. albicans*, and similar disruptions of this core have been observed by the indazole ring of the nonselective inhibitor SNX-2112 in human[41] and *C. albicans*,[42] and the methoxy-substituted aryl ring of PU3 in human (Figure 6B).[72,75] Notably, the RAP R^2 aryl ring penetrates more deeply into this site and engages F124 in $\pi-\pi$ stacking interaction (Figures 6 and 7), potentially offsetting the energetic cost of repacking the hydrophobic core.

The *C. neoformans* structures reveal two packing arrangements of the RAP R^2 aryl groups (Figure 6B and Supporting Figure S6). In four of the complexes (chain A of **10**, chains A and

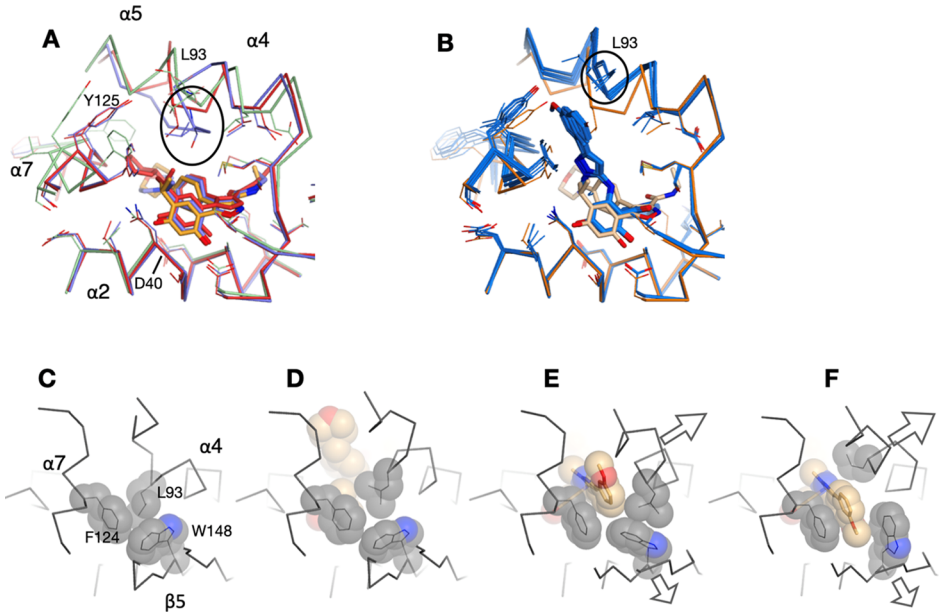

Figure 7. Ligand-driven reorganization of the *C. neoformans* binding pocket. (A) Overlay of the human (light blue, 2VCI), *C. albicans* (red, 6CJS), and *C. neoformans* (orange, 7K9S) complexes with AUY922. (B) Overlay of the *C. neoformans* NBD in complex with AUY422 (orange, 7K9S) and RAP compounds **10** (7K9W), **18** (7K9V), and **19** (7K9U) (dark blue). (C−F) Residues L93, F125, and W128 from helices α4, α7, and strand β5, respectively, are in packing contact in the apo (6CJI, C) and AUY922 (7K9S, D) complexes, but are disrupted by the R^2 aryl ring of the RAPs (7K9W, E/F). The two chains in the co-crystals of the *C. neoformans* NBD with **10** reveal different rotamers of the *meta*-methoxy aryl ring, shown in (E) and (F).

https://dx.doi.org/10.1021/acs.jmedchem.0c01777
J. Med. Chem. 2021, 64, 1139−1169

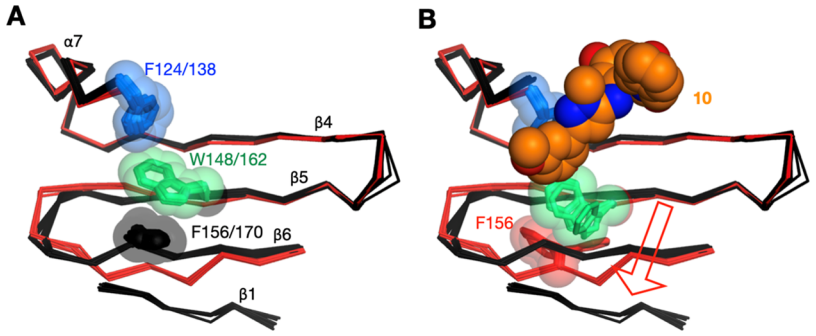

Figure 8. RAP binding disrupts the β-sheet. (A) Overlay of the *C. neoformans* and human structures from Figure 5 were divided into two sets. Set A includes all of the eight human structures [1YER, 1YES, 4EGK, 4NH7 (two chains), 2VCI, 2XJX, and 1UY6] and the nine *C. neoformans* apo and AUY922 structures [7K9R (three chains) and 7K9S (six chains)] and is shown in black Cα trace. Set B includes the six fungal RAP complexes [7K9U (two chains), 7K9V (two chains), and 7K9W (two chains)] and is shown in red Cα trace. Selected side chains from set A are shown in stick representation with van der Waals surface and fungal/human numbering. (B) The same backbone traces are represented, but with the side chains from set B as well as the RAP inhibitor **10** in space filling representation. Note that strand β1 is present only in the structures from set A.

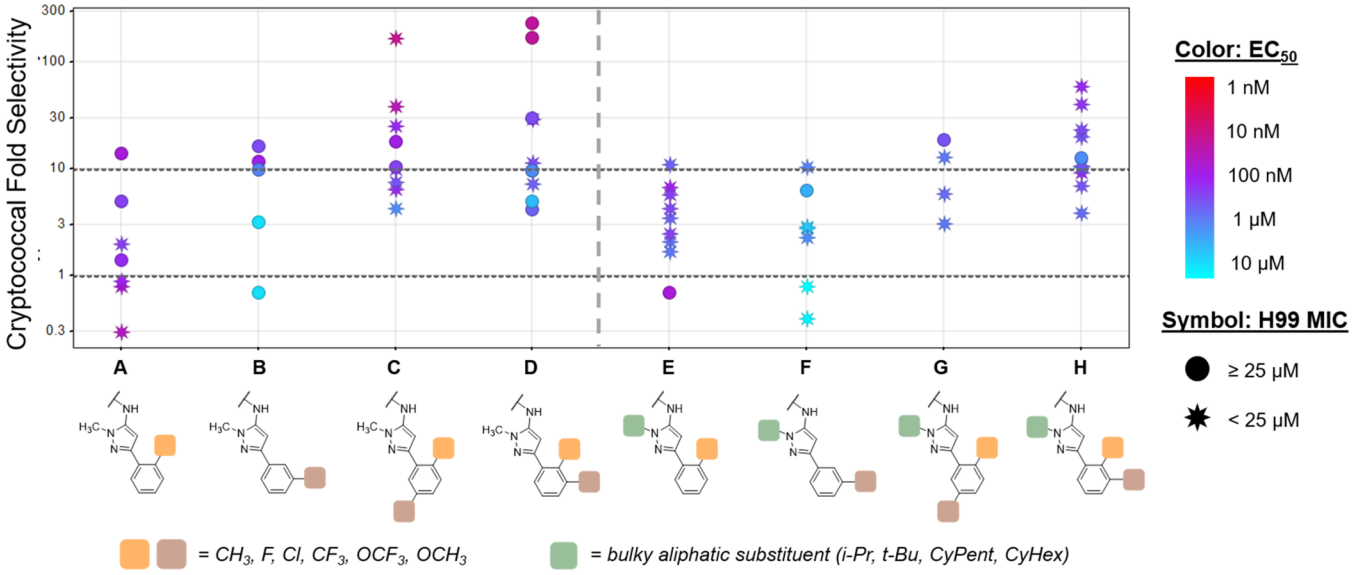

Figure 9. Scatter plots of cryptococcal selectivity, biochemical potency, and whole-cell activity for Table 4 RAPs, binned by the aminopyrazole substructure class as defined by the R^1 and R^2 substitution patterns. The y-axis depicts cryptococcal fold-selectivity on a logarithmic scale. Points are colored by H99 lysate EC_{50} on a logarithmic scale, on a gradient ranging from cyan (10 μM) to red (1 nM). Point symbols indicate whole-cell activity class, with circles corresponding to compounds with little to no whole-cell activity (H99 MIC $\geq$ 25 μM) and stars indicating whole-cell-active compounds with an H99 MIC < 25 μM.

B of **18**, and chain A of **19**), the aryl ring is in the position shown in Figure 7E, while in the other two (chain B of **10** and **19**), the conformer is as in Figure 7F. Thus, the pocket can adjust to two rotamers of the ligand aryl ring relative to the aminopyrazole ring. These structures, in combination with the SNX-2112 and AT13387 structures, demonstrate the plasticity of this induced binding pocket in both fungal and human Hsp90s. While we expect that the RAPs can induce similar rearrangements in the human protein, the weaker K_d's strongly suggest that the energetics of repacking differs between the two species. Although there is no obvious trend to show how the aryl ring substituents may favor different binding states, these structures clearly show that ring substitution is a viable strategy to modulate the binding affinity within this series of inhibitors.

The insertion of RAP aryl rings not only displaces and remodels the α4-α5 lid but also has smaller but significant effects on β5 due to backbone shifts at residue W148 (Figures 7E,F and 8). This has a domino effect that affects neighboring strand β6 by displacing F156, ultimately resulting in the loss of the N-terminal β1 strand of the sheet (Figure 8). In turn, the disruption of strand β1 results in the shift in α1 since the N-terminus of this helix is no longer anchored to the protein (Figures 5 and 8).

Each of the three major ligand-induced conformational changes seen in the *C. neoformans* RAP complexes (disruption of the L93/F125/W128 core, fusion of the lid helices, and disruption of the N-terminus) have been observed in other NBD complexes, but not in the same structures (Supporting Table 7). Given the current data, it is challenging to propose a single unifying model to explain how these changes are correlated to each other and to ligand binding. We propose, however, that the fusion of the lid helices is not directly correlated with the other observed changes and is most likely driven by direct interactions with the ligands. Support for this model can be found in the structures with AUY922, which are known for all three species under consideration. The binding of AUY922 to the *C. albicans* NBD results in a fused lid helix and disrupted N-terminus, but does not disrupt the core, while none of these changes are present in the human AUY922 complex. In addition, a fused lid

https://dx.doi.org/10.1021/acs.jmedchem.0c01777
J. Med. Chem. 2021, 64, 1139−1169

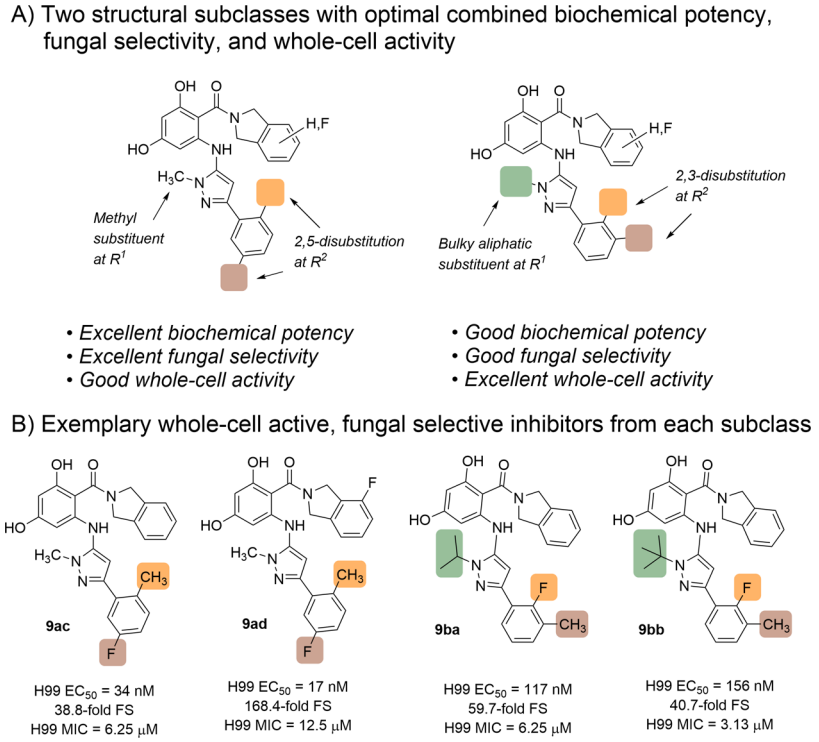

Figure 10. (A) Two predominant structural classes among RAPs with optimal combined biochemical potency/fungal selectivity/whole-cell activity profile, each with slightly divergent activity profiles. (B) Representative structures and activities of top inhibitors **9ac**, **9ad**, **9ba**, and **9bb** from these subclasses.

helix is seen in two of the six AUY922 complexes with the *C. neoformans* NBDs, but all have an intact L93/F125/W128 core and an ordered N-terminus. The second pattern that emerges from the set of complexes is that the disruption of the N-terminal region co-occurs with the disruption of the W148/F156 stack between strands β5 and β6. This stack is disrupted in some, but not all, of the ligand complexes that disrupt the L93/F125/W128 core. These include the six *C. neoformans*/RAP structures presented here and the *C. albicans* complexes with AUY922 and CMLD013075.[42] Complexes with SNX-2112 (human, *C. albicans*) and PU3 (human) are able to disrupt the core packing, but do not reach deeply enough into the induced pocket to affect the position of W148, and consequently, these ligands do not disrupt the β1/α1 N-terminus. It is notable that N-terminal remodeling has been observed in approximately half of the available *C. neoformans* and *C. albicans* structures, but never in a human structure. This may simply reflect the selection of structures that are currently available, or it may be because the fungal NBDs are more prone to structural rearrangements in regions outside of the lid. Overall, these results reflect the complex interplay between the ligands and the proteins and support the idea that Hsp90 inhibitors can be designed with species-specific properties.

Summary of Structure–Activity Relationships and Insights from Modeling. With X-ray crystallographic structures providing an improved understanding of the binding modes of R^1-methylated, R^2 monosubstituted RAPs, we next attempted to further rationalize the observed structure–activity and structure–property relationships across different RAP structural subtypes. Figure 9 shows a scatter plot summarizing the cryptococcal fold-selectivity (y-axis), biochemical potency (color), and whole-cell activity (symbol) of the cohort of inhibitors from Table 4, binned on the x-axis based on their patterns of substitution at R^1 (methyl vs bulky aliphatic substituents) as well as at the R^2 phenyl ring (2-substituted, 3-substituted, 2,3-disubstituted, and 2,5-disubstituted). From this plot, we can glean generalized SAR trends through head-to-head comparisons of different cohorts. For example, in comparing groups A–B and E–F, it is clear that *ortho*-monosubstituted compounds in group A generally have very good (low nM) biochemical potencies but are limited in their fungal selectivity. In contrast, *meta*-monosubstitutions (groups B and F) generally lead to suppression of biochemical potency, in some cases to the micromolar range. Interestingly, for the *meta*-monosubstituted subset B, selectivity does not appear to track as cleanly with biochemical activity compared to the *ortho*-monosubstituted subset A. Also apparent is the general overall improvement in biochemical potency and selectivity that is achieved when incorporating a second substituent at R^2 (groups C/D/G/H as compared to groups A/B/E/F). It is also notable that group to group, these improvements in selectivity do sometimes come at a cost: for example, the most potent and selective *N*-methylated, 2,3-disubstituted inhibitors (group D) tend to have poor whole-cell activity, and highly selective inhibitors bearing bulky R^1 substituents are generally less potent than their *N*-methylated counterparts (*cf.* groups G/H and groups C/D).

In judging these structural subclasses by their full complement of relevant parameters, two clear "optimal" themes emerge (Figure 10A): first, for compounds that are *N*-methylated at R^1, overall whole-cell activity is best among R^2-disubstituted compounds where the substituents have a 2,5 relationship (group C); in contrast, compounds bearing bulky aliphatic groups at R^1 generally exhibit improved potency and selectivity when R^2 is 2,3-disubstituted (group H). Interestingly, these two orthogonal subsets also diverge somewhat in the nature of their "optimal" properties; while group C is exemplary in biochemical

https://dx.doi.org/10.1021/acs.jmedchem.0c01777
J. Med. Chem. 2021, 64, 1139–1169

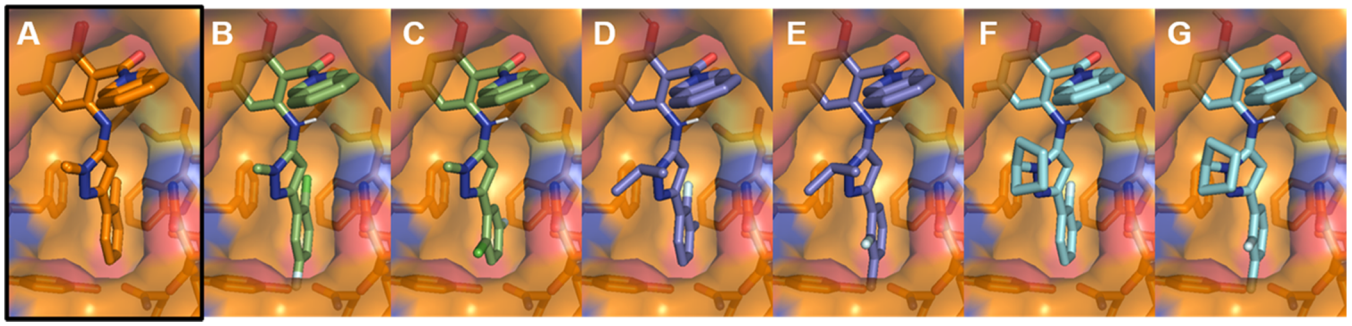

Figure 11. Results of computational modeling using RAP-liganded X-ray crystal structures. (A) X-ray crystal structure (7K9V) with compound **18** bound at Chain A. (B, C) Comparative views of two rotamers of compound **9an** docked into structure 7K9V Chain A. Docking scores are −15.3 and −14.5 kcal/mol, respectively. (D, E) Comparative views of two rotamers of compound **9ba** docked into structure 7K9V Chain A. Docking scores are −14.7 and −14.5 kcal/mol, respectively. (F, G) Comparative views of two rotamers of compound **9bc** docked into structure 7K9V Chain A. Docking scores are −14.2 and −14.4 kcal/mol, respectively.

potency and selectivity, group H is stronger in terms of whole-cell anticryptococcal activity; this feature is even more pronounced when considering the relative whole-cell potencies, which for simplicity are not represented here. In Figure 10B, we provide representative leading members of each of these two classes, as starting points for future optimizations of potency; selectivity; whole-cell activity; and additional absorption, distribution, metabolism, and excretion (ADME) parameters including metabolic stability.

We next attempted to model these various structural subclasses into our existing X-ray structures to rationalize structure−activity trends observed among the R^2-disubstituted inhibitors. In doing so, it is important to consider that due to the inherent plasticity of the Hsp90 NBD and the number and scope of remodeling events which have so far been documented across different species and in co-complex with different ligand structural subclasses, any effort to model other RAP structural subclasses into these rigid, RAP-induced receptors is of only limited and speculative utility. Nonetheless, in each RAP-liganded X-ray structure, the R^1-methyl substituent is projected outward and solvent-exposed; we posit that expansion of this group to a larger lipophilic moiety is likely to create entropic penalties due to bulk water disruption, which may in part explain the general overall trend of lowered biochemical EC_{50}'s as the size and lipophilicity of this substituent increases. Given the proximity of this solvent-exposed group to a polar region of the binding pocket periphery, it is also possible that incompatible sterics and polarities also compound this issue. In addition, since the overall structural disruptions of the NBD appear to be induced by the R^2 aryl ring, we postulate that the added steric demands imposed by a second substituent on this ring may be the source of further improvements to selectivity. While we are reluctant to definitively propose binding modes for the R^2-disubstituted RAPs, we have performed computational (Glide) docking[76,77] of the 24 RAPs from Table 4 to explore whether the pockets induced by compounds **10**, **18**, and **19** are large enough to accommodate larger R^1 and R^2 substituents in similar binding poses without any further protein structure remodeling (Figure 11 and Supporting Table 8). Glide docking with positioning restricted to the reference RAP ligand core produced excellently scored poses (−14.3 to −15.5 kcal/mol), for 20 out of the 24 compounds into at least one of the six independent chains with a core atom root-mean-square deviation (RMSD) to the native ligand of <0.1 Å. Notably, each compound also produced at least one high-scored docking pose for each of the two types of R^2 rotamers that were observed for compound **10** in the independent chains of the 7K9W structure, underscoring the flexibility of this pocket to accommodate disubstituted R^2 aryl rings in multiple orientations. Select docking poses of compounds **9an**, **9ba**, and **9bc**, which illustrate this phenomenon, are depicted in Figure 11B−G.

Out of the set of RAPs docked, only the R^1-cyclohexyl-substituted compounds (**9j**, **9az**, **9bd**, and **9bi**) failed to produce any poses in any of the six chains under the applied constraints, which we ascribe to the entropic and steric factors described above. For the remaining 20 compounds, very high docking scores were obtained across compounds with widely varying biochemical potencies and selectivities; as such, it is difficult to fully rationalize the divergent activities on the basis of this structural modeling. However, this limited computational study does confirm an overall compatibility of the R^2-disubstituted RAPs with the RAP-induced binding pocket. In addition, the accommodation of multiple R^2 substituents and in multiple orientations suggests that the potency gains observed for disubstituted compounds may in part arise due to additional beneficial van der Waals interactions and an improved occupancy of the deep hydrophobic cavity in the R^2-induced pocket.[78,79] What is not clear from this modeling, however, is whether these added R^1/R^2 substituents may induce further changes to the protein structure, nor do they explain what role the size and nature of the R^1/R^2 groups play in other important improvements such as whole-cell permeance and reduced mammalian cytotoxicity. Given the number of unexpected ligand-induced conformations that have been observed in fungal Hsp90 structures to date, further crystallographic work is needed to fully understand the binding modes of the optimized R^2-disubstituted compounds described herein.

CONCLUSIONS

Continuing in our pursuit of fungal-selective, resorcylate inhibitors of the protein-folding chaperone Hsp90, and building on early leads from our prior study of resorcylate aminopyrazoles (RAPs), we have used a rational structure−property approach to improve the whole-cell fungal permeance of a lead series which exhibits high selectivity for cryptococcal Hsp90. Toward this goal, we have achieved synthesis of 22 new fungal-selective RAPs that effectively inhibit growth of *C. neoformans* whole cells at low-to-sub-micromolar concentrations. Further pharmacological and biological characterization of these RAPs showed that despite moderate improvements in both micro-

https://dx.doi.org/10.1021/acs.jmedchem.0c01777
J. Med. Chem. 2021, 64, 1139−1169

somal stability and whole-cell anticryptococcal activity, further optimization of fungal permeance is still needed to achieve an adequate therapeutic window for use in infection-relevant contexts. We have also solved the first X-ray crystal structures of *C. neoformans* Hsp90 in various states, including structures in complex with three fungal-selective RAPs. Conformational rearrangements induced by RAPs, while unique within the direct binding site, create downstream conformational reorganizations that are consistent with other changes induced by a resorcylate compound that selectively binds *C. albicans* Hsp90. Further studies to parlay these foundational findings into improved fungal-selective Hsp90 inhibitors for use as chemical biological probes and eventually therapeutics are ongoing.

EXPERIMENTAL SECTION

Fungal Strains and Culture Conditions. The strain used in this study was *C. neoformans* H99.[80] Archive of this strain was maintained at −80 °C in 25% glycerol. Active cultures were maintained on solid (2% agar) yeast extract peptone (YPD, 1% yeast extract, 2% bacopeptone, and 2% glucose) at 4 °C for no more than 1 month.

Antifungal Sensitivity Testing. Minimum inhibitory concentrations (MICs) were determined in flat-bottom, 96-well-plate format using RPMI medium (Gibco SKU no. 318000-089, 3.5% MOPS, 2% glucose, pH 7.0). A modified broth microdilution protocol was used as previously described,[23,81] except that a relative viable cell number was monitored by standard dye-reduction assay after a 3 h incubation with resazurin at 37 °C. All compounds were formulated in dimethyl sulfoxide (DMSO, Sigma-Aldrich Co.). Each compound was tested in duplicate in at least two independent experiments.

Mammalian Cell Culture and Cytotoxicity Testing. The cell lines NIH 3T3 (CRL-1658) and HepG2 (HB-8065) were purchased from the American Type Culture Collection (ATCC). The cells were maintained in RPMI medium supplemented with 10% fetal bovine serum at 37 °C under 5% CO_2. Experiments were performed using cells within 10 passages post recovery from low-passage stocks maintained in liquid nitrogen and confirmed negative for mycoplasma contamination by PCR-based assay. The cells were plated in a 384-well format at a density of 2000 per well (HepG2) or 2500 per well (NIH 3T3) in RPMI supplemented with 10% fetal bovine serum (FBS). Following overnight adherence, twofold dilutions of test inhibitors were added to wells and plates were incubated for 72 h. Subsequent determination of relative viable cell number was performed using standard resazurin dye-reduction assay with incubation at 37 °C for 3 h and measurement in a Tecan Spark microplate reader using SparkControl software (version 2.2). Nonlinear four-parameter curve fitting of raw dose−response data was performed in GraphPad Prism 7 to determine IC_{50} values. Results reported are representative of two independent experiments, each performed with technical triplicate.

FP Assays. FP assays performed with whole-cell lysates and purified *C. neoformans* Hsp90 NBD were performed as previously described.[62] In calculating fold-selectivity for compounds, a normalization factor of 0.84 was applied based on the EC_{50} values determined in human and fungal cell lysate for geldanamycin, the same Hsp90 inhibitor used to generate the FP probe itself.

NBD Expression and Purification. Recombinant Hsp90 NBDs were expressed and purified as previously described.[42,62]

Analytical LC-MS/MS Conditions. Compound levels for *in vitro* metabolic stability assays were monitored by LC-MS/MS using an AB Sciex (Framingham, MA) 4000 QTRAP mass spectrometer coupled to a Shimadzu (Columbia, MD) Prominence LC. The parent ion and the two most prominent daughter ions were followed to confirm compound identity, although only the most abundant daughter was used for quantitation. Analytes were detected with the mass spectrometer in negative multiple reaction monitoring (MRM) mode for the following compounds: **9i** 541.3-404.0; **9j** 541.2-404.0; **9n** 477.1-358.0; **9o** 551.3-432.0; **9ac** 457.1-337.9; **9ad** 475.2-338.1; **9ae** 475.1-337.9; **9ah** 475.2-338.0; **9ak** 477.1-357.9. The following compounds were detected in positive MRM mode: **9d** 483.2-308.0; **9v** 487.2-312.0; **9af** 459.2-340.1; **9am** 463.1-344.1; **9ar** 529.1-410.1; **9av** 497.2-322.0; **9ax** 501.2-326.0; **9az** 527.2-326.0; **9ba** 487.2-326.1; **9bb** 501.2-326.0; **9bc** 513.2-326.0; **9bd** 527.2-326.1; **9be** 491.2-330.1; **9bf** 505.2-330.0; **9bg** 523.2-330.1; **9bi** 531.2-330.1. An Agilent (Santa Clara, CA) C18 XDB column (5 μm, 50 mm × 4.6 mm) was used for chromatography for compounds detected in negative mode under the following conditions: Buffer A: dH_2O + 0.1% formic acid, Buffer B: methanol + 0.1% formic acid, 0−1.0 min 5% B, 1.0−2 min gradient to 100% B, 2−3.5 min 100% B, 3.5−3.6 min gradient to 5% B, 3.6−4.5 5% B. Tolbutamide (transition 269.1-169.9) from Sigma (St. Louis, MO) was used as an internal standard (IS). Conditions for compounds evaluated in positive mode were nearly identical, except the gradient conditions: 0−1.0 min 5% B, 1.0−1.5 min gradient to 100% B, 1.5−3.0 min 100% B, 3.0−3.2 min gradient to 5% B, 3.2−4.5 5% B, and *N*-benzylbenzamide (Sigma) was used as the internal standard (transition 212.1−91.1). Solvents (methanol and water) and formic acid were all of LC-MS/MS grade ("Optima") and purchased from Fisher Scientific (Waltham, MA).

Mouse Liver Microsome Stability. Female ICR/CD-1 mouse microsome fractions were purchased from BioIVT (Westbury, NY), and the protocol provided with the microsomes for assessment of compound stability was followed as detailed herein. All chemical reagents aside from the aforementioned solvents were purchased from Sigma (St. Louis, MO). Microsome protein (0.5 mg/mL) was added to a glass screw cap tube; then, 50 mM Tris, pH 7.5 solution, containing the compound of interest in DMSO (final DMSO concentration, 0.1%) was added on ice. The final concentration of compound after addition of all reagents was 2 μM. A nicotinamide adenine dinucleotide phosphate (NADPH)-regenerating system (1.7 mg/mL NADP, 7.8 mg/mL glucose-6-phosphate, 6 U/mL glucose-6-phosphate dehydrogenase in 2% w/v $NaHCO_3$/10 mm $MgCl_2$) was added for analysis of Phase I metabolism after both the microsome/compound mixture and regenerating system were warmed to 37 °C for 5 min. The tube was then placed in a 37 °C shaking water bath. At varying time points after addition of the NADPH regenerating system, the reaction was stopped by the addition of 0.5 mL of methanol containing an internal standard (IS) and formic acid such that the final concentration of tolbutamide IS was 50 ng/mL and that of *N*-benzylbenzamide IS was 100 ng/mL, and acid was 0.1%. Time 0 samples were quenched with methanol prior to addition of compound. The samples were incubated 10 min at room temperature and then spun at 16 100*g* for 5 min in a microcentrifuge at 4 °C. The supernatant was analyzed by LC-MS/MS. The method described in McNaney et al.[69] was used with modification for determination of metabolic stability half-life by substrate depletion. A "% remaining" value was used to assess the metabolic stability of a compound over time. The LC-MS/MS peak area of the incubated sample at each time point was divided by the LC-MS/MS peak area of the time 0 (T0) sample and multiplied by 100. The natural log (LN) of the % remaining of compound was then plotted versus time (in minutes) and a linear regression curve plotted going through *y*-intercept at LN(100). The metabolism of some compounds failed to show linear kinetics at a later time point, so those time points were excluded. The half-life ($T_{1/2}$) was calculated as $T_{1/2} = -0.693/\text{slope}$. To determine intrinsic clearance,[82−85] which allows for comparison of data obtained using different volumes and protein concentrations, the following calculations were employed:

$$V(\mu\text{L/mg}) = \frac{\text{volume of incubation } (\mu\text{L})}{\text{protein in the incubation (mg)}}$$

$$\text{intrinsic clearance } (\text{CL}_{\text{int}})(\mu\text{L/min /mg protein}) = \frac{Vx0.693}{t_{1/2}}$$

Statistical Methods. For FP experiments in support of SAR studies, GraphPad Prism 5.0 was used to perform curve fitting and calculate the concentrations of compounds resulting in 50% reduction in maximal polarization signal (EC_{50}). All curve fits demonstrated a correlation coefficient (R^2) > 0.95. The number of independent experiments performed and the number of technical replicates in each experiment are provided in the legends of figures and tables

https://dx.doi.org/10.1021/acs.jmedchem.0c01777
J. Med. Chem. 2021, 64, 1139−1169

characterizing the biochemical and biological activities of compounds. In calculating the error of selectivity determinations, the fractional error of measurements in each species was summed to yield a composite error for the derived ratio.

Protein Crystallization and Structure Determination. Aliquots of purified *C. neoformans* NBD (residues 1−211 or 1−215) were crystallized either alone (apo) or in the presence of AUY922 or RAPs **10**, **18**, and **19**. Crystals were obtained by mixing one part of protein solution at 10−15 mg/mL (20 mM Hepes, pH 7.5, 500 mM NaCl, 8% glycerol, 10% DMSO with or without 2 mM ligand) with one part of reservoir solution. Crystals were obtained by sitting-drop vapor diffusion at 21 °C. The best diffracting crystals were produced with a reservoir containing 20−25% PEG6K, 0.1 M Hepes, pH 7, and 1 M $LiCl_2$.

Crystals were cryo-protected by passage through paratone before flash-cooling in liquid nitrogen. Diffraction data were collected at the APS or NSLS II synchrotrons, as indicated in Supplementary Tables 5 and 6. Data were processed and integrated with XDS[86] and Aimless,[87] and structures were determined by molecular replacement using *C. albicans* Hsp90 NBD (PDB ID 6CJI) as a search model for the apo structure. The apo structure was then used to solve the RAP complexes by molecular replacement. Model building was done with Coot,[88] and the structures were refined with Phenix.[89] Software used in this project was curated by SBGrid.[90]

Computational Docking. Molecular docking of the 24 compounds listed in Table 4 was performed using six separate docking grids (7K9U Chain A, 7K9U Chain B, 7K9V Chain A, 7K9V Chain B, 7K9W Chain A, and 7K9W Chain B) using the Glide docking program (Schrödinger Maestro Version 12.4.079). Proteins were treated using Schrödinger's Protein Preparation Wizard with retention of waters, optimization of hydrogen bonds, and restrained minimization converging heavy atoms to RMSD 0.3 Å. Protein structures were kept rigid during docking experiments. Docking grids were prepared using a receptor-based box centered at the native ligand for each chain. Ligands were prepared using Schrodinger's LigPrep and kept at a neutral ionization state. Docking was run at Standard precision with flexible ligands, with the docking restricted to a reference position (identified using Maximum Common Substructure) defined by the 5-((1*H*-pyrazol-5-yl)amino)benzene-1,3-diol core substructure from the native ligand of each chain. The output was set to report up to five poses per ligand, and Epik state penalties were included in the calculation of docking score. All of the output docking poses fell into one of the two possible R^2 aryl-ring rotamers as originally observed for compound **10** in the 7K9W X-ray structure. Where two R^2 aryl-ring rotamers were present, the highest-scored poses for each of the two rotamers were kept for analysis; otherwise, only the highest-scored pose for each compound into each chain was kept. Tabular results for docking each compound into each chain are reported in Supporting Table 8.

Chemistry Methods. *General Methods.* ^{1}H NMR spectra were recorded at 400 or 500 MHz at ambient temperature. ^{13}C NMR spectra were recorded at 101 or 126 MHz at ambient temperature. ^{19}F NMR spectra were recorded at 470 MHz at ambient temperature. Chemical shifts are reported in parts per million. Data for ^{1}H NMR are reported as follows: chemical shift, multiplicity (app = apparent, br = broad, s = singlet, d = doublet, t = triplet, q = quartet, sxt = sextet, hept = heptet, m = multiplet,), coupling constants, and integration. All ^{13}C NMR spectra were recorded with complete proton decoupling. Analytical thin-layer chromatography was performed using 0.25 mm silica gel 60-F plates. Silica flash chromatography was performed using prepacked columns (SI-HC, puriFlash or Premium Universal, Yamazen) on either an Interchim puriFlash450 or Yamazen Smart Flash EPCLC W-Prep2XY system. All mass-guided preparative high-performance liquid chromatography (HPLC) experiments were performed using an acetonitrile/water gradient (mobile phase modified with 0.01% formic acid) on a Waters FractionLynx system equipped with a 600 HPLC pump, a micromass ZQ quadrupole, Waters 996 diode array, and Sedere Sedex 75 ELS detectors, using an XBridge Prep C18 5 μM OBD 19 mm diameter column of either 100 or 250 mm length. Isolated yields refer to chromatographically and spectroscopically pure compounds, unless otherwise stated. All reactions were carried out in oven-dried glassware under a nitrogen atmosphere unless otherwise noted. Analytical UPLC−MS experiments were performed using a Waters Acquity (ultraperformance liquid chromatography) with a binary solvent manager, an SQ mass spectrometer, a Waters 2996 photodiode array (PDA) detector, and an evaporative light-scattering detector (ELSD). All microwave experiments were performed on a CEM Discover microwave reactor, using a sealed 10 or 35 mL vessel with temperatures monitored by an external sensor. All compounds tested in biological assays were determined to be >95% pure by UPLC−MS-ELSD analysis.

α-Cyanoketone Synthesis. α-Cyanoketones **3a**, **3c**, **3e**, **3g**, **3h**, **3i**, **3k**, and **3l** were obtained from commercial sources.

General Procedure A. To a flame-dried nitrogen-flushed round-bottom flask equipped with a magnetic stir bar were added anhydrous THF (4 mL) and *n*BuLi solution (3 mmol, 1.2 equiv). The solution was cooled to −78 °C in a dry ice/acetone bath. To the reaction flask was added a solution of MeCN (0.26 mL, 5 mmol, 2 equiv, 2 M in THF) dropwise over 2 min. The mixture was stirred for 1 h at −78 °C. A solution of methyl ester **2** (2.5 mmol, 2 M in THF) was prepared and added to the reaction flask dropwise over 2 min. The reaction was stirred at −78 °C for 30 min and then at room temperature for 2 h. The reaction was quenched with 1 M HCl (30 mL), extracted with EtOAc (3 × 50 mL), washed with brine, dried with Na_2SO_4, and concentrated under reduced pressure. Purification by silica flash chromatography (2−40% EtOAc in hexanes) afforded the desired α-cyanoketone product **3**.

*3-Oxo-3-(2-(trifluoromethyl)phenyl)propanenitrile (**3b**).* **3b** was prepared from methyl 3-(trifluoromethyl)benzoate (0.78 mL, 5 mmol) according to General Procedure A. **3b** (799 mg, 3.75 mmol, 74% yield). ^{1}H NMR (400 MHz, $CDCl_3$) δ 7.82−7.75 (m, 1H), 7.73−7.64 (m, 2H), 7.54−7.48 (m, 1H), 3.95 (s, 2H).

*3-Oxo-3-(2-(trifluoromethoxy)phenyl)propanenitrile (**3e**).* **3e** was prepared from methyl 2-(trifluoromethoxy)benzoate (1.10 g, 5 mmol) according to General Procedure A. **3e** (1.08 g, 4.73 mmol, 94% yield). ^{1}H NMR (400 MHz, $CDCl_3$) δ 7.88 (dd, J = 7.9, 1.8 Hz, 1H), 7.70−7.63 (m, 1H), 7.49−7.41 (m, 1H), 7.41−7.33 (m, 1H), 4.05 (s, 2H).

*3-Oxo-3-(3-(trifluoromethoxy)phenyl)propanenitrile (**3i**).* **3i** was prepared from methyl 3-(trifluoromethoxy)benzoate (1.10 g, 5 mmol) according to General Procedure A. **3i** (979 mg, 4.27 mmol, 85% yield). ^{1}H NMR (400 MHz, $CDCl_3$) δ 7.86−7.81 (m, 1H), 7.79−7.75 (m, 1H), 7.62−7.55 (m, 1H), 7.53−7.48 (m, 1H), 4.13 (s, 2H).

*3-(2,3-Dimethylphenyl)-3-oxopropanenitrile (**3l**).* **3l** was prepared from methyl 2,3-dimethylbenzoate (985 mg, 6 mmol) according to General Procedure A. **3l** (647 mg, 3.74 mmol, 62% yield). ^{1}H NMR (400 MHz, $CDCl_3$) δ 7.37 (d, J = 7.7 Hz, 2H), 7.21 (t, J = 7.7 Hz, 1H), 3.99 (s, 2H), 2.40 (s, 3H), 2.34 (s, 3H).

*3-(5-Fluoro-2-methylphenyl)-3-oxopropanenitrile (**3m**).* **3m** was prepared from methyl 5-fluoro-2-methyl-benzoate (1.01 g, 5 mmol) according to General Procedure A. **3m** (706 mg, 3.98 mmol, 66% yield). ^{1}H NMR (400 MHz, $CDCl_3$) δ 7.34−7.27 (m, 2H), 7.20 (td, J = 8.1, 2.6 Hz, 1H), 4.02 (s, 2H), 2.52 (s, 3H).

*3-(2-Fluoro-3-methylphenyl)-3-oxopropanenitrile (**3n**).* **3n** was prepared from methyl 2-fluoro-3-methyl-benzoate (1.01 g, 6 mmol) according to General Procedure A. **3n** (1020 mg, 5.76 mmol, 95% yield). ^{1}H NMR (400 MHz, $CDCl_3$) δ 7.76 (t, J = 7.3 Hz, 1H), 7.51−7.43 (m, 1H), 7.22−7.13 (m, 1H), 4.12−4.05 (m, 2H), 2.34 (s, 3H).

*3-(2,3-Difluorophenyl)-3-oxopropanenitrile (**3o**).* **3o** was prepared from methyl 2,3-difluorobenzoate (1.03 g, 6 mmol) according to General Procedure A. **3o** (694 mg, 3.83 mmol, 63% yield). ^{1}H NMR (400 MHz, $CDCl_3$) δ 7.76−7.68 (m, 1H), 7.53−7.43 (m, 1H), 7.30−7.21 (m, 1H), 4.11 (d, J = 2.4 Hz, 2H).

*3-(2-Methyl-3-(trifluoromethyl)phenyl)-3-oxopropanenitrile (**3p**).* **3p** was prepared from methyl 2-methyl-3-(trifluoromethyl)benzoate (501 mg, 2.3 mmol) according to General Procedure A. **3p** (449 mg, 1.98 mmol, 85% yield). ^{1}H NMR (400 MHz, $CDCl_3$) δ 7.84 (d, J = 7.9 Hz, 1H), 7.67 (d, J = 7.8 Hz, 1H), 7.44 (t, J = 7.9 Hz, 1H), 4.00 (s, 2H), 2.57 (s, 3H).

*3-(3-Chloro-2-fluorophenyl)-3-oxopropanenitrile (**3q**).* **3q** was prepared from methyl 3-chloro-2-fluoro-benzoate (471 mg, 2.5 mmol) according to General Procedure A. **3q** (443 mg, 2.24 mmol,

https://dx.doi.org/10.1021/acs.jmedchem.0c01777
J. Med. Chem. 2021, 64, 1139−1169

89% yield). ^{1}H NMR (400 MHz, $CDCl_3$) δ 7.89−7.81 (m, 1H), 7.73−7.64 (m, 1H), 7.30−7.19 (m, 1H), 4.11 (s, 2H).

*3-(2-Fluoro-3-(trifluoromethoxy)phenyl)-3-oxopropanenitrile (**3r**).* To a 20 mL scintillation vial were added 2-fluoro-3-(trifluoromethoxy)benzoic acid (504 mg, 2.25 mmol), concentrated sulfuric acid (0.2 mL), and methanol (6 mL, 0.38 M). The vial was sealed, and the reaction was heated at 75 °C for 18 h. The reaction was cooled to room temperature, diluted with ethyl acetate (50 mL), washed with saturated sodium bicarbonate solution (3 × 50 mL), washed with brine (50 mL), dried with Na_2SO_4, and concentrated under reduced pressure. The crude methyl ester was carried on without further purification and treated according to General Procedure A. **3r** (445 mg, 1.80 mmol, 80% yield). ^{1}H NMR (400 MHz, $CDCl_3$) δ 7.96−7.88 (m, 1H), 7.66−7.58 (m, 1H), 7.39−7.31 (m, 1H), 4.12 (d, J = 2.7 Hz, 2H).

*3-(2,5-Difluorophenyl)-3-oxopropanenitrile (**3s**).* **3s** was prepared from methyl 2,5-difluorobenzoate (516 mg, 3 mmol) according to General Procedure A. **3s** (248 mg, 1.37 mmol, 45% yield). ^{1}H NMR (400 MHz, $CDCl_3$) δ 7.72−7.60 (m, 1H), 7.40−7.28 (m, 1H), 7.25−7.14 (m, 1H), 4.10 (d, J = 2.7 Hz, 2H).

*3-(2-Chloro-5-fluorophenyl)-3-oxopropanenitrile (**3t**).* **3t** was prepared from methyl 2-chloro-5-fluoro-benzoate (471 mg, 2.5 mmol) according to General Procedure A. **3t** (441 mg, 2.23 mmol, 89% yield). ^{1}H NMR (400 MHz, $CDCl_3$) δ 7.53−7.45 (m, 1H), 7.42−7.36 (m, 1H), 7.31−7.22 (m, 1H), 4.19 (s, 2H).

*3-(5-Chloro-2-fluorophenyl)-3-oxopropanenitrile (**3u**).* **3u** was prepared from methyl 5-chloro-2-fluoro-benzoate (471 mg, 2.5 mmol) according to General Procedure A. **3u** (445 mg, 2.25 mmol, 90% yield). ^{1}H NMR (400 MHz, $CDCl_3$) δ 7.94 (m, 1H), 7.59 (m, 1H), 7.18 (m, 1H), 4.08 (d, J = 2.6 Hz, 2H).

*3-(2-Fluoro-5-methylphenyl)-3-oxopropanenitrile (**3v**).* **3v** was prepared from methyl 2-fluoro-5-methyl-benzoate (505 mg, 3 mmol) according to General Procedure A. **3v** (323 mg, 1.82 mmol, 60% yield). ^{1}H NMR (400 MHz, $CDCl_3$) δ 7.74 (dd, J = 7.1, 2.4 Hz, 1H), 7.45−7.34 (m, 1H), 7.08 (dd, J = 11.3, 8.4 Hz, 1H), 4.08 (dd, J = 2.5, 0.6 Hz, 2H), 2.38 (s, 3H).

*3-(2-Fluoro-5-(trifluoromethyl)phenyl)-3-oxopropanenitrile (**3w**).* **3w** was prepared from methyl 2-fluoro-5-(trifluoromethyl)benzoate (511 mg, 2.3 mmol) according to General Procedure A. **3w** (489 mg, 2.11 mmol, 91% yield). ^{1}H NMR (400 MHz, $CDCl_3$) δ 8.29−8.21 (m, 1H), 7.94−7.86 (m, 1H), 7.42−7.33 (m, 1H), 4.14−4.10 (m, 2H).

*3-(2-Fluoro-5-(trifluoromethoxy)phenyl)-3-oxopropanenitrile (**3x**).* To a 20 mL scintillation vial were added 2-fluoro-5-(trifluoromethoxy)benzoic acid (504 mg, 2.25 mmol), concentrated sulfuric acid (0.2 mL), and methanol (6 mL, 0.38 M). The vial was sealed, and the reaction was heated at 75 °C for 18 h. The reaction was cooled to room temperature, diluted with ethyl acetate (50 mL), washed with saturated sodium bicarbonate solution (3 × 50 mL), washed with brine (50 mL), dried with Na_2SO_4, and concentrated under reduced pressure. The crude methyl ester was carried on without further purification and treated according to General Procedure A. **3x** (414 mg, 1.68 mmol, 74% yield). ^{1}H NMR (400 MHz, $CDCl_3$) δ 7.83 (dd, J = 5.9, 2.9 Hz, 1H), 7.53−7.46 (m, 1H), 7.31−7.25 (m, 1H), 4.13−4.09 (m, 2H).

*3-(2,6-Difluorophenyl)-3-oxopropanenitrile (**3y**).* **3y** was prepared from methyl 2,6-difluorobenzoate (258 mg, 1.5 mmol) according to General Procedure A. **3y** (169 mg, 0.93 mmol, 62% yield). ^{1}H NMR (400 MHz, $CDCl_3$) δ 7.60−7.50 (m, 1H), 7.09−6.99 (m, 2H), 4.02−3.94 (m, 2H).

*3-(4-Chloro-2-fluorophenyl)-3-oxopropanenitrile (**3z**).* **3z** was prepared from methyl 4-chloro-2-fluoro-benzoate (1.13 g, 6 mmol) according to General Procedure A. **3z** (1.08 g, 5.46 mmol, 91% yield). ^{1}H NMR (400 MHz, $CDCl_3$) δ 8.00−7.87 (m, 1H), 7.34−7.28 (m, 1H), 7.28−7.20 (m, 1H), 4.10−4.03 (m, 2H).

*3-(2-Chloro-4-fluorophenyl)-3-oxopropanenitrile (**3aa**).* **3aa** was prepared from methyl 2-chloro-4-fluoro-benzoate (1.13 g, 6 mmol) according to General Procedure A. **3aa** (1.11 g, 5.62 mmol, 93% yield). ^{1}H NMR (400 MHz, $CDCl_3$) δ 7.79−7.70 (m, 1H), 7.25−7.19 (m, 1H), 7.16−7.06 (m, 1H), 4.15 (s, 2H).

5-Aminopyrazole Synthesis. 5-Aminopyrazoles **4a**, **4f**, and **4s** were obtained from commercial sources.

General Procedure B. To a microwave vial equipped with a magnetic stir bar were added α-cyanoketone **3** (1 equiv), methyl hydrazine (1.1 equiv), and anhydrous methanol (1 M). The vial was capped and heated in a microwave reactor maintaining 120 °C for 90 min. The vial was cooled to room temperature and the reaction was concentrated under reduced pressure. The crude residue was purified by silica flash chromatography (5-60% EtOAc in CH_2Cl_2) to afford the desired 5-aminopyrazole.

General Procedure C. To a microwave vial equipped with a magnetic stir bar were added α-cyanoketone **3** (1 equiv), *N*-alkylhydrazine hydrochloride (1.1 equiv), triethylamine (1.5 equiv), and anhydrous methanol (1 M). The vial was capped and heated in a microwave reactor maintaining 120 °C for 90 min. The vial was cooled to room temperature and the reaction was concentrated under reduced pressure. The crude residue was purified by silica flash chromatography (5−50% EtOAc in hexanes) to afford the desired 5-aminopyrazole.

*3-(2-Chlorophenyl)-1-methyl-1H-pyrazol-5-amine (**4b**).* **4b** was prepared from 2-chlorobenzoylacetonitrile **3a** (898 mg, 5 mmol, 1 equiv) according to General Procedure B. **4b** (508 mg, 2.45 mmol, 48% yield). ^{1}H NMR (400 MHz, $CDCl_3$) δ 7.76 (dd, J = 7.8, 1.8 Hz, 1H), 7.41 (dd, J = 7.8, 1.5 Hz, 1H), 7.32−7.18 (m, 2H), 6.11 (s, 1H), 3.75 (s, 3H), 3.56 (s, 2H).

*1-Methyl-3-(2-(trifluoromethyl)phenyl)-1H-pyrazol-5-amine (**4c**).* **4c** was prepared from **3b** (710 mg, 3.33 mmol, 1 equiv) according to General Procedure B. **4c** (501 mg, 2.1 mmol, 62% yield). ^{1}H NMR (400 MHz, $CDCl_3$) δ 7.74−7.60 (m, 2H), 7.54 (t, J = 7.6 Hz, 1H), 7.42 (t, J = 7.7 Hz, 1H), 5.85−5.77 (m, 1H), 3.77−3.72 (m, 3H), 3.69−3.51 (m, 2H).

*1-(tert-Butyl)-3-(o-tolyl)-1H-pyrazol-5-amine (**4d**).* **4d** was prepared from *o*-toluoylacetonitrile **3c** (239 mg, 1.5 mmol, 1 equiv) and *tert*-butylhydrazine hydrochloride (206 mg, 1.65 mmol, 1.1 equiv) according to General Procedure C. **4d** (221 mg, 0.96 mmol, 64% yield). ^{1}H NMR (400 MHz, $CDCl_3$) δ 7.56−7.51 (m, 1H), 7.37−7.30 (m, 1H), 7.23−7.12 (m, 2H), 5.77 (s, 1H), 3.56 (s, 2H), 2.51 (s, 3H), 1.69 (s, 9H).

*1-Methyl-3-(o-tolyl)-1H-pyrazol-5-amine (**4e**).* **4e** was prepared from *o*-toluoylacetonitrile **3c** (239 mg, 1.5 mmol, 1 equiv) according to General Procedure B. **4e** (135 mg, 0.72 mmol, 47% yield). ^{1}H NMR (400 MHz, $CDCl_3$) δ 7.55−7.46 (m, 1H), 7.23−7.17 (m, 3H), 5.73 (s, 1H), 3.74 (s, 3H), 3.51 (s, 2H), 2.46 (s, 3H).

*1-Isopropyl-3-(2-methoxyphenyl)-1H-pyrazol-5-amine (**4g**).* **4g** was prepared from 2-methoxybenzoylacetonitrile **3d** (175 mg, 1 mmol, 1 equiv) and isopropylhydrazine hydrochloride (122 mg, 1.1 mmol, 1.1 equiv) according to General Procedure C. **4g** (191 mg, 0.83 mmol, 82% yield). ^{1}H NMR (400 MHz, $CDCl_3$) δ 8.00−7.86 (m, 1H), 7.26−7.24 (m, 1H), 7.08−6.87 (m, 2H), 6.13 (s, 1H), 4.50−4.32 (m, 1H), 3.88 (s, 3H), 3.45 (s, 2H), 1.52 (d, J = 6.7 Hz, 6H).

*1-Cyclohexyl-3-(2-methoxyphenyl)-1H-pyrazol-5-amine (**4h**).* **4h** was prepared from 2-methoxybenzoylacetonitrile **3d** (175 mg, 1 mmol, 1 equiv) and cyclohexylhydrazine hydrochloride (166 mg, 1.1 mmol, 1.1 equiv) according to General Procedure C. **4h** (231 mg, 0.85 mmol, 84% yield). ^{1}H NMR (400 MHz, $CDCl_3$) δ 7.99−7.84 (m, 1H), 7.26−7.18 (m, 1H), 7.08−6.89 (m, 2H), 6.12 (s, 1H), 4.06−3.91 (m, 1H), 3.88 (s, 3H), 3.45 (s, 2H), 2.12−1.86 (m, 6H), 1.79−1.67 (m, 1H), 1.49−1.20 (m, 3H).

*1-Cyclopentyl-3-(2-methoxyphenyl)-1H-pyrazol-5-amine (**4i**).* **4i** was prepared from 2-methoxybenzoylacetonitrile **3d** (175 mg, 1.1 mmol, 1 equiv) and cyclopentylhydrazine hydrochloride (150 mg, 1.1 mmol, 1.1 equiv) according to General Procedure C. **4i** (204 mg, 0.79 mmol, 79% yield). ^{1}H NMR (400 MHz, $CDCl_3$) δ 8.01−7.80 (m, 1H), 7.27−7.20 (m, 2H), 7.05−6.84 (m, 2H), 6.13 (s, 1H), 4.64−4.30 (m, 1H), 3.88 (s, 3H), 3.47 (s, 2H), 2.24−2.11 (m, 2H), 2.11−1.89 (m, 4H), 1.74−1.61 (m, 2H).

*1-Isobutyl-3-(2-methoxyphenyl)-1H-pyrazol-5-amine (**4j**).* **4j** was prepared from 2-methoxybenzoylacetonitrile **3d** (175 mg, 1 mmol, 1 equiv) and isobutylhydrazine hydrochloride (137 mg, 1.1 mmol, 1.1 equiv) according to General Procedure C. **4j** (206 mg, 0.84 mmol, 84% yield). ^{1}H NMR (400 MHz, $CDCl_3$) δ 7.93−7.85 (m, 1H), 7.30−7.22

https://dx.doi.org/10.1021/acs.jmedchem.0c01777
J. Med. Chem. 2021, 64, 1139−1169

(m, 1H), 7.05−6.90 (m, 2H), 6.12 (s, 1H), 3.88 (s, 3H), 3.80 (d, J = 7.4 Hz, 2H), 3.44 (s, 2H), 2.36−2.19 (m, 1H), 0.97 (d, J = 6.6 Hz, 6H).

*1-(tert-Butyl)-3-(2-methoxyphenyl)-1H-pyrazol-5-amine (**4k**).* **4k** was prepared from 2-methoxybenzoylacetonitrile **3d** (168 mg, 0.96 mmol, 1 equiv) and *tert*-butylhydrazine hydrochloride (131 mg, 1.05 mmol, 1.1 equiv) according to General Procedure C. **4k** (193 mg, 0.79 mmol, 81% yield). ^{1}H NMR (400 MHz, $CDCl_3$) δ 8.01−7.92 (m, 1H), 7.25−7.19 (m, 1H), 7.05−6.95 (m, 1H), 6.92 (d, J = 8.3 Hz, 1H), 6.18 (s, 1H), 3.88 (s, 3H), 3.56 (s, 2H), 1.69 (s, 9H).

*1-Methyl-3-(2-(trifluoromethoxy)phenyl)-1H-pyrazol-5-amine (**4l**).* **4l** was prepared from **3e** (458 mg, 2 mmol, 1 equiv) according to General Procedure B. **4l** (348 mg, 1.35 mmol, 67% yield). ^{1}H NMR (400 MHz, $CDCl_3$) δ 8.03−7.96 (m, 1H), 7.33−7.27 (m, 3H), 6.03 (s, 1H), 3.74 (s, 3H), 3.54 (s, 2H).

*1-(tert-Butyl)-3-(2-(trifluoromethoxy)phenyl)-1H-pyrazol-5-amine (**4m**).* **4m** was prepared from **3e** (343 mg, 1.5 mmol, 1 equiv) and *tert*-butylhydrazine hydrochloride (206 mg, 1.65 mmol, 1.1 equiv) according to General Procedure C. **4m** (303 mg, 1.01 mmol, 67% yield). ^{1}H NMR (400 MHz, $CDCl_3$) δ 8.10−8.00 (m, 1H), 7.37−7.22 (m, 4H), 6.06 (s, 1H), 3.56 (s, 2H), 1.74−1.65 (m, 9H).

*1-(tert-Butyl)-3-(3-methoxyphenyl)-1H-pyrazol-5-amine (**4n**).* **4n** was prepared from 3-methoxybenzoylacetonitrile **3f** (219 mg, 1.25 mmol, 1 equiv) and *tert*-butylhydrazine hydrochloride (171 mg, 1.38 mmol, 1.1 equiv) according to General Procedure C. **4n** (288 mg, 1.17 mmol, 93% yield). ^{1}H NMR (400 MHz, $CDCl_3$) δ 7.35−7.29 (m, 2H), 7.28−7.21 (m, 1H), 6.84−6.76 (m, 1H), 5.89 (s, 1H), 3.85 (s, 3H), 3.59 (s, 2H), 1.75−1.59 (m, 9H).

*1-(tert-Butyl)-3-(m-tolyl)-1H-pyrazol-5-amine (**4o**).* **4o** was prepared from *m*-toluoylacetonitrile **3g** (199 mg, 1.25 mmol, 1 equiv) and *tert*-butylhydrazine hydrochloride (171 mg, 1.38 mmol, 1.1 equiv) according to General Procedure C. **4o** (276 mg, 1.20 mmol, 96% yield). ^{1}H NMR (400 MHz, $CDCl_3$) δ 7.62−7.57 (m, 1H), 7.56−7.48 (m, 1H), 7.23 (t, J = 7.6 Hz, 1H), 7.10−7.01 (m, 1H), 5.89 (s, 1H), 3.58 (s, 2H), 2.37 (s, 3H), 1.69 (s, 9H).

*1-(tert-Butyl)-3-(3-(trifluoromethyl)phenyl)-1H-pyrazol-5-amine (**4p**).* **4p** was prepared from 3-(trifluoromethyl)benzoylacetonitrile **3h** (266 mg, 1.25 mmol, 1 equiv) and *tert*-butylhydrazine hydrochloride (171 mg, 1.38 mmol, 1.1 equiv) according to General Procedure C. **4p** (255 mg, 0.90 mmol, 71% yield). ^{1}H NMR (400 MHz, $CDCl_3$) δ 8.04−7.95 (m, 1H), 7.93−7.85 (m, 1H), 7.52−7.39 (m, 2H), 5.93 (s, 1H), 3.63 (s, 2H), 1.70 (s, 9H).

*1-Methyl-3-(3-(trifluoromethoxy)phenyl)-1H-pyrazol-5-amine (**4q**).* **4q** was prepared from **3i** (344 mg, 1.5 mmol, 1 equiv) according to General Procedure B. **4q** (246 mg, 0.96 mmol, 63% yield). ^{1}H NMR (400 MHz, $CDCl_3$) δ 7.70−7.60 (m, 1H), 7.60−7.55 (m, 1H), 7.37 (t, J = 8.0 Hz, 1H), 7.15−7.06 (m, 1H), 5.86 (s, 1H), 3.72 (s, 3H), 3.57 (s, 2H).

*1-(tert-Butyl)-3-(3-(trifluoromethoxy)phenyl)-1H-pyrazol-5-amine (**4r**).* **4r** was prepared from **3i** (344 mg, 1.65 mmol, 1 equiv) and *tert*-butylhydrazine hydrochloride (206 mg, 1.65 mmol, 1.1 equiv) according to General Procedure C. **4r** (248 mg, 0.83 mmol, 55% yield). ^{1}H NMR (400 MHz, $CDCl_3$) δ 7.74−7.63 (m, 1H), 7.62−7.57 (m, 1H), 7.35 (t, J = 8.0 Hz, 1H), 7.12−7.04 (m, 1H), 5.89 (s, 1H), 3.60 (s, 2H), 1.69 (s, 9H).

*1-(tert-Butyl)-3-(3-fluorophenyl)-1H-pyrazol-5-amine (**4t**).* **4t** was prepared from 3-fluorobenzoylacetonitrile **3j** (245 mg, 1.5 mmol, 1 equiv) and *tert*-butylhydrazine hydrochloride (206 mg, 1.65 mmol, 1.1 equiv) according to General Procedure C. **4t** (222 mg, 0.95 mmol, 63% yield). ^{1}H NMR (400 MHz, $CDCl_3$) δ 7.54−7.40 (m, 2H), 7.35−7.25 (m, 1H), 6.98−6.88 (m, 1H), 5.89 (s, 1H), 3.61 (s, 2H), 1.69 (s, 9H).

*3-(3-Chlorophenyl)-1-methyl-1H-pyrazol-5-amine (**4u**).* **4u** was prepared from 3-chlorobenzoylacetonitrile **3k** (898 mg, 5 mmol, 1 equiv) according to General Procedure B. **4u** (614 mg, 2.96 mmol, 59% yield). ^{1}H NMR (400 MHz, $CDCl_3$) δ 7.72 (s, 1H), 7.61 (d, J = 7.6 Hz, 1H), 7.33−7.21 (m, 2H), 5.86 (s, 1H), 3.75 (s, 3H), 3.60 (s, 2H).

*1-(tert-Butyl)-3-(3-chlorophenyl)-1H-pyrazol-5-amine (**4v**).* **4v** was prepared from 3-chorobenzoylacetonitrile **3k** (224 mg, 1.25 mmol, 1 equiv) and *tert*-butylhydrazine hydrochloride (171 mg, 1.38 mmol, 1.1 equiv) according to General Procedure C. **4v** (232 mg, 0.93 mmol, 74% yield). ^{1}H NMR (400 MHz, $CDCl_3$) δ 7.77−7.73 (m, 1H), 7.64−7.58 (m, 1H), 7.31−7.24 (m, 1H), 7.24−7.17 (m, 1H), 5.88 (s, 1H), 3.61 (s, 2H), 1.69 (s, 9H).

*3-(3-Chlorophenyl)-1-cyclohexyl-1H-pyrazol-5-amine (**4w**).* **4w** was prepared from 3-chlorobenzoylacetonitrile **3k** (269 mg, 1.5 mmol, 1 equiv) and cyclohexylhydrazine hydrochloride (226 mg, 1.5 mmol, 1 equiv) according to General Procedure C. **4w** (328 mg, 1.19 mmol, 79% yield). ^{1}H NMR (400 MHz, $CDCl_3$) δ 7.72 (t, J = 2.0 Hz, 1H), 7.61−7.54 (m, 1H), 7.26−7.20 (m, 1H), 7.20−7.15 (m, 1H), 5.81 (s, 1H), 3.95−3.81 (m, 1H), 3.52 (s, 2H), 2.00−1.82 (m, 6H), 1.70 (d, J = 12.0 Hz, 1H), 1.50−1.24 (m, 3H).

*3-(2,3-Dimethylphenyl)-1-methyl-1H-pyrazol-5-amine (**4x**).* **4x** was prepared from **3l** (350 mg, 2 mmol, 1 equiv) according to General Procedure B. **4x** (197 mg, 0.98 mmol, 48% yield). ^{1}H NMR (400 MHz, $CDCl_3$) δ 7.32−7.26 (m, 2H), 7.13−7.08 (m, 2H), 5.66 (s, 1H), 3.73 (s, 3H), 3.51 (s, 2H), 2.33 (s, 3H), 2.31 (s, 3H).

*3-(5-Fluoro-2-methylphenyl)-1-methyl-1H-pyrazol-5-amine (**4y**).* **4y** was prepared from **3m** (298 mg, 1.68 mmol, 1 equiv) according to General Procedure B. **4y** (194 mg, 0.95 mmol, 56% yield). ^{1}H NMR (400 MHz, $CDCl_3$) δ 7.32−7.22 (m, 1H), 7.18−7.10 (m, 1H), 6.93−6.84 (m, 1H), 5.72 (s, 1H), 3.72 (s, 3H), 3.54 (s, 2H), 2.41 (s, 3H).

*3-(2-Fluoro-3-methylphenyl)-1-methyl-1H-pyrazol-5-amine (**4z**).* **4z** was prepared from **3n** (461 mg, 2.6 mmol, 1 equiv) according to General Procedure B. **4z** (299 mg, 1.46 mmol, 55% yield). ^{1}H NMR (400 MHz, $CDCl_3$) δ 7.77−7.68 (m, 1H), 7.13−6.97 (m, 2H), 6.07−5.93 (m, 1H), 3.74 (s, 3H), 3.56 (s, 2H), 2.33−2.28 (m, 3H).

*3-(2,3-Difluorophenyl)-1-methyl-1H-pyrazol-5-amine (**4aa**).* **4aa** was prepared from **3o** (221 mg, 1.22 mmol, 1 equiv) according to General Procedure B. **4aa** (142 mg, 0.68 mmol, 55% yield). ^{1}H NMR (400 MHz, $CDCl_3$) δ 7.74−7.62 (m, 1H), 7.11−6.99 (m, 2H), 6.05 (d, J = 4.0 Hz, 1H), 3.75 (s, 3H), 3.55 (s, 2H).

*1-Methyl-3-(2-methyl-3-(trifluoromethyl)phenyl)-1H-pyrazol-5-amine (**4ab**).* **4ab** was prepared from **3p** (284 mg, 1.25 mmol, 1 equiv) according to General Procedure B. **4ab** (138 mg, 0.54 mmol, 43% yield). ^{1}H NMR (400 MHz, $CDCl_3$) δ 7.65−7.57 (m, 2H), 7.32−7.27 (m, 1H), 5.68 (s, 1H), 3.79−3.75 (m, 3H), 3.66 (s, 2H), 2.51 (d, J = 1.8 Hz, 3H).

*3-(3-Chloro-2-fluorophenyl)-1-methyl-1H-pyrazol-5-amine (**4ac**).* **4ac** was prepared from **3q** (247 mg, 1.25 mmol, 1 equiv) according to General Procedure B. **4ac** (180 mg, 0.80 mmol, 63% yield). ^{1}H NMR (400 MHz, $CDCl_3$) δ 7.86 (t, J = 7.4 Hz, 1H), 7.30 (t, J = 7.3 Hz, 1H), 7.08 (m, 1H), 6.05 (d, J = 4.2 Hz, 1H), 3.76 (s, 3H), 3.71−3.49 (m, 2H).

*3-(2-Fluoro-3-(trifluoromethoxy)phenyl)-1-methyl-1H-pyrazol-5-amine (**4ad**).* **4ad** was prepared from **3r** (247 mg, 1 mmol, 1 equiv) according to General Procedure B. **4ad** (202 mg, 0.73 mmol, 73% yield). ^{1}H NMR (400 MHz, $CDCl_3$) δ 7.92−7.85 (m, 1H), 7.25−7.09 (m, 2H), 6.09−5.99 (m, 1H), 3.74 (s, 3H), 3.60 (s, 2H).

*3-(2,5-Difluorophenyl)-1-methyl-1H-pyrazol-5-amine (**4ae**).* **4ae** was prepared from **3s** (248 mg, 1.37 mmol, 1 equiv) according to General Procedure B. **4ae** (193 mg, 0.92 mmol, 67% yield). ^{1}H NMR (400 MHz, $CDCl_3$) δ 7.68−7.59 (m, 1H), 7.12−6.98 (m, 1H), 6.98−6.82 (m, 1H), 6.04 (d, J = 4.1 Hz, 1H), 3.74 (s, 3H), 3.54 (s, 2H).

*3-(2-Chloro-5-fluorophenyl)-1-methyl-1H-pyrazol-5-amine (**4af**).* **4af** was prepared from **3t** (247 mg, 1.25 mmol, 1 equiv) according to General Procedure B. **4af** (159 mg, 0.71 mmol, 56% yield). ^{1}H NMR (400 MHz, $CDCl_3$) δ 7.57−7.49 (m, 1H), 7.41−7.31 (m, 1H), 6.98−6.85 (m, 1H), 6.15 (s, 1H), 3.74 (s, 3H), 3.69−3.43 (m, 2H).

*3-(5-Chloro-2-fluorophenyl)-1-methyl-1H-pyrazol-5-amine (**4ag**).* **4ag** was prepared from **3u** (247 mg, 1.25 mmol, 1 equiv) according to General Procedure B. **4ag** (183 mg, 0.81 mmol, 64% yield). ^{1}H NMR (400 MHz, $CDCl_3$) δ 7.98−7.88 (m, 1H), 7.20−7.13 (m, 1H), 7.08−6.93 (m, 1H), 6.03 (d, J = 4.1 Hz, 1H), 3.74 (s, 3H), 3.53 (s, 2H).

*3-(2-Fluoro-5-methylphenyl)-1-methyl-1H-pyrazol-5-amine (**4ah**).* **4ah** was prepared from **3v** (323 mg, 1.82 mmol, 1 equiv) according to General Procedure B. **4ah** (271 mg, 1.32 mmol, 72% yield). ^{1}H NMR (400 MHz, $CDCl_3$) δ 7.81−7.64 (m, 1H), 7.14−6.80 (m, 2H), 6.13−5.91 (m, 1H), 3.81−3.66 (m, 3H), 3.66−3.46 (m, 2H), 2.33 (s, 3H).

https://dx.doi.org/10.1021/acs.jmedchem.0c01777
J. Med. Chem. 2021, 64, 1139−1169

*3-(2-Fluoro-5-(trifluoromethyl)phenyl)-1-methyl-1H-pyrazol-5-amine (**4ai**).* **4ai** was prepared from **3w** (289 mg, 1.25 mmol, 1 equiv) according to General Procedure B. **4ai** (109 mg, 0.42 mmol, 33% yield). ^{1}H NMR (400 MHz, $CDCl_3$) δ 8.33−8.24 (m, 1H), 7.54−7.43 (m, 1H), 7.23−7.13 (m, 1H), 6.10−6.00 (m, 1H), 3.78 (s, 3H), 3.69 (s, 2H).

*3-(2-Fluoro-5-(trifluoromethoxy)phenyl)-1-methyl-1H-pyrazol-5-amine (**4aj**).* **4aj** was prepared from **3x** (247 mg, 1 mmol, 1 equiv) according to General Procedure B. **4aj** (163 mg, 0.59 mmol, 59% yield). ^{1}H NMR (400 MHz, $CDCl_3$) δ 7.86−7.81 (m, 1H), 7.11−7.05 (m, 2H), 6.04 (dd, J = 4.1, 0.7 Hz, 1H), 3.75 (s, 3H), 3.59 (s, 2H).

*3-(2,6-Difluorophenyl)-1-methyl-1H-pyrazol-5-amine (**4ak**).* **4ak** was prepared from **3y** (169 mg, 0.93 mmol, 1 equiv) according to General Procedure B. **4ak** (48 mg, 0.23 mmol, 24% yield). ^{1}H NMR (400 MHz, $CDCl_3$) δ 7.26−7.15 (m, 1H), 6.94 (t, J = 8.3 Hz, 2H), 5.90 (d, J = 1.9 Hz, 1H), 3.77 (s, 3H), 3.53 (s, 2H).

*3-(4-Chloro-2-fluorophenyl)-1-methyl-1H-pyrazol-5-amine (**4al**).* **4al** was prepared from **3z** (296 mg, 1.5 mmol, 1 equiv) according to General Procedure B. **4al** (172 mg, 0.76 mmol, 50% yield). ^{1}H NMR (400 MHz, $CDCl_3$) δ 7.90 (t, J = 8.3 Hz, 1H), 7.17−7.08 (m, 2H), 6.01 (d, J = 4.1 Hz, 1H), 3.75 (s, 3H), 3.70−3.51 (m, 2H).

*3-(2-Chloro-4-fluorophenyl)-1-methyl-1H-pyrazol-5-amine (**4am**).* **4am** was prepared from **3aa** (296 mg, 1.5 mmol, 1 equiv) according to General Procedure B. **4am** (135 mg, 0.60 mmol, 39% yield). ^{1}H NMR (400 MHz, $CDCl_3$) δ 7.80−7.69 (m, 1H), 7.21−7.09 (m, 1H), 7.09−6.95 (m, 1H), 6.06 (s, 1H), 3.74 (s, 3H), 3.60 (s, 2H).

*1-(tert-Butyl)-3-(2,3-dimethylphenyl)-1H-pyrazol-5-amine (**4ao**).* **4ao** was prepared from **3l** (260 mg, 1.5 mmol, 1 equiv) and *tert*-butylhydrazine hydrochloride (206 mg, 1.65 mmol, 1.1 equiv) according to General Procedure C. **4ao** (122 mg, 0.50 mmol, 33% yield). ^{1}H NMR (400 MHz, $CDCl_3$) δ 7.33−7.27 (m, 1H), 7.12−7.03 (m, 2H), 5.69 (s, 1H), 3.60 (s, 2H), 2.37 (s, 3H), 2.30 (s, 3H), 1.69 (s, 9H).

*3-(5-Fluoro-2-methylphenyl)-1-isopropyl-1H-pyrazol-5-amine (**4ap**).* **4ap** was prepared from **3m** (177 mg, 1 mmol, 1 equiv) and isopropylhydrazine hydrochloride (82 mg, 1.1 mmol, 1.1 equiv) according to General Procedure C. **4ap** (93 mg, 0.40 mmol, 40% yield). ^{1}H NMR (400 MHz, $CDCl_3$) δ 7.30−7.23 (m, 1H), 7.23−7.08 (m, 1H), 6.92−6.83 (m, 1H), 5.72 (s, 1H), 4.51−4.32 (m, 1H), 3.65 (s, 2H), 2.43 (s, 3H), 1.51 (d, J = 6.6 Hz, 6H).

*1-(tert-Butyl)-3-(5-fluoro-2-methylphenyl)-1H-pyrazol-5-amine (**4aq**).* **4aq** was prepared from **3m** (266 mg, 1.5 mmol, 1 equiv) and *tert*-butylhydrazine hydrochloride (206 mg, 1.65 mmol, 1.1 equiv) according to General Procedure C. **4aq** (118 mg, 0.48 mmol, 31% yield). ^{1}H NMR (400 MHz, $CDCl_3$) δ 7.32−7.27 (m, 1H), 7.17−7.10 (m, 1H), 6.89−6.79 (m, 1H), 5.78 (s, 1H), 3.58 (s, 2H), 2.46 (s, 3H), 1.68 (s, 9H).

*1-Cyclopentyl-3-(5-fluoro-2-methylphenyl)-1H-pyrazol-5-amine (**4ar**).* **4ar** was prepared from **3m** (177 mg, 1 mmol, 1 equiv) and cyclopentylhydrazine hydrochloride (150 mg, 1.1 mmol, 1.1 equiv) according to General Procedure C. **4ar** (202 mg, 0.78 mmol, 78% yield). ^{1}H NMR (400 MHz, $CDCl_3$) δ 7.34−7.24 (m, 1H), 7.18−7.10 (m, 1H), 6.88 (m, 1H), 5.75 (s, 1H), 4.67−4.53 (m, 1H), 2.43 (s, 3H), 2.23−1.87 (m, 6H), 1.67 (m, 2H).

*1-Cyclohexyl-3-(5-fluoro-2-methylphenyl)-1H-pyrazol-5-amine (**4as**).* **4as** was prepared from **3m** (177 mg, 1 mmol, 1 equiv) and cyclohexylhydrazine hydrochloride (166 mg, 1.1 mmol, 1.1 equiv) according to General Procedure C. **4as** (185 mg, 0.68 mmol, 68% yield). ^{1}H NMR (400 MHz, $CDCl_3$) δ 7.29−7.21 (m, 1H), 7.18−7.08 (m, 1H), 6.93−6.83 (m, 1H), 5.75−5.70 (m, 1H), 4.08−3.92 (m, 1H), 3.77 (s, 2H), 2.42 (s, 3H), 2.04−1.85 (m, 7H), 1.71 (d, J = 12.6 Hz, 1H), 1.50−1.29 (m, 2H).

*3-(2-Fluoro-3-methylphenyl)-1-isopropyl-1H-pyrazol-5-amine (**4at**).* **4at** was prepared from **3n** (177 mg, 1 mmol, 1 equiv) and isopropylhydrazine hydrochloride (82 mg, 1.1 mmol, 1.1 equiv) according to General Procedure C. **4at** (149 mg, 0.64 mmol, 64% yield). ^{1}H NMR (400 MHz, $CDCl_3$) δ 7.83 (td, J = 7.4, 2.0 Hz, 1H), 7.13−6.99 (m, 2H), 6.03 (d, J = 4.1 Hz, 1H), 4.46 (hept, J = 6.6 Hz, 1H), 3.73 (s, 1H), 2.30 (d, J = 2.3 Hz, 3H), 1.52 (d, J = 6.6 Hz, 6H).

*1-(tert-Butyl)-3-(2-fluoro-3-methylphenyl)-1H-pyrazol-5-amine (**4au**).* **4au** was prepared from **3n** (266 mg, 1.5 mmol, 1 equiv) and *tert*-butylhydrazine hydrochloride (206 mg, 1.65 mmol, 1.1 equiv) according to General Procedure C. **4au** (238 mg, 0.96 mmol, 64% yield). ^{1}H NMR (400 MHz, $CDCl_3$) δ 7.86−7.78 (m, 1H), 7.11−6.94 (m, 2H), 6.10−5.97 (m, 1H), 3.55 (s, 2H), 2.33−2.25 (m, 3H), 1.69 (s, 9H).

*1-Cyclopentyl-3-(2-fluoro-3-methylphenyl)-1H-pyrazol-5-amine (**4av**).* **4av** was prepared from **3n** (177 mg, 1 mmol, 1 equiv) and cyclopentylhydrazine hydrochloride (150 mg, 1.1 mmol, 1.1 equiv) according to General Procedure C. **4av** (208 mg, 0.80 mmol, 80% yield). ^{1}H NMR (400 MHz, $CDCl_3$) δ 7.91−7.79 (m, 1H), 7.20−6.99 (m, 2H), 6.09−6.02 (m, 1H), 4.74−4.49 (m, 1H), 2.37−2.23 (m, 3H), 2.24−1.88 (m, 6H), 1.80−1.56 (m, 2H).

*1-Cyclohexyl-3-(2-fluoro-3-methylphenyl)-1H-pyrazol-5-amine (**4aw**).* **4aw** was prepared from **3n** (266 mg, 1.5 mmol, 1 equiv) and cyclohexylhydrazine hydrochloride (226 mg, 1 mmol, 1 equiv) according to General Procedure C. **4aw** (322 mg, 1.18 mmol, 78% yield). ^{1}H NMR (400 MHz, $CDCl_3$) δ 7.82−7.72 (m, 1H), 7.10−6.97 (m, 2H), 6.02 (d, J = 4.2 Hz, 1H), 4.02−3.86 (m, 1H), 3.47 (s, 2H), 2.30 (d, J = 2.4 Hz, 3H), 2.07−1.83 (m, 6H), 1.78−1.68 (m, 1H), 1.49−1.22 (m, 3H).

*3-(2,3-Difluorophenyl)-1-isopropyl-1H-pyrazol-5-amine (**4ax**).* **4ax** was prepared from **3o** (181 mg, 1 mmol, 1 equiv) and isopropylhydrazine hydrochloride (82 mg, 1.1 mmol, 1.1 equiv) according to General Procedure C. **4ax** (128 mg, 0.54 mmol, 54% yield). ^{1}H NMR (400 MHz, $CDCl_3$) δ 7.84−7.74 (m, 1H), 7.14−6.99 (m, 2H), 6.08−6.02 (m, 1H), 4.52−4.37 (m, 1H), 3.76−3.55 (m, 2H), 1.52 (d, J = 6.4 Hz, 6H).

*1-(tert-Butyl)-3-(2,3-difluorophenyl)-1H-pyrazol-5-amine (**4ay**).* **4ay** was prepared from **3o** (272 mg, 1.5 mmol, 1 equiv) and *tert*-butylhydrazine hydrochloride (206 mg, 1.65 mmol, 1.1 equiv) according to General Procedure C. **4ay** (244 mg, 0.97 mmol, 64% yield). ^{1}H NMR (400 MHz, $CDCl_3$) δ 7.83−7.71 (m, 1H), 7.13−6.96 (m, 2H), 6.12−6.04 (m, 1H), 3.78−3.51 (m, 2H), 1.69 (s, 9H).

*1-Cyclopentyl-3-(2,3-difluorophenyl)-1H-pyrazol-5-amine (**4az**).* **4az** was prepared from **3o** (181 mg, 1 mmol, 1 equiv) and cyclopentylhydrazine hydrochloride (150 mg, 1.1 mmol, 1.1 equiv) according to General Procedure C. **4az** (193 mg, 0.73 mmol, 73% yield). ^{1}H NMR (400 MHz, $CDCl_3$) δ 7.82−7.73 (m, 1H), 7.11−6.98 (m, 2H), 6.05 (d, J = 4.1 Hz, 1H), 4.55 (p, J = 7.4 Hz, 1H), 3.85−3.53 (m, 2H), 2.27−1.91 (m, 6H), 1.78−1.59 (m, 2H).

*1-Cyclohexyl-3-(2,3-difluorophenyl)-1H-pyrazol-5-amine (**4bb**).* **4bb** was prepared from **3o** (181 mg, 1.5 mmol, 1 equiv) and cyclohexylhydrazine hydrochloride (166 mg, 1.1 mmol, 1.1 equiv) according to General Procedure C. **4bb** (237 mg, 0.85 mmol, 85% yield). ^{1}H NMR (400 MHz, $CDCl_3$) δ 7.92−7.83 (m, 1H), 7.10 (t, J = 6.1 Hz, 2H), 6.10 (d, J = 3.8 Hz, 1H), 4.24−4.04 (m, 1H), 2.22−2.05 (m, 1H), 2.03−1.86 (m, 5H), 1.74−1.66 (m, 1H), 1.51−1.26 (m, 3H).

Recorcylate Amide Bromide Synthesis. *2-Bromo-4,6-dimethoxybenzaldehyde (**S1**).* To a 250 mL round-bottom flask equipped with a magnetic stir bar were added 3,5-dimethoxybromobenzene (10.0 g, 46.1 mmol) and DMF (23 mL, 2 M). The mixture was cooled to 0 °C, and $POCl_3$ (12.8 mL, 138 mmol, 3 equiv) was added dropwise over 5 min. The reaction was warmed to room temperature and then heated to 90 °C for 6 h. The reaction was cooled to room temperature and poured into ice water (200 mL). The reaction was quenched with a slow addition of KOH (55 g) to reach pH 14. The slurry was warmed to room temperature and stirred for 16 h. The aqueous phase was extracted with Et_2O (3 × 200 mL), and the combined organic extracts were washed with water (3 × 100 mL) and brine (150 mL), dried with Na_2SO_4, and concentrated under reduced pressure. No further purification was required affording aldehyde **S1** as a brown solid (10.4 g, 92% yield). ^{1}H NMR (400 MHz, $CDCl_3$) δ 10.31 (s, 1H), 6.78 (d, J = 2.2 Hz, 1H), 6.44 (d, J = 2.2 Hz, 1H), 3.95−3.80 (m, 6H). UPLC/MS [M + H] = 245.359, t_R = 1.41 min.

*2-Bromo-4,6-dihydroxybenzaldehyde (**6**).* To a flamed-dried 250 mL round-bottom flask equipped with a magnetic stir bar was added 2-bromo-4,6-dimethoxybenzaldehyde **S1** (10 g, 40.8 mmol). The flask was fitted with a rubber septum, evacuated, and backfilled with N_2.

https://dx.doi.org/10.1021/acs.jmedchem.0c01777
J. Med. Chem. 2021, 64, 1139−1169

Anhydrous CH_2Cl_2 (150 mL, 0.27 M) was added, and the mixture was cooled to 0 °C. In a separate round-bottom flask, a solution of BBr_3 (11.6 mL, 122 mmol, 3 equiv) in anhydrous CH_2Cl_2 (30 mL, 4 M) was prepared. The BBr_3 solution was added dropwise via a cannula over 15 min. The reaction was slowly warmed to room temperature as the ice bath melted and stirred for 18 h. The reaction was poured into ice water (300 mL), extracted with EtOAc (3 × 200 mL), washed with brine (300 mL), dried with Na_2SO_4, and concentrated under reduced pressure. The crude product was purified by silica flash chromatography (5−50% acetone in hexanes) affording aldehyde **6** (6.61 g, 75% yield) as a light purple solid. ^{1}H NMR (400 MHz, DMSO-d_6) δ 12.19 (s, 1H), 9.97 (s, 1H), 6.71 (d, J = 2.1 Hz, 1H), 6.30 (d, J = 2.0 Hz, 1H). UPLC/MS [M + H] = 216.956, t_R = 1.29 min.

*2,4-Bis(benzyloxy)-6-bromobenzaldehyde (**7**).* To a 200 mL round-bottom flask equipped with a magnetic stir bar were added 2-bromo-4,6-dihydroxybenzaldehyde **6** (3.33 g, 15.3 mmol), K_2CO_3 (5.3 g, 38.3 mmol, 2.5 equiv), benzyl bromide (4.6 mL, 38.3 mmol, 2.5 equiv), and MeCN (45 mL, 0.33 M). The flask was fitted with a reflux condenser, and the reaction was heated at reflux in a 90 °C oil bath for 16 h. The reaction was cooled to room temperature, and the salts were removed by vacuum filtration and washed with EtOAc (100 mL). The filtrate was concentrated under reduced pressure and purified by silica flash chromatography (2−40% EtOAc in hexanes) affording aldehyde **7** (5.0 g, 82% yield) as a colorless solid. ^{1}H NMR (400 MHz, $CDCl_3$) δ 10.39 (s, 1H), 7.49−7.29 (m, 10H), 6.89 (d, J = 2.1 Hz, 1H), 6.57 (d, J = 2.2 Hz, 1H), 5.13 (s, 2H), 5.07 (s, 2H); ^{13}C NMR (101 MHz, $CDCl_3$) δ 188.86, 163.47, 162.92, 135.66, 135.43, 128.94, 128.87, 128.71, 128.40, 127.76, 127.18, 126.64, 117.63, 113.07, 100.33, 70.96, 70.76. UPLC/MS [M + H] = 397.337, t_R = 2.30 min.

General Procedure D. To a 100 mL round-bottom flask equipped with a magnetic stir bar were added 2,4-bis(benzyloxy)-6-bromobenzaldehyde **7** (1.59 g, 4 mmol), *t*-BuOH (12 mL), and THF (10 mL). In a separate flask, sodium chlorite (1.09 g, 12 mmol, 3 equiv) and sodium monobasic phosphate monohydrate (4.14 g, 30 mmol, 7.5 equiv) were dissolved in H_2O (10 mL). The aqueous solution was added to the reaction portion-wise over 2 min, turning the reaction bright yellow. 2-Methyl-2-butene (5.1 mL, 48 mmol, 12 equiv) was added, and the reaction was stirred for 30 min until the yellow color dissipated and the reaction turned colorless again. The reaction was quenched with 3 M HCl (30 mL) and extracted with EtOAc (3 × 50 mL). The combined organic extracts were washed with saturated NH_4Cl solution (2 × 50 mL), washed with brine (50 mL), dried with Na_2SO_4, and concentrated under reduced pressure. The resulting benzoic acid was immediately used without purification.

In a 100 mL round-bottom flask equipped with a magnetic stir bar, the crude benzoic acid was dissolved in CH_2Cl_2 (12 mL) and THF (12 mL). Amine (4.40 mmol, 1.1 equiv), *N*,*N*-diisopropylethylamine (DIPEA, 1.74 mL, 10 mmol, 2.5 equiv), and HATU (1.83 g, 4.80 mmol, 1.2 equiv) were added. The reaction was stirred at room temperature for 3 h. The reaction was quenched with saturated $NaHCO_3$ solution (30 mL), extracted with CH_2Cl_2 (3 × 50 mL), washed with brine (75 mL), dried with Na_2SO_4, and concentrated under reduced pressure. The crude product was purified by silica flash chromatography (5−60% EtOAc in hexane) to afford the desired amide **8**.

*(2,4-Bis(benzyloxy)-6-bromophenyl)(isoindolin-2-yl)methanone (**8a**).* **8a** was prepared according to General Procedure D from isoindoline hydrochloride (685 mg, 4.40 mmol, 1.1 equiv). **8a** (1.67 g, 3.24 mmol) was obtained in 81% yield as a colorless solid. ^{1}H NMR (400 MHz, $CDCl_3$) δ 7.48−7.22 (m, 13H), 7.15 (d, J = 7.3 Hz, 1H), 6.85 (d, J = 2.1 Hz, 1H), 6.59 (d, J = 2.1 Hz, 1H), 5.16−5.05 (m, 2H), 5.02 (d, J = 7.1 Hz, 4H), 4.68−4.45 (m, 2H); ^{13}C NMR (101 MHz, $CDCl_3$) δ 165.90, 160.46, 156.51, 136.54, 136.47, 136.16, 136.03, 128.86, 128.70, 128.48, 128.12, 127.86, 127.71, 127.62, 127.04, 123.27, 122.74, 122.19, 120.39, 110.63, 100.80, 70.75, 70.63, 53.32, 51.89. UPLC/MS [M + H] = 514.231, t_R = 2.10 min.

*(2,4-Bis(benzyloxy)-6-bromophenyl)(4-fluoroisoindolin-2-yl)-methanone (**8b**).* **8b** was prepared according to General Procedure D from 4-fluoroisoindoline (290 mg, 2.11 mmol). **8b** (585 mg, 1.10 mmol) was obtained in 57% yield. ^{1}H NMR (400 MHz, $CDCl_3$) δ 7.47−7.21 (m, 11H), 7.15−6.87 (m, 2H), 6.86−6.80 (m, 1H), 6.68−6.54 (m, 1H), 5.09−4.99 (m, 6H), 4.67−4.40 (m, 2H). UPLC/MS [M + H] = 532.195, t_R = 2.09 min.

*(2,4-Bis(benzyloxy)-6-bromophenyl)(5-fluoroisoindolin-2-yl)-methanone (**8c**).* **8c** was prepared according to General Procedure D from 5-fluoroisoindoline hydrochloride (382 mg, 2.2 mmol). **8c** (917 mg, 1.72 mmol) was obtained in 86% yield.

^{1}H NMR (400 MHz, $CDCl_3$) δ 7.55−7.32 (m, 5H), 7.33−7.19 (m, 6H), 7.13−6.92 (m, 2H), 6.87−6.78 (m, 1H), 6.58 (dd, J = 2.2, 1.2 Hz, 1H), 5.09−4.90 (m, 6H), 4.60−4.38 (m, 2H). UPLC/MS [M + H] = 532.438, t_R = 2.08 min.

RAP Synthesis. *General Procedure E.* **E1a**: To a flame-dried 2D vial equipped with a magnetic stir bar was added resorcylate amide bromide **8a−c** (0.15 mmol, 1 equiv), aminopyrazole **4a−bb** (0.165 mmol, 1.1 equiv), $Pd(OAc)_2$ (15 μmol, 0.1 equiv), xantphos (30 μmol, 0.2 equiv), and Cs_2CO_3 (0.3 mmol, 2 equiv). The vial was fitted with a rubber septum, evacuated, backfilled with N_2, and anhydrous toluene (0.6 mL, 0.25 M) was added. The septum was replaced with a cap, and the vial was sealed with PTFE tape. The reaction was heated at 130 °C for 16 h in a heating block. The reaction was cooled to room temperature and filtered through silica plug eluting with EtOAc (12 mL). The filtrate was concentrated and used without further purification.

E1b: To a flame-dried microwave vial equipped with a magnetic stir bar were added resorcylate amide bromide **8a−c** (0.15 mmol, 1 equiv), aminopyrazole **4a−bb** (0.165 mmol, 1.1 equiv), $Pd_2(dba)_3$ (6 μmol, 0.04 equiv), xanthphos (15 μmol, 0.1 equiv), and sodium phenoxide (0.225 mmol, 1.5 equiv). The vial was fitted with a rubber septum, evacuated, backfilled with N_2, and anhydrous 1,4-dioxane (0.1 M reaction concentration) was added. The septum was replaced with a microwave cap, and the reaction was heated in a microwave holding at 170 °C for 2 h. The reaction was cooled to room temperature and filtered through a silica plug eluting with EtOAc (8× reaction volume). The filtrate was concentrated and used without further purification.

E2a: In a 2D vial equipped with a magnetic stir bar were added benzyl-protected RAP (1 equiv), MeOH (2 mL), and Pd/C (20% wt). The vial was fitted with a rubber septum and a hydrogen balloon. Hydrogen was bubbled through the solution for 10 min; then, the reaction was stirred under hydrogen atmosphere for 16 h or until full conversion was observed by UPLC/MS. The reaction was filtered through celite plug eluting with MeOH (6 mL) and EtOAc (6 mL) and concentrated. The crude material was purified by mass-guided preparative HPLC.

E2b: In a 2D vial equipped with a magnetic stir bar was added benzyl-protected RAP (1 equiv), EtOAc (2 mL), and $Pd(OH)_2/C$ (20% wt). The vial was fitted with a rubber septum and a hydrogen balloon. Hydrogen was bubbled through the solution for 10 min; then, the reaction was stirred under hydrogen atmosphere for 16 h or until full conversion was observed by UPLC/MS. The reaction was filtered through celite plug eluting with MeOH (6 mL) and EtOAc (6 mL) and concentrated. The crude material was purified by mass-guided preparative HPLC.

*(2-((3-(2-Fluorophenyl)-1-methyl-1H-pyrazol-5-yl)amino)-4,6-dihydroxyphenyl)(isoindolin-2-yl)methanone (**9a**).* Amide bromide **8a** (45 mg, 0.087 mmol, 1 equiv) was coupled to 5-amino-3-(2-fluorophenyl)-1-methylpyrazole **4a** (18.4 mg, 0.096 mmol, 1.1 equiv) according to General Procedure **E1a**. The resulting product was deprotected according to General Procedure **E2a**. **9a** (16.7 mg, 0.037 mmol) was obtained in a 43% yield over two steps. ^{1}H NMR (500 MHz, DMSO-d_6) δ 9.64 (s, 1H), 9.31 (s, 1H), 7.89 (dt, J = 1.90, 7.8 Hz, 1H), 7.29−7.35 (m, 3H), 7.24−7.29 (m, 2H), 7.22−7.24 (m, 1H), 7.21 (s, 2H), 7.20 (s, 1H), 6.36 (d, J = 3.9 Hz, 1H), 5.89 (d, J = 2.0 Hz, 1H), 5.62 (d, J = 2.0 Hz, 1H), 4.63−4.86 (m, 4H), 3.63 (s, 3H); ^{13}C NMR (126 MHz, DMSO-d_6) δ 166.5, 160.3, 159.4, 158.3, 155.7, 143.9, 142.8, 141.6, 141.6, 129.2, 129.1, 127.6, 127.4, 124.6, 123.0, 121.3, 121.2, 116.3, 116.1, 104.5, 99.8, 99.7, 94.6, 93.0, 40.6, 35.2.

*(2-((3-(2-Chlorophenyl)-1-methyl-1H-pyrazol-5-yl)amino)-4,6-dihydroxyphenyl)(isoindolin-2-yl)methanone (**9b**).* Amide bromide **8a** (51 mg, 0.1 mmol, 1 equiv) was coupled to **4b** (23 mg, 0.11 mmol, 1.1 equiv) according to General Procedure **E1a**. The resulting product was deprotected according to General Procedure **E2a**. **9b** (3.4 mg,

https://dx.doi.org/10.1021/acs.jmedchem.0c01777
J. Med. Chem. 2021, 64, 1139−1169

0.007 mmol) was obtained in 7% yield over two steps. ^{1}H NMR (500 MHz, DMSO-d_6): δ 9.64 (s, 1H), 9.32 (s, 1H), 7.78−7.72 (m, 1H), 7.50−7.45 (m, 1H), 7.38−7.29 (m, 4H), 7.29−7.25 (m, 2H), 7.21 (s, 1H), 6.48 (s, 1H), 5.90 (d, J = 2.1 Hz, 1H), 5.65 (d, J = 2.1 Hz, 1H), 4.82−4.69 (m, 4H), 3.62 (s, 3H); ^{13}C NMR (126 MHz, DMSO-d_6): δ 166.34, 159.23, 155.52, 145.71, 143.74, 140.82, 132.16, 130.72, 130.20, 129.88, 128.88, 127.23, 127.14, 122.86, 104.28, 100.19, 94.50, 92.87, 35.04. UPLC/MS [M + H] = 461.337, t_R = 2.36 min.

*(2,4-Dihydroxy-6-((1-methyl-3-(2-(trifluoromethyl)phenyl)-1H-pyrazol-5-yl)amino)phenyl)(isoindolin-2-yl)methanone (**9c**).* Amide bromide **8a** (77 mg, 0.15 mmol, 1 equiv) was coupled to **4c** (40 mg, 0.165 mmol, 1.1 equiv) according to General Procedure **E1a**. The resulting product was deprotected according to General Procedure **E2a**. **9c** (13 mg, 0.026 mmol) was obtained in 17% yield over two steps. ^{1}H NMR (500 MHz, DMSO-d_6): δ 9.63−9.59 (m, 1H), 9.32 (s, 1H), 7.78 (dd, J = 8.0, 1.3 Hz, 1H), 7.68−7.63 (m, 1H), 7.63−7.60 (m, 1H), 7.58−7.53 (m, 1H), 7.41−7.25 (m, 4H), 7.23 (s, 1H), 6.18 (s, 1H), 5.91 (d, J = 2.1 Hz, 1H), 5.64 (d, J = 2.1 Hz, 1H), 4.75 (s, 4H), 3.61 (s, 3H); ^{13}C NMR (126 MHz, DMSO-d_6): δ 166.32, 159.22, 155.48, 146.45, 143.68, 140.85, 137.21, 133.27, 132.20, 131.56, 128.06, 127.25, 126.09, 125.26, 122.88, 104.34, 99.67, 94.51, 92.87, 35.02. UPLC/MS [M + H] = 495.601, t_R = 1.49 min.

*(2-((1-(tert-Butyl)-3-(o-tolyl)-1H-pyrazol-5-yl)amino)-4,6-dihydroxyphenyl)(isoindolin-2-yl)methanone (**9d**).* Amide bromide **8a** (62 mg, 0.120 mmol, 1 equiv) was coupled to **4d** (30 mg, 0.132 mmol, 1.1 equiv) according to General Procedure **E1b**. The resulting product was deprotected according to General Procedure **E2a**. **9d** (18.5 mg, 0.038 mmol) was obtained in 32% yield over two steps. ^{1}H NMR (500 MHz, DMSO-d_6): δ 9.69 (s, 1H), 9.29 (s, 1H), 7.58−7.51 (m, 1H), 7.38−7.32 (m, 2H), 7.32−7.26 (m, 2H), 7.24−7.16 (m, 3H), 6.98 (s, 1H), 6.37 (s, 1H), 5.85 (d, J = 2.1 Hz, 1H), 5.70 (d, J = 2.1 Hz, 1H), 4.81 (s, 4H), 2.48 (s, 3H), 1.55 (s, 9H); ^{13}C NMR (126 MHz, DMSO-d_6): δ 167.36, 159.88, 156.00, 147.57, 145.54, 139.92, 137.13, 135.37, 133.63, 131.35, 128.69, 127.73, 127.45, 126.14, 123.31, 103.48, 103.20, 94.24, 92.56, 59.70, 29.89, 21.90 UPLC/MS [M + H] = 483.575, t_R = 1.81 min.

*(2,4-Dihydroxy-6-((1-methyl-3-(o-tolyl)-1H-pyrazol-5-yl)amino)-phenyl)(5-fluoroisoindolin-2-yl)methanone (**9e**).* Compound **9e** was obtained according to the route and procedures described in ref 62. (2-Bromo-4,6-bis(methoxymethoxy)phenyl)(5-fluoroisoindolin-2-yl)-methanone (78 mg, 0.177 mmol, 1 equiv), 2-methyl-5-(*o*-tolyl)pyrazol-3-amine (**4e**) (22 mg, 0.195 mmol, 1.1 equiv), $Pd_2(dba)_3$ (8.1 mg, 5 mol %), xantphos (10.3 mg, 10 mol %), sodium phenoxide (31 mg, 0.266 mmol, 1.5 equiv), and anhydrous dioxane (2 mL) were heated to 120 °C in a 2 dram vial under an atmosphere of nitrogen. The reaction was cooled to room temperature, diluted with ethyl acetate, and passed through a prewetted 3 mL hydromatrix cartridge eluting with ethyl acetate. The eluents were dried with sodium sulfate, filtered, and condensed by rotary evaporation. Purification on a short silica column with a gradient of 25% to 40% acetone in hexanes afforded a yellow gum, which was then dissolved in methanol (5 mL) and 2 M aqueous HCl (0.53 mL). The reaction was heated to 50 °C overnight, cooled to room temperature, and the solvent was removed by rotary evaporation. The crude residue was purified by mass-guided preparative HPLC to afford **9e** (24.2 mg, 28% yield over two steps). ^{1}H NMR (500 MHz, $CDCl_3$) δ 7.41 (d, J = 7.34 Hz, 1H), 7.06−7.17 (m, 4H), 6.92 (dt, J = 1.96, 8.56 Hz, 1H), 6.86 (br d, J = 8.31 Hz, 1H), 6.81 (s, 1H), 6.10 (s, 1H), 5.97 (d, J = 0.98 Hz, 1H), 5.78 (d, J = 1.47 Hz, 1H), 4.91 (br s, 2H), 4.72−4.86 (m, 2H), 3.64 (s, 3H), 2.33 (s, 3H); ^{13}C NMR (126 MHz, $CDCl_3$) δ 168.8, 161.8, 160.5, 156.4, 150.4, 144.8, 140.6, 136.0, 132.9, 132.0, 130.9, 129.1, 128.0, 126.0, 124.2, 124.1, 115.1, 114.9, 110.2, 110.0, 100.0, 95.9, 94.0, 52.9, 52.4, 40.9, 21.2. UPLC/MS [M + H] = 459.393, t_R = 1.70 min.

*(2,4-Dihydroxy-6-((3-(2-methoxyphenyl)-1-methyl-1H-pyrazol-5-yl)amino)phenyl)(isoindolin-2-yl)methanone (**9f**).* Compound **9f** was obtained from (2-bromo-4,6-bis(methoxymethoxy)phenyl)-(isoindolin-2-yl)methanone[62] and 5-(2-methoxyphenyl)-2-methyl-pyrazol-3-amine (**4f**) according to the same procedures described above for **9e**. **9f** (17.8 mg) was obtained in 35% yield over two steps. ^{1}H NMR (500 MHz, $CDCl_3$) δ 7.76 (dd, J = 1.47, 7.83 Hz, 1H), 7.21−7.25 (m, 3H), 7.17−7.21 (m, 3H), 6.90 (br t, J = 7.50 Hz, 1H), 6.85 (d, J = 8.31 Hz, 1H), 6.72 (s, 1H), 6.49 (s, 1H), 5.97 (d, J = 0.98 Hz, 1H), 5.76 (d, J = 1.96 Hz, 1H), 4.94−5.09 (m, 2H), 4.81−4.93 (m, 2H), 3.75 (s, 3H), 3.66 (s, 3H); ^{13}C NMR (126 MHz, $CDCl_3$) δ 168.8, 160.5, 156.8, 156.4, 147.1, 145.3, 140.3, 136.7, 129.0, 128.3, 127.7, 122.9, 122.3, 120.9, 111.4, 103.1, 101.6, 95.6, 93.8, 77.5, 55.5, 53.0, 40.9, 35.1. UPLC/MS [M + H] = 457.409, t_R = 1.56 min.

*(2,4-Dihydroxy-6-((1-isopropyl-3-(2-methoxyphenyl)-1H-pyrazol-5-yl)amino)phenyl)(isoindolin-2-yl)methanone (**9g**).* Amide bromide **8a** (77 mg, 0.150 mmol, 1 equiv) was coupled to **4g** (38 mg, 0.165 mmol, 1.1 equiv) according to General Procedure **E1a**. The resulting product was deprotected according to General Procedure **E2a**. **9g** (22 mg, 0.046 mmol) was obtained in 37% yield over two steps. ^{1}H NMR (500 MHz, DMSO-d_6): δ 9.58 (s, 1H), 9.25 (s, 1H), 7.91 (m, 1H), 7.42−7.21 (m, 5H), 7.12−6.94 (m, 3H), 6.46 (s, 1H), 5.84 (d, J = 2.1 Hz, 1H), 5.54 (d, J = 2.1 Hz, 1H), 4.77 (m, 4H), 4.50−4.37 (p, J = 6.6 Hz, 1H), 3.85−3.78 (m, 3H), 1.35 (d, J = 6.6 Hz, 6H); ^{13}C NMR (126 MHz, DMSO-d_6): δ 166.62, 159.35, 156.32, 155.64, 145.20, 145.08, 139.03, 136.90, 128.51, 127.40, 127.25, 123.03, 122.49, 120.49, 111.89, 103.84, 102.14, 94.11, 92.40, 55.49, 47.87, 22.45. UPLC/MS [M + H] = 485.231, t_R = 1.52 min.

*(2-((1-Cyclohexyl-3-(2-methoxyphenyl)-1H-pyrazol-5-yl)amino)-4,6-dihydroxyphenyl)(isoindolin-2-yl)methanone (**9h**).* Amide bromide **8a** (77 mg, 0.150 mmol, 1 equiv) was coupled to **4h** (45 mg, 0.165 mmol, 1.1 equiv) according to General Procedure **E1a**. The resulting product was deprotected according to General Procedure **E2a**. **9h** (20 mg, 0.039 mmol) was obtained in 26% yield over two steps. ^{1}H NMR (500 MHz, DMSO-d_6): δ 9.66 (s, 1H), 9.33 (s, 1H), 8.01−7.96 (m, 1H), 7.43 (t, J = 4.4 Hz, 2H), 7.40−7.31 (m, 3H), 7.17−7.09 (m, 2H), 7.09−7.02 (m, 1H), 6.56 (s, 1H), 5.94 (d, J = 2.1 Hz, 1H), 5.65 (d, J = 2.1 Hz, 1H), 4.86 (s, 4H), 4.15−4.05 (m, 1H), 3.89 (s, 3H), 1.99−1.81 (m, 6H), 1.69−1.65 (m, 1H), 1.36−1.19 (m, 3H); ^{13}C NMR (126 MHz, DMSO-d_6): δ 166.49, 159.16, 156.15, 155.46, 144.91, 144.86, 138.97, 136.70, 128.33, 127.25, 127.07, 122.84, 122.30, 120.32, 111.72, 103.76, 102.07, 94.01, 92.29, 55.32, 55.25, 32.34, 25.12, 24.91. UPLC/MS [M + H] = 526.363, t_R = 3.06 min.

*(2-((1-Cyclohexyl-3-(2-methoxyphenyl)-1H-pyrazol-5-yl)amino)-4,6-dihydroxyphenyl)(4-fluoroisoindolin-2-yl)methanone (**9i**).* Amide bromide **8b** (48 mg, 0.090 mmol, 1 equiv) was coupled to **4h** (27 mg, 0.099 mmol, 1.1 equiv) according to General Procedure **E1b**. The resulting product was deprotected according to General Procedure **E2a**. **9i** (19 mg, 0.035 mmol) was obtained in 39% yield over two steps. ^{1}H NMR (500 MHz, DMSO-d_6): δ 9.59 (s, 1H), 9.26 (s, 1H), 7.93−7.85 (m, 1H), 7.37−7.30 (m, 1H), 7.28−7.22 (m, 1H), 7.19 (d, J = 7.6 Hz, 1H), 7.10 (t, J = 8.8 Hz, 1H), 7.07−7.00 (m, 2H), 7.00−6.93 (m, 1H), 6.46 (s, 1H), 5.85 (d, J = 2.1 Hz, 1H), 5.57 (d, J = 2.1 Hz, 1H), 4.92−4.68 (m, 4H), 4.07−3.97 (m, 1H), 3.79 (s, 3H), 1.91−1.70 (m, 7H), 1.61−1.57 (m, 1H), 1.28−1.14 (m, 3H), ^{13}C NMR (126 MHz, DMSO-d_6): δ 166.43, 159.25, 156.11, 155.52, 144.96, 144.87, 138.97, 128.29, 127.01, 122.24, 120.29, 113.63 (d, J = 19.4 Hz), 111.67, 103.45, 102.04, 93.99, 92.49, 79.16, 55.27, 32.34, 25.11, 24.91. UPLC/MS [M + H] = 543.598, t_R = 1.79 min.

*(2-((1-Cyclohexyl-3-(2-methoxyphenyl)-1H-pyrazol-5-yl)amino)-4,6-dihydroxyphenyl)(5-fluoroisoindolin-2-yl)methanone (**9j**).* Amide bromide **8c** (48 mg, 0.90 mmol, 1 equiv) was coupled to **4h** (27 mg, 0.099 mmol, 1.1 equiv) according to General Procedure **E1b**. The resulting product was deprotected according to General Procedure **E2a**. **9j** (19 mg, 0.034 mmol) was obtained in 38% yield over two steps. ^{1}H NMR (500 MHz, DMSO-d_6): δ 9.57 (s, 1H), 9.24 (s, 1H), 7.91−7.86 (m, 1H), 7.43−7.32 (m, 1H), 7.27−7.22 (m, 1H), 7.22−7.18 (m, 1H), 7.11−7.06 (m, 1H), 7.04−7.01 (m, 2H), 6.45 (s, 1H), 5.84 (d, J = 2.1 Hz, 1H), 5.57 (d, J = 2.1 Hz, 1H), 4.73 (s, 6H), 3.80 (s, 3H), 1.93−1.71 (m, 6H), 1.66−1.55 (m, 1H), 1.31−1.13 (m, 3H); ^{13}C NMR (126 MHz, DMSO-d_6): δ 166.44, 159.20, 156.12, 155.48, 144.91, 144.88, 139.00, 128.30, 127.05, 124.54, 122.27, 120.30, 114.22, 111.68, 110.06, 103.62, 102.01, 94.00, 92.44, 79.17, 55.30, 48.58, 32.35, 25.12. UPLC/MS [M + H] = 543.322, t_R = 1.79 min.

*(2-((1-Cyclopentyl-3-(2-methoxyphenyl)-1H-pyrazol-5-yl)-amino)-4,6-dihydroxyphenyl)(isoindolin-2-yl)methanone (**9k**).* Amide bromide **8a** (77 mg, 0.150 mmol, 1 equiv) was coupled to **4i**

https://dx.doi.org/10.1021/acs.jmedchem.0c01777
J. Med. Chem. 2021, 64, 1139−1169

(42 mg, 0.165 mmol, 1.1 equiv) according to General Procedure **E1a**. The resulting product was deprotected according to General Procedure **E2a**. **9k** (30.5 mg, 0.060 mmol) was obtained in 40% yield over two steps. ^{1}H NMR (500 MHz, DMSO-d_6): δ 9.59 (s, 1H), 7.92−7.87 (m, 1H), 7.39−7.32 (m, 2H), 7.30−7.22 (m, 3H), 7.10−7.01 (m, 2H), 7.01−6.93 (m, 1H), 6.47 (s, 1H), 5.86 (d, J = 2.1 Hz, 1H), 5.55 (d, J = 2.1 Hz, 1H), 4.77 (s, 4H), 4.58 (p, J = 7.3 Hz, 1H), 3.81 (s, 3H), 2.04−1.78 (m, 6H), 1.67−1.47 (m, 2H); ^{13}C NMR (126 MHz, DMSO-d_6): δ 166.52, 159.21, 156.18, 155.48, 145.00, 144.83, 139.60, 136.76, 128.38, 127.26, 127.10, 122.86, 122.30, 120.37, 111.75, 103.72, 101.94, 94.04, 92.39, 56.91, 55.34, 32.25, 24.16. UPLC/MS [M + H] = 511.295, t_R = 1.74 min.

*(2,4-Dihydroxy-6-((1-isobutyl-3-(2-methoxyphenyl)-1H-pyrazol-5-yl)amino)phenyl)(isoindolin-2-yl)methanone (**9l**).* Amide bromide **8a** (77 mg, 0.150 mmol, 1 equiv) was coupled to **4j** (40 mg, 0.165 mmol, 1.1 equiv) according to General Procedure **E1a**. The resulting product was deprotected according to General Procedure **E2a**. **9l** (20.7 mg, 0.0415 mmol) was obtained in 28% yield over two steps. ^{1}H NMR (500 MHz, DMSO-d_6): δ 9.63 (s, 1H), 9.29 (s, 1H), 7.90−7.84 (m, 1H), 7.34 (s, 2H), 7.31−7.24 (m, 3H), 7.08 (s, 1H), 7.07−7.04 (m, 1H), 6.98−6.94 (m, 1H), 6.50 (s, 1H), 5.87 (d, J = 2.1 Hz, 1H), 5.67 (d, J = 2.1 Hz, 1H), 4.77 (s, 4H), 3.82 (s, 3H), 3.72 (d, J = 7.3 Hz, 2H), 2.14−2.03 (m, 1H), 0.78 (d, J = 6.7 Hz, 6H); ^{13}C NMR (126 MHz, DMSO-d_6): δ 167.03, 159.72, 156.66, 155.95, 145.55, 144.68, 140.56, 137.11, 128.92, 127.72, 127.56, 123.31, 122.57, 120.83, 112.24, 104.24, 101.43, 94.67, 92.89, 55.82, 55.00, 29.14, 20.25. UPLC/MS [M + H] = 499.343, t_R = 1.74 min.

*(2-((1-(tert-Butyl)-3-(2-methoxyphenyl)-1H-pyrazol-5-yl)amino)-4,6-dihydroxyphenyl)(isoindolin-2-yl)methanone (**9m**).* Amide bromide **8a** (77 mg, 0.150 mmol, 1 equiv) was coupled to **4k** (40 mg, 0.165 mmol, 1.1 equiv) according to General Procedure **E1a**. The resulting product was deprotected according to General Procedure **E2a**. **9m** (12.4 mg, 0.025 mmol) was obtained in 12.5% yield over two steps. ^{1}H NMR (500 MHz, DMSO-d_6): δ 9.67 (s, 1H), 9.26 (s, 1H), 7.94−7.89 (m, 1H), 7.41−7.33 (m, 2H), 7.31−7.24 (m, 3H), 7.08−7.02 (m, 1H), 6.97 (s, 1H), 6.94−6.91 (m, 1H), 6.54 (d, J = 0.7 Hz, 1H), 5.84 (d, J = 2.1 Hz, 1H), 5.62 (d, J = 2.1 Hz, 1H), 4.81 (s, 4H), 3.81 (s, 3H), 1.55 (s, 9H); ^{13}C NMR (126 MHz, DMSO-d_6): δ 167.35, 159.83, 156.68, 155.97, 145.81, 143.75, 139.66, 137.12, 128.81, 127.73, 127.46, 123.31, 122.73, 120.82, 112.21, 105.28, 103.41, 94.12, 92.51, 59.69, 55.81, 29.91. UPLC/MS [M + H] = 499.343, t_R = 1.62 min.

*(2,4-Dihydroxy-6-((1-methyl-3-(2-(trifluoromethoxy)phenyl)-1H-pyrazol-5-yl)amino)phenyl)(isoindolin-2-yl)methanone (**9n**).* Amide bromide **8a** (77 mg, 0.15 mmol, 1 equiv) was coupled to **4l** (42 mg, 0.165 mmol, 1.1 equiv) according to General Procedure **E1b**. The resulting product was deprotected according to General Procedure **E2a**. **9n** (36 mg, 0.70 mmol) was obtained in 47% yield over two steps. ^{1}H NMR (500 MHz, DMSO-d_6): δ 9.63 (s, 1H), 9.29 (s, 1H), 8.00−7.92 (m, 1H), 7.44−7.36 (m, 3H), 7.32 (s, 2H), 7.28−7.23 (m, 3H), 6.35 (s, 1H), 5.92 (d, J = 2.1 Hz, 1H), 5.62 (d, J = 2.1 Hz, 1H), 4.75 (s, 4H), 3.63 (s, 3H); ^{13}C NMR (126 MHz, DMSO-d_6): δ 166.34, 159.27, 155.52, 145.02, 143.73, 143.28, 141.43, 136.73, 128.92, 128.62, 127.64, 127.25, 126.95, 122.85, 121.53, 121.22, 119.18, 104.39, 99.57, 94.56, 92.88, 35.17. UPLC/MS [M + H] = 511.162, t_R = 1.49 min.

*(2-((1-(tert-Butyl)-3-(2-(trifluoromethoxy)phenyl)-1H-pyrazol-5-yl)amino)-4,6-dihydroxyphenyl)(isoindolin-2-yl)methanone (**9o**).* Amide bromide **8a** (64 mg, 0.125 mmol, 1 equiv) was coupled to **4m** (41 mg, 0.138 mmol, 1.1 equiv) according to General Procedure **E1b**. The resulting product was deprotected according to General Procedure **E2a**. **9o** (14.7 mg, 0.027 mmol) was obtained in 22% yield over two steps. ^{1}H NMR (500 MHz, DMSO-d_6): δ 9.69 (s, 1H), 9.26 (s, 1H), 8.02−7.97 (m, 1H), 7.45−7.37 (m, 3H), 7.37−7.31 (m, 2H), 7.32−7.26 (m, 2H), 7.02 (s, 1H), 6.44 (s, 1H), 5.86 (d, J = 2.1 Hz, 1H), 5.62 (d, J = 2.1 Hz, 1H), 4.80 (s, 4H), 1.56 (s, 9H); ^{13}C NMR (126 MHz, DMSO-d_6): δ 166.78, 159.40, 155.50, 144.95, 141.74, 140.21, 136.60, 128.80, 128.69, 127.62, 127.27, 127.04, 122.83, 121.57, 121.28, 119.24, 103.26, 103.19, 93.90, 92.08, 59.77, 29.32.UPLC/MS [M + H] = 553.609, t_R = 1.87 min.

*(2-((1-(tert-Butyl)-3-(3-methoxyphenyl)-1H-pyrazol-5-yl)amino)-4,6-dihydroxyphenyl)(isoindolin-2-yl)methanone (**9p**).* Amide bromide **8a** (77 mg, 0.150 mmol, 1 equiv) was coupled to **4n** (40 mg, 0.165 mmol, 1.1 equiv) according to General Procedure **E1b**. The resulting product was deprotected according to General Procedure **E2a**. **9p** (32.3 mg, 0.065 mmol) was obtained in 43% yield over two steps. ^{1}H NMR (500 MHz, DMSO-d_6): δ 9.70 (s, 1H), 9.28 (s, 1H), 7.38−7.32 (m, 3H), 7.32−7.25 (m, 4H), 6.97 (s, 1H), 6.86−6.80 (m, 1H), 6.58 (d, J = 0.6 Hz, 1H), 5.86 (d, J = 2.1 Hz, 1H), 5.67 (d, J = 2.1 Hz, 1H), 4.99−4.66 (m, 4H), 3.78 (s, 3H), 1.56 (s, 9H); ^{13}C NMR (126 MHz, DMSO-d_6): δ 166.90, 159.49, 159.42, 155.54, 146.34, 145.08, 140.43, 136.66, 135.22, 129.55, 127.28, 122.86, 117.14, 112.72, 110.05, 103.03, 100.57, 93.82, 92.24, 59.36, 55.02, 29.41 UPLC/MS [M + H] = 499.255, t_R = 1.66 min.

*(2-((1-(tert-butyl)-3-(m-tolyl)-1H-pyrazol-5-yl)amino)-4,6-dihydroxyphenyl)(isoindolin-2-yl)methanone (**9q**).* Amide bromide **8a** (77 mg, 0.150 mmol, 1 equiv) was coupled to **4o** (38 mg, 0.165 mmol, 1.1 equiv) according to General Procedure **E1b**. The resulting product was deprotected according to General Procedure **E2a**. **9q** (34.7 mg, 0.072 mmol) was obtained in 48% yield over two steps. ^{1}H NMR (500 MHz, DMSO-d_6): δ 9.70 (s, 1H), 9.28 (s, 1H), 7.61−7.57 (m, 1H), 7.57−7.52 (m, 1H), 7.40−7.32 (m, 2H), 7.32−7.21 (m, 3H), 7.11−7.04 (m, 1H), 7.00−6.96 (m, 1H), 6.53 (s, 1H), 5.86 (d, J = 2.1 Hz, 1H), 5.69 (d, J = 2.1 Hz, 1H), 5.06−4.62 (m, 4H), 2.32 (s, 3H), 1.56 (s, 9H); ^{13}C NMR (126 MHz, DMSO-d_6): δ 166.92, 159.43, 155.55, 146.55, 145.06, 140.42, 137.50, 136.67, 133.72, 128.37, 127.82, 127.29, 125.19, 122.86, 121.91, 103.06, 100.22, 93.84, 92.26, 59.31, 29.44, 21.10. UPLC/MS [M + H] = 483.247, t_R = 1.85 min.

*(2-((1-(tert-Butyl)-3-(3-(trifluoromethyl)phenyl)-1H-pyrazol-5-yl)-amino)-4,6-dihydroxyphenyl)(isoindolin-2-yl)methanone (**9r**).* Amide bromide **8a** (77 mg, 0.150 mmol, 1 equiv) was coupled to **4p** (46.7 mg, 0.165 mmol, 1.1 equiv) according to General Procedure **E1b**. The resulting product was deprotected according to General Procedure **E2a**. **9r** (49.8 mg, 0.093 mmol) was obtained in 62% yield over two steps. ^{1}H NMR (500 MHz, DMSO-d_6): δ 9.72 (s, 1H), 9.29 (s, 1H), 8.10−8.02 (m, 2H), 7.64−7.57 (m, 2H), 7.41−7.31 (m, 2H), 7.31−7.24 (m, 2H), 7.03 (s, 1H), 6.75 (s, 1H), 5.88 (d, J = 2.1 Hz, 1H), 5.70 (d, J = 2.1 Hz, 1H), 5.04−4.59 (m, 4H), 1.58 (s, 9H); ^{13}C NMR (126 MHz, DMSO-d_6): δ 167.33, 159.89, 156.01, 145.47, 145.35, 141.49, 137.11, 130.13, 129.91 (q, J = 30.8 Hz), 128.95, 127.73, 125.82, 124.14−123.94 (m), 123.65, 123.30, 121.23−121.03 (m), 103.64, 101.20, 94.43, 92.85, 60.13, 29.80. UPLC/MS [M + H] = 537.270, t_R = 1.94 min.

*(2,4-Dihydroxy-6-((1-methyl-3-(3-(trifluoromethoxy)phenyl)-1H-pyrazol-5-yl)amino)phenyl)(isoindolin-2-yl)methanone (**9s**).* Amide bromide **8a** (77 mg, 0.15 mmol, 1 equiv) was coupled to **4q** (42 mg, 0.165 mmol, 1.1 equiv) according to General Procedure **E1b**. The resulting product was deprotected according to General Procedure **E2a**. **9s** (43 mg, 0.084 mmol) was obtained in 56% yield over two steps. ^{1}H NMR (500 MHz, DMSO-d_6): δ 9.64 (s, 1H), 9.30 (s, 1H), 7.76−7.70 (m, 1H), 7.69−7.64 (m, 1H), 7.47 (t, J = 8.0 Hz, 1H), 7.34−7.29 (m, 2H), 7.29−7.23 (m, 3H), 7.22 (s, 1H), 6.58 (s, 1H), 5.91 (d, J = 2.1 Hz, 1H), 5.66 (d, J = 2.1 Hz, 1H), 4.92−4.51 (m, 4H), 3.63 (s, 3H); ^{13}C NMR (126 MHz, DMSO-d_6): δ 166.40, 159.27, 155.55, 148.90−148.76 (m), 146.67, 142.02, 136.68, 135.92, 130.55, 127.24, 123.63, 122.84, 121.15, 119.45, 119.11, 116.59, 104.27, 97.13, 94.52, 93.09, 35.10. UPLC/MS [M + H] = 511.162, t_R = 1.62 min.

*(2-((1-(tert-Butyl)-3-(3-(trifluoromethoxy)phenyl)-1H-pyrazol-5-yl)amino)-4,6-dihydroxyphenyl)(isoindolin-2-yl)methanone (**9t**).* Amide bromide **8a** (77 mg, 0.150 mmol, 1 equiv) was coupled to **4r** (49 mg, 0.165 mmol, 1.1 equiv) according to General Procedure **E1b**. The resulting product was deprotected according to General Procedure **E2a**. **9t** (39.4 mg, 0.071 mmol) was obtained in 47% yield over two steps. ^{1}H NMR (500 MHz, DMSO-d_6): δ 9.71 (s, 1H), 9.28 (s, 1H), 7.82−7.77 (m, 1H), 7.73−7.68 (m, 1H), 7.50 (t, J = 8.0 Hz, 1H), 7.40−7.32 (m, 2H), 7.32−7.21 (m, 3H), 7.02 (s, 1H), 6.69 (s, 1H), 5.87 (d, J = 2.1 Hz, 1H), 5.68 (d, J = 2.1 Hz, 1H), 5.05−4.58 (m, 4H), 1.57 (s, 9H); ^{13}C NMR (126 MHz, DMSO-d_6): δ 167.33, 159.89, 156.01, 149.38−149.25 (m), 145.44, 145.40, 141.38, 137.11, 136.64, 131.01, 127.73, 124.08, 121.61, 119.79, 119.57, 117.16, 103.60, 101.30, 94.40, 92.80, 60.10, 29.79. UPLC/MS [M + H] = 553.278, t_R = 544.246 min.

https://dx.doi.org/10.1021/acs.jmedchem.0c01777
J. Med. Chem. 2021, 64, 1139−1169

*(2-((3-(3-Fluorophenyl)-1-methyl-1H-pyrazol-5-yl)amino)-4,6-dihydroxyphenyl)(isoindolin-2-yl)methanone (**9u**).* Amide bromide **8a** (45 mg, 0.087 mmol, 1 equiv) was coupled to 2-methyl-5-(3-fluorophenyl)pyrazol-3-amine **4s** (18 mg, 0.096 mmol, 1.1 equiv) according to General Procedure **E1a**. The resulting product was deprotected according to General Procedure **E2a**. **9u** (24.7 mg, 0.056 mmol) was obtained in 64% yield over two steps. ^{1}H NMR (400 MHz, methanol-d_4) δ 7.45−7.39 (m, 1H), 7.38−7.26 (m, 2H), 7.26−7.21 (m, 4H), 7.01−6.89 (m, 1H), 6.38 (s, 1H), 5.96 (d, J = 2.1 Hz, 1H), 5.79 (d, J = 2.1 Hz, 1H), 4.95−4.72 (m, 4H), 3.71 (s, 3H); (500 MHz, DMSO-d_6): δ 9.63 (s, 1H), 9.29 (s, 1H), 7.59−7.53 (m, 1H), 7.50−7.46 (m, 1H), 7.41−7.35 (m, 1H), 7.35−7.29 (m, 2H), 7.30−7.25 (m, 2H), 7.19 (s, 1H), 7.10−7.03 (m, 1H), 6.54 (s, 1H), 5.89 (d, J = 2.1 Hz, 1H), 5.64 (d, J = 2.1 Hz, 1H), 4.84−4.68 (m, 4H), 3.61 (s, 3H); ^{13}C NMR (126 MHz, DMSO-d_6): δ 166.83, 162.99 (d, J = 242.2 Hz), 159.70, 155.99, 147.48 (d, J = 2.4 Hz), 144.29, 142.26, 136.54 (d, J = 8.2 Hz), 130.93 (d, J = 8.5 Hz), 127.69, 123.30, 121.06, 114.28 (d, J = 21.7 Hz), 111.51 (d, J = 22.4 Hz), 104.64, 97.54, 94.90, 93.42, 35.51. UPLC/MS [M + H] = 445.408, t_R = 2.31 min.

*(2-((1-(tert-Butyl)-3-(3-fluorophenyl)-1H-pyrazol-5-yl)amino)-4,6-dihydroxyphenyl)(isoindolin-2-yl)methanone (**9v**).* Amide bromide **8a** (77 mg, 0.150 mmol, 1 equiv) was coupled to **4t** (38.5 mg, 0.165 mmol, 1.1 equiv) according to General Procedure **E1b**. The resulting product was deprotected according to General Procedure **E2a**. **9v** (32.8 mg, 0.067 mmol) was obtained in 45% yield over two steps. ^{1}H NMR (500 MHz, DMSO-d_6): δ 9.71 (s, 1H), 9.28 (s, 1H), 7.64−7.59 (m, 1H), 7.59−7.51 (m, 1H), 7.44−7.38 (m, 1H), 7.37−7.32 (m, 2H), 7.32−7.25 (m, 2H), 7.11−7.04 (m, 1H), 7.00 (s, 1H), 6.65 (s, 1H), 5.87 (d, J = 2.1 Hz, 1H), 5.67 (d, J = 2.1 Hz, 1H), 4.97−4.71 (m, 4H), 1.56 (s, 9H); ^{13}C NMR (126 MHz, DMSO-d_6): δ 166.88, 162.58 (d, J = 242.3 Hz), 159.43, 155.56, 145.35 (d, J = 2.6 Hz), 144.99, 140.75, 136.67, 136.31 (d, J = 8.1 Hz), 130.50 (d, J = 8.6 Hz), 127.29, 122.86, 120.65 (d, J = 2.7 Hz), 113.75 (d, J = 21.0 Hz), 111.06 (d, J = 22.4 Hz), 103.11, 100.80, 93.91, 92.30, 59.58, 29.37. UPLC/MS [M + H] = 487.501, t_R = 1.82 min.

*(2-((3-(3-Chlorophenyl)-1-methyl-1H-pyrazol-5-yl)amino)-4,6-dihydroxyphenyl)(isoindolin-2-yl)methanone (**9w**).* Amide bromide **8a** (129 mg, 0.25 mmol, 1 equiv) was coupled to **4u** (57 mg, 0.275 mmol, 1.1 equiv) according to General Procedure **E1b**. The resulting product was deprotected according to General Procedure **E2b**. **9w** (20.4 mg, 0.044 mmol) was obtained in 18% yield over two steps. ^{1}H NMR (500 MHz, DMSO-d_6): δ 9.43 (s, 1H), 9.07 (s, 1H), 7.49 (t, J = 1.9 Hz, 1H), 7.45−7.39 (m, 1H), 7.11 (t, J = 7.9 Hz, 1H), 7.09−7.00 (m, 5H), 6.95 (s, 1H), 6.30 (s, 1H), 5.65 (d, J = 2.1 Hz, 1H), 5.40 (d, J = 2.1 Hz, 1H), 4.65−4.33 (m, 4H), 3.36 (s, 3H); ^{13}C NMR (126 MHz, DMSO-d_6): δ 166.38, 159.25, 155.56, 146.72, 143.76, 141.87, 136.95, 135.67, 133.40, 130.40, 127.23, 126.92, 124.13, 123.14, 122.83, 104.20, 96.93, 94.49, 93.01, 35.06. UPLC/MS [M + H] = 461.175, t_R = 1.54 min.

*(2-((1-(tert-Butyl)-3-(3-chlorophenyl)-1H-pyrazol-5-yl)amino)-4,6-dihydroxyphenyl)(isoindolin-2-yl)methanone (**9x**).* Amide bromide **8a** (77 mg, 0.150 mmol, 1 equiv) was coupled to **4v** (41 mg, 0.165 mmol, 1.1 equiv) according to General Procedure **E1b**. The resulting product was deprotected according to General Procedure **E2b**. **9x** (6.4 mg, 0.013 mmol) was obtained in 9% yield over two steps. ^{1}H NMR (500 MHz, DMSO-d_6): δ 9.70 (s, 1H), 9.27 (s, 1H), 7.79 (t, J = 1.9 Hz, 1H), 7.77−7.69 (m, 1H), 7.39 (t, J = 7.9 Hz, 1H), 7.37−7.33 (m, 2H), 7.33−7.27 (m, 3H), 7.00 (s, 1H), 6.66 (s, 1H), 5.85 (d, J = 2.1 Hz, 1H), 5.67 (d, J = 2.1 Hz, 1H), 4.93−4.69 (m, 4H), 1.56 (s, 9H); ^{13}C NMR (126 MHz, DMSO-d_6): δ 166.84, 159.40, 155.53, 145.03, 144.90, 140.81, 136.31, 135.90, 133.40, 130.43, 127.27, 126.88, 124.08, 123.20, 122.85, 103.11, 100.71, 93.90, 92.29, 59.59, 29.35. UPLC/MS [M + H] = 503.236, t_R = 1.86 min.

*(2-((3-(3-Chlorophenyl)-1-cyclohexyl-1H-pyrazol-5-yl)amino)-4,6-dihydroxyphenyl)(isoindolin-2-yl)methanone (**9y**).* Amide bromide **8a** (77 mg, 0.150 mmol, 1 equiv) was coupled to **4w** (46 mg, 0.165 mmol, 1.1 equiv) according to General Procedure **E1b**. The resulting product was deprotected according to General Procedure **E2b**. **9y** (85 mg, 0.016 mmol) was obtained in 11% yield over two steps. ^{1}H NMR (500 MHz, DMSO-d_6): δ 9.59 (s, 1H), 9.25 (s, 1H), 7.76 (t, J = 1.9 Hz, 1H), 7.71−7.65 (m, 1H), 7.36 (t, J = 7.9 Hz, 1H), 7.34−7.25 (m, 5H), 7.10 (s, 1H), 6.55 (s, 1H), 5.86 (d, J = 2.1 Hz, 1H), 5.61 (d, J = 2.1 Hz, 1H), 4.75 (s, 4H), 4.07−3.98 (m, 1H), 1.90−1.70 (m, 6H), 1.61−1.55 (m, 1H), 1.26−1.13 (m, 3H); ^{13}C NMR (126 MHz, DMSO-d_6): δ 166.42, 159.16, 155.49, 146.69, 144.42, 140.58, 136.65, 135.92, 133.37, 130.38, 127.24, 126.83, 124.07, 123.18, 122.82, 104.02, 97.97, 94.27, 92.75, 55.44, 40.43, 32.24, 24.85. UPLC/MS [M + H] = 529.319, t_R = 1.90 min.

*(2-((3-(2,3-Dimethylphenyl)-1-methyl-1H-pyrazol-5-yl)amino)-4,6-dihydroxyphenyl)(isoindolin-2-yl)methanone (**9z**).* Amide bromide **8a** (77 mg, 0.15 mmol, 1 equiv) was coupled to **4x** (33.2 mg, 0.165 mmol, 1.1 equiv) according to General Procedure **E1a**. The resulting product was deprotected according to General Procedure **E2a**. **9z** (5.5 mg, 0.012 mmol) was obtained in 8% yield over two steps. ^{1}H NMR (500 MHz, DMSO-d_6): 9.60 (s, 1H), 9.30 (s, 1H), 7.34 (s, 2H), 7.31−7.26 (m, 2H), 7.24−7.18 (m, 1H), 7.17 (s, 1H), 7.13−7.09 (m, 1H), 7.06 (t, J = 7.5 Hz, 1H), 6.13 (s, 1H), 5.88 (d, J = 2.1 Hz, 1H), 5.66 (d, J = 2.1 Hz, 1H), 4.82−4.70 (m, 4H), 3.60 (s, 3H), 2.30 (s, 3H), 2.26 (s, 3H); ^{13}C NMR (126 MHz, DMSO-d_6): δ 166.40, 159.24, 155.50, 149.40, 143.88, 140.45, 136.76, 133.87, 133.85, 128.76, 127.25, 126.92, 125.06, 122.87, 104.09, 99.74, 94.34, 92.74, 34.85, 20.36, 16.59. UPLC/MS [M + H] = 455.303, t_R = 1.52 min.

*(2-((3-(2,3-Dimethylphenyl)-1-methyl-1H-pyrazol-5-yl)amino)-4,6-dihydroxyphenyl)(4-fluoroisoindolin-2-yl)methanone (**9aa**).* Amide bromide **8b** (66.6 mg, 0.125 mmol, 1 equiv) was coupled to **4x** (27.7 mg, 0.138 mmol, 1.1 equiv) according to General Procedure **E1b**. The resulting product was deprotected according to General Procedure **E2a**. **9aa** (17.5 mg, 0.037 mmol) was obtained in 30% yield over two steps. ^{1}H NMR (500 MHz, DMSO-d_6): δ 9.66 (s, 1H), 9.34 (s, 1H), 7.40−7.30 (m, 1H), 7.25−7.14 (m, 3H), 7.15−7.08 (m, 2H), 7.05 (t, J = 7.5 Hz, 1H), 6.14 (s, 1H), 5.89 (d, J = 2.1 Hz, 1H), 5.68 (d, J = 2.1 Hz, 1H), 4.83−4.70 (m, 4H), 3.17 (s, 3H), 2.30 (s, 3H), 2.26 (s, 3H); ^{13}C NMR (126 MHz, DMSO-d_6): δ 166.42, 159.39, 157.13 (d, J = 241.2 Hz), 155.58, 149.41, 144.01, 140.43, 136.76, 133.84 (d, J = 4.3 Hz), 129.93, 128.77, 126.89, 125.06, 123.23, 119.19, 113.69 (d, J = 19.2 Hz), 103.74, 99.74, 94.34, 92.89, 34.86, 20.37, 16.59. UPLC/MS [M + H] = 473.751, t_R = 1.54min.

*(2-((3-(2,3-Dimethylphenyl)-1-methyl-1H-pyrazol-5-yl)amino)-4,6-dihydroxyphenyl)(5-fluoroisoindolin-2-yl)methanone (**9ab**).* Amide bromide **8c** (53.2 mg, 0.1 mmol, 1 equiv) was coupled to **4x** (22.1 mg, 0.11 mmol, 1.1 equiv) according to General Procedure **E1b**. The resulting product was deprotected according to General Procedure **E2a**. **9ab** (8.2 mg, 0.017 mmol) was obtained in 17% yield over two steps. ^{1}H NMR (500 MHz, DMSO-d_6): δ 9.60 (s, 1H), 9.30 (s, 1H), 7.38−7.34 (m, 1H), 7.24−7.18 (m, 2H), 7.17 (s, 1H), 7.13−7.03 (m, 3H), 6.12 (s, 1H), 5.88 (d, J = 2.1 Hz, 1H), 5.66 (d, J = 2.0 Hz, 1H), 5.05−4.42 (m, 4H), 3.60 (s, 3H), 2.29 (s, 3H), 2.26 (s, 3H); ^{13}C NMR (126 MHz, DMSO-d_6): δ 166.35, 159.28, 155.51, 149.38, 143.93, 140.44, 138.77, 136.74, 133.83 (d, J = 2.8 Hz), 128.75, 126.89, 125.04, 110.01 (d, J = 24.7 Hz), 103.93, 99.74, 94.32, 92.81, 34.85, 20.35, 16.58. UPLC/MS [M + H] = 473.670, t_R = 1.53 min.

*(2-((3-(5-Fluoro-2-methylphenyl)-1-methyl-1H-pyrazol-5-yl)-amino)-4,6-dihydroxyphenyl)(isoindolin-2-yl)methanone (**9ac**).* Amide bromide **8a** (77 mg, 0.15 mmol, 1 equiv) was coupled to **4y** (34 mg, 0.165 mmol, 1.1 equiv) according to General Procedure **E1a**. The resulting product was deprotected according to General Procedure **E2a**. **9ac** (9 mg, 0.020 mmol) was obtained in 13% yield over two steps. ^{1}H NMR (500 MHz, DMSO-d_6): δ 9.60 (s, 1H), 9.29 (s, 1H), 7.36−7.22 (m, 6H), 7.20 (s, 1H), 7.01 (td, J = 8.4, 2.9 Hz, 1H), 6.34 (s, 1H), 5.89 (d, J = 2.0 Hz, 1H), 5.66 (d, J = 2.0 Hz, 1H), 4.78−4.70 (m, 4H), 3.61 (s, 3H), 2.41 (s, 3H); ^{13}C NMR (126 MHz, DMSO-d_6): δ 160.37, 154.39 (d, J = 240.2 Hz), 153.23, 149.51, 141.62, 137.82, 134.93, 130.69, 128.85 (d, J = 7.4 Hz), 126.51 (d, J = 7.8 Hz), 124.91 (d, J = 2.8 Hz), 121.23, 116.84, 108.17 (d, J = 21.8 Hz), 107.62 (d, J = 21.1 Hz), 98.17, 93.52, 88.41, 86.87, 29.00, 14.55. UPLC/MS [M + H] = 459.452, t_R = 1.43 min.

*(2-((3-(5-Fluoro-2-methylphenyl)-1-methyl-1H-pyrazol-5-yl)-amino)-4,6-dihydroxyphenyl)(4-fluoroisoindolin-2-yl)methanone (**9ad**).* Amide bromide **8b** (66.6 mg, 0.125 mmol, 1 equiv) was coupled to **4y** (28.2 mg, 0.138 mmol, 1.1 equiv) according to General Procedure

https://dx.doi.org/10.1021/acs.jmedchem.0c01777
J. Med. Chem. 2021, 64, 1139−1169

E1b. The resulting product was deprotected according to General Procedure **E2a**. **9ad** (27 mg, 0.056 mmol) was obtained in 45% yield over two steps. ^{1}H NMR (500 MHz, DMSO-d_6): δ 9.66 (s, 1H), 9.34 (s, 1H), 7.36−7.30 (m, 1H), 7.30−7.26 (m, 1H), 7.26−7.21 (m, 2H), 7.20−7.15 (m, 1H), 7.08 (t, J = 8.8 Hz, 1H), 7.00 (td, J = 8.4, 2.9 Hz, 1H), 6.34 (s, 1H), 5.90 (d, J = 2.1 Hz, 1H), 5.68 (d, J = 2.1 Hz, 1H), 4.87−4.71 (m, 4H), 3.62 (s, 3H), 2.40 (s, 3H); ^{13}C NMR (126 MHz, DMSO-d_6): δ 166.39, 160.39 (d, J = 240.5 Hz), 159.37, 147.62 (d, J = 2.3 Hz), 143.98, 140.95, 134.80 (d, J = 7.9 Hz), 132.51 (d, J = 8.0 Hz), 130.88 (d, J = 2.9 Hz), 129.85, 119.14, 114.12 (d, J = 22.1 Hz), 113.71 (d, J = 7.1 Hz), 113.55 (d, J = 8.8 Hz), 103.85, 99.51, 94.43, 93.12, 89.17 (d, J = 104.5 Hz), 35.02, 20.57. UPLC/MS [M + H] = 477.489, t_R = 1.53 min.

*(2-((3-(5-Fluoro-2-methylphenyl)-1-methyl-1H-pyrazol-5-yl)amino)-4,6-dihydroxyphenyl)(5-fluoroisoindolin-2-yl)methanone (**9ae**)*. Amide bromide **8c** (66.6 mg, 0.125 mmol, 1 equiv) was coupled to **4y** (28.2 mg, 0.138 mmol, 1.1 equiv) according to General Procedure **E1b**. The resulting product was deprotected according to General Procedure **E2a**. **9ae** (19 mg, 0.40 mmol) was obtained in 32% yield over two steps. ^{1}H NMR (500 MHz, DMSO-d_6): δ 9.61 (s, 1H), 9.30 (s, 1H), 7.37−7.31 (m, 1H), 7.29−7.25 (m, 1H), 7.25−7.22 (m, 1H), 7.22−7.16 (m, 2H), 7.12−7.04 (m, 1H), 7.04−6.98 (m, 1H), 6.32 (s, 1H), 5.89 (d, J = 2.1 Hz, 1H), 5.66 (d, J = 2.1 Hz, 1H), 4.80−4.65 (m, 4H), 3.62 (s, 3H), 2.40 (s, 3H); ^{13}C NMR (126 MHz, DMSO-d_6): δ 166.32, 160.35 (d, J = 240.5 Hz), 159.26, 155.54, 147.60 (d, J = 2.4 Hz), 143.90, 140.96, 134.80 (d, J = 7.7 Hz), 132.49 (d, J = 8.1 Hz), 130.87 (d, J = 2.9 Hz), 124.50 (d, J = 8.8 Hz), 114.22, 114.05, 113.67, 113.51, 109.96 (d, J = 23.2 Hz), 104.03, 99.51, 94.41, 93.04, 35.01, 20.56. UPLC/MS [M + H] = 477.489, t_R = 1.52 min.

*(2-((3-(2-Fluoro-3-methylphenyl)-1-methyl-1H-pyrazol-5-yl)amino)-4,6-dihydroxyphenyl)(isoindolin-2-yl)methanone (**9af**)*. Amide bromide **8a** (77 mg, 0.150 mmol, 1 equiv) was coupled to **4z** (33.8 mg, 0.165 mmol, equiv) according to General Procedure **E1a**. The resulting product was deprotected according to General Procedure **E2a**. **9af** (13.7 mg, 0.030 mmol) was obtained in 20% yield over two steps. ^{1}H NMR (500 MHz, DMSO-d_6): δ 9.61 (s, 1H), 9.29 (s, 1H), 7.74−7.67 (m, 1H), 7.35−7.29 (m, 2H), 7.29−7.23 (m, 2H), 7.21 (s, 1H), 7.20−7.15 (m, 1H), 7.08 (t, J = 7.6 Hz, 1H), 6.35 (d, J = 4.1 Hz, 1H), 5.89 (d, J = 2.1 Hz, 1H), 5.64 (d, J = 2.0 Hz, 1H), 4.81−4.67 (m, 4H), 3.62 (s, 3H), 2.24 (d, J = 2.1 Hz, 3H); ^{13}C NMR (126 MHz, DMSO-d_6): δ 166.33, 159.21, 157.64 (d, J = 246.4 Hz), 155.51, 143.78, 142.88, 141.33, 130.20, 127.19, 125.07−124.96 (m), 124.79 (d, J = 17.8 Hz), 123.88, 122.81, 120.73, 104.26, 99.46, 94.47, 35.04, 14.29 (d, J = 5.0 Hz). UPLC/MS [M + H] = 459.496, t_R = 1.49 min.

*(2-((3-(2-Fluoro-3-methylphenyl)-1-methyl-1H-pyrazol-5-yl)amino)-4,6-dihydroxyphenyl)(4-fluoroisoindolin-2-yl)methanone (**9ag**)*. Amide bromide **8b** (66.6 mg, 0.125 mmol, 1 equiv) was coupled to **4z** (28.2 mg, 0.138 mmol, 1.1 equiv) according to General Procedure **E1b**. The resulting product was deprotected according to General Procedure **E2a**. **9ag** (39 mg, 0.082 mmol) was obtained in 66% yield over two steps. ^{1}H NMR (500 MHz, DMSO-d_6): δ 9.68−9.64 (m, 1H), 9.34 (s, 1H), 7.73−7.66 (m, 1H), 7.35−7.27 (m, 1H), 7.25 (s, 1H), 7.20−7.13 (m, 2H), 7.10−7.03 (m, 2H), 6.33 (d, J = 4.1 Hz, 1H), 5.91 (d, J = 2.1 Hz, 1H), 5.68 (d, J = 2.0 Hz, 1H), 4.87−4.67 (m, 4H), 3.63 (s, 3H), 2.23 (d, J = 2.1 Hz, 3H); ^{13}C NMR (126 MHz, DMSO-d_6): δ 166.36, 159.34, 157.65 (d, J = 247.1 Hz), 155.61, 144.25, 142.85, 141.38, 130.21, 124.92 (d, J = 4.1 Hz), 124.76, 123.87 (d, J = 3.6 Hz), 120.73 (d, J = 12.5 Hz), 119.08, 113.59 (d, J = 19.1 Hz), 103.95, 99.49 (d, J = 10.2 Hz), 94.50, 93.29, 79.16, 35.05, 14.28 (d, J = 4.8 Hz). UPLC/MS [M + H] = 477.489, t_R = 1.44 min.

*(2-((3-(2-Fluoro-3-methylphenyl)-1-methyl-1H-pyrazol-5-yl)amino)-4,6-dihydroxyphenyl)(5-fluoroisoindolin-2-yl)methanone (**9ah**)*. Amide bromide **8c** (53.2 mg, 0.1 mmol, 1 equiv) was coupled to **4z** (22.6 mg, 0.11 mmol, 1.1 equiv) according to General Procedure **E1b**. The resulting product was deprotected according to General Procedure **E2a**. **9ah** (18 mg, 0.038 mmol) was obtained in 38% yield over two steps. ^{1}H NMR (500 MHz, DMSO-d_6): δ 9.62 (s, 1H), 9.26 (s, 0H), 7.73−7.66 (m, 1H), 7.35−7.29 (m, 1H), 7.22 (s, 1H), 7.20−7.12 (m, 2H), 7.11−7.02 (m, 2H), 6.32 (d, J = 4.1 Hz, 1H), 5.89 (d, J = 2.1 Hz, 1H), 5.66 (d, J = 2.1 Hz, 1H), 4.84−4.56 (m, 4H), 3.63 (s, 3H), 2.24 (d, J = 2.1 Hz, 3H); ^{13}C NMR (126 MHz, DMSO-d_6): δ 166.30, 160.78, 159.24, 156.66 (d, J = 244.7 Hz), 155.55, 143.88, 142.11 (d, J = 181.7 Hz), 130.16, 125.03−124.87 (m), 124.75 (d, J = 7.8 Hz), 124.41, 123.85 (d, J = 4.3 Hz), 120.74 (d, J = 12.4 Hz), 114.34 (d, J = 24.9 Hz), 109.81 (d, J = 25.6 Hz), 104.12, 99.50 (d, J = 10.4 Hz), 94.48, 93.18, 35.05, 14.26 (d, J = 4.8 Hz). UPLC/MS [M + H] = 477.445, t_R = 1.51 min.

*(2-((3-(2,3-Difluorophenyl)-1-methyl-1H-pyrazol-5-yl)amino)-4,6-dihydroxyphenyl)(isoindolin-2-yl)methanone (**9ai**)*. Amide bromide **8a** (77 mg, 0.150 mmol, 1 equiv) was coupled to **4aa** (34.5 mg, 0.165 mmol, 1.1 equiv) according to General Procedure **E1a**. The resulting product was deprotected according to General Procedure **E2a**. **9ai** (5.7 mg, 0.012 mmol) was obtained in 8% yield over two steps. ^{1}H NMR (500 MHz, DMSO-d_6): δ 9.61 (s, 1H), 9.30 (s, 1H), 7.70−7.63 (m, 1H), 7.35−7.28 (m, 3H), 7.27−7.22 (m, 3H), 7.22−7.16 (m, 1H), 6.37 (d, J = 3.7 Hz, 1H), 5.90 (d, J = 2.0 Hz, 1H), 5.65 (d, J = 2.1 Hz, 1H), 4.79−4.66 (m, 4H), 3.64 (s, 3H); ^{13}C NMR (126 MHz, DMSO-d_6): δ 166.28, 159.19, 155.53, 143.71, 141.77, 136.38, 132.64, 127.16, 124.43, 122.90, 122.78, 104.41, 94.60, 93.20, 35.16. UPLC/MS [M + H] = 463.241, t_R = 1.45 min.

*(2,4-Dihydroxy-6-((1-methyl-3-(2-methyl-3-(trifluoromethyl)-phenyl)-1H-pyrazol-5-yl)amino)phenyl)(isoindolin-2-yl)methanone (**9aj**)*. Amide bromide **8a** (64 mg, 0.125 mmol, 1 equiv) was coupled to **4ab** (35 mg, 0.138 mmol, 1.1 equiv) according to General Procedure **E1b**. The resulting product was deprotected according to General Procedure **E2a**. **9aj** (3.4 mg, 0.007 mmol) was obtained in 6% yield over two steps. ^{1}H NMR (500 MHz, DMSO-d_6): δ 9.60 (s, 1H), 9.30 (s, 1H), 7.66 (t, J = 7.8 Hz, 2H), 7.38 (t, J = 7.8 Hz, 1H), 7.34−7.31 (m, 3H), 7.31−7.25 (m, 2H), 7.23 (s, 1H), 6.27 (s, 1H), 5.89 (d, J = 2.1 Hz, 1H), 5.68 (d, J = 2.0 Hz, 1H), 4.83−4.69 (m, 4H), 3.62 (s, 3H), 2.49 (s, 3H); ^{13}C NMR (126 MHz, DMSO-d_6): δ 166.34, 159.22, 155.52, 147.64, 143.75, 140.96, 136.17, 133.85, 133.27, 127.23, 125.93, 122.84, 104.25, 100.08, 94.47, 93.01, 34.99, 16.38; ^{19}F NMR (470 MHz, DMSO-d_6): δ −59.28. UPLC/MS [M + H] = 509.514, t_R = 1.56 min.

*(2-((3-(3-Chloro-2-fluorophenyl)-1-methyl-1H-pyrazol-5-yl)amino)-4,6-dihydroxyphenyl)(isoindolin-2-yl)methanone (**9ak**)*. Amide bromide **8a** (64 mg, 0.125 mmol, 1 equiv) was coupled to **4ac** (31 mg, 0.138 mmol, 1.1 equiv) according to General Procedure **E1b**. The resulting product was deprotected according to General Procedure **E2b**. **9ak** (18 mg, 0.037 mmol) was obtained in 30% yield over two steps. ^{1}H NMR (500 MHz, DMSO-d_6): δ 9.62 (s, 1H), 9.31 (s, 1H), 7.87−7.80 (m, 1H), 7.51−7.44 (m, 1H), 7.33−7.27 (m, 2H), 7.27−7.19 (m, 4H), 6.38 (d, J = 4.0 Hz, 1H), 5.90 (d, J = 2.1 Hz, 1H), 5.66 (d, J = 2.1 Hz, 1H), 4.87−4.60 (m, 4H), 3.64 (s, 3H); ^{13}C NMR (126 MHz, DMSO-d_6): δ 166.29, 159.20, 155.55, 154.13 (d, J = 250.7 Hz), 143.69, 141.84−141.68 (m), 136.63, 129.05, 127.16, 126.21 (d, J = 3.6 Hz), 125.29 (d, J = 4.3 Hz), 122.86, 122.77, 120.45 (d, J = 18.0 Hz), 104.41, 99.55 (d, J = 9.8 Hz), 94.61, 93.22, 35.18; ^{19}F NMR (470 MHz, DMSO-d_6) δ −116.80 to −124.29 (m). UPLC/MS [M + H] = 479.219, t_R = 1.46 min.

*(2-((3-(2-Fluoro-3-(trifluoromethoxy)phenyl)-1-methyl-1H-pyrazol-5-yl)amino)-4,6-dihydroxyphenyl)(isoindolin-2-yl)methanone (**9al**)*. Amide bromide **8a** (64 mg, 0.125 mmol, 1 equiv) was coupled to **4ad** (38 mg, 0.138 mmol, 1.1 equiv) according to General Procedure **E1b**. The resulting product was deprotected according to General Procedure **E2a**. **9al** (29 mg, 0.056 mmol) was obtained in 45% yield over two steps. ^{1}H NMR (500 MHz, DMSO-d_6): δ 9.63 (s, 1H), 9.32 (s, 1H), 7.93−7.86 (m, 1H), 7.49−7.41 (m, 1H), 7.34−7.20 (m, 6H), 6.40 (d, J = 3.7 Hz, 1H), 5.91 (d, J = 2.1 Hz, 1H), 5.67 (d, J = 2.1 Hz, 1H), 4.81−4.64 (m, 4H), 3.65 (s, 3H); ^{13}C NMR (126 MHz, DMSO-d_6): δ 166.32, 159.23, 155.57, 150.83 (d, J = 254.4 Hz), 143.69, 141.93 (d, J = 1.9 Hz), 141.50, 136.65, 136.23−136.00 (m), 127.18, 126.41 (d, J = 3.3 Hz), 125.00 (d, J = 4.5 Hz), 123.32 (d, J = 9.5 Hz), 122.79, 122.19, 121.12, 119.07, 104.49, 99.50 (d, J = 9.2 Hz), 94.68, 93.28, 35.22; ^{19}F NMR (470 MHz, DMSO-d_6) δ −57.82 (d, J = 4.9 Hz), −134.22 to −134.33 (m). UPLC/MS [M + H] = 529.562, t_R = 1.54 min.

*(2-((3-(2,5-Difluorophenyl)-1-methyl-1H-pyrazol-5-yl)amino)-4,6-dihydroxyphenyl)(isoindolin-2-yl)methanone (**9am**)*. Amide bromide **8a** (77 mg, 0.150 mmol, 1 equiv) was coupled to **4ae** (34.5 mg, 0.165 mmol, 1.1 equiv) according to General Procedure **E1a**. The

https://dx.doi.org/10.1021/acs.jmedchem.0c01777
J. Med. Chem. 2021, 64, 1139−1169

resulting product was deprotected according to General Procedure **E2a**. **9am** (14.6 mg, 0.032 mmol) was obtained in 21% yield over two steps. ^{1}H NMR (500 MHz, DMSO-d_6): δ 9.62 (s, 1H), 9.30 (s, 1H), 7.62−7.56 (m, 1H), 7.34−7.23 (m, 6H), 7.19−7.11 (m, 1H), 6.38 (d, J = 4.0 Hz, 1H), 5.90 (d, J = 2.1 Hz, 1H), 5.63 (d, J = 2.1 Hz, 1H), 4.84−4.60 (m, 4H), 3.64 (s, 3H); ^{13}C NMR (126 MHz, DMSO-d_6): δ 166.28, 159.19, 157.26, 155.53, 154.23 (d, J = 243.9 Hz), 143.70, 141.85 (d, J = 2.4 Hz), 141.70, 127.19, 122.80, 118.04−117.56 (m), 115.52−114.98 (m), 113.10−112.60 (m), 104.44, 99.60 (d, J = 10.1 Hz), 94.61, 93.15, 35.17 (d, J = 241.7 Hz); ^{19}F NMR (470 MHz, DMSO-d_6) δ −118.66 to −118.78 (m), −121.71 to −121.84 (m) UPLC/MS [M + H] = 463.241, t_R = 1.46 min.

(2-((3-(2-Chloro-5-fluorophenyl)-1-methyl-1H-pyrazol-5-yl)-amino)-4,6-dihydroxyphenyl)(isoindolin-2-yl)methanone (***9an***). Amide bromide **8a** (64 mg, 0.125 mmol, 1 equiv) was coupled to **4af** (31 mg, 0.138 mmol, 1.1 equiv) according to General Procedure **E1b**. The resulting product was deprotected according to General Procedure **E2b**. **9an** (18 mg, 0.038 mmol) was obtained in 30% yield over two steps. ^{1}H NMR (500 MHz, DMSO-d_6): δ 9.62 (s, 1H), 9.32 (s, 1H), 7.56−7.48 (m, 2H), 7.33−7.29 (m, 2H), 7.28−7.22 (m, 3H), 7.22−7.15 (m, 1H), 6.56 (s, 1H), 5.91 (d, J = 2.1 Hz, 1H), 5.66 (d, J = 2.0 Hz, 1H), 4.80−4.69 (m, 4H), 3.64 (s, 3H); ^{13}C NMR (126 MHz, DMSO-d_6): δ 166.30, 160.66 (d, J = 243.7 Hz), 159.21, 155.54, 144.63 (d, J = 1.9 Hz), 143.70, 141.25, 136.60, 133.85 (d, J = 8.5 Hz), 132.11 (d, J = 8.7 Hz), 127.21, 125.85 (d, J = 3.0 Hz), 122.82, 115.74 (d, J = 22.7 Hz), 115.64 (d, J = 22.1 Hz), 104.43, 100.19, 94.61, 93.12, 35.15; ^{19}F NMR (470 MHz, DMSO-d_6) δ −115.27 to −115.40 (m). UPLC/MS [M + H] = 479.259, t_R = 1.53 min.

(2-((3-(5-Chloro-2-fluorophenyl)-1-methyl-1H-pyrazol-5-yl)-amino)-4,6-dihydroxyphenyl)(isoindolin-2-yl)methanone (***9ao***). Amide bromide **8a** (64 mg, 0.125 mmol, 1 equiv) was coupled to **4ag** (31 mg, 0.138 mmol, 1.1 equiv) according to General Procedure **E1b**. The resulting product was deprotected according to General Procedure **E2b**. **9ao** (18 mg, 0.037 mmol) was obtained in 30% yield over two steps. ^{1}H NMR (500 MHz, DMSO-d_6): δ 9.63 (s, 1H), 9.32 (s, 1H), 7.89−7.82 (m, 1H), 7.39−7.33 (m, 1H), 7.33−7.21 (m, 6H), 6.38 (d, J = 4.0 Hz, 1H), 5.91 (d, J = 2.1 Hz, 1H), 5.65 (d, J = 2.1 Hz, 1H), 4.96−4.53 (m, 4H), 3.64 (s, 3H); ^{13}C NMR (126 MHz, DMSO-d_6): δ 166.30, 159.21, 157.66 (d, J = 248.4 Hz), 155.55, 143.69, 141.92 (d, J = 2.3 Hz), 141.36 (d, J = 2.1 Hz), 136.61, 128.57−128.40 (m), 127.19, 126.41 (d, J = 4.3 Hz), 122.87 (d, J = 13.3 Hz), 122.79, 118.19 (d, J = 24.2 Hz), 104.49, 99.62 (d, J = 9.9 Hz), 94.67, 93.25, 35.20; ^{19}F NMR (470 MHz, DMSO-d_6) δ −118.55 to −118.64 (m). UPLC/MS [M + H] = 479.219, t_R = 1.57 min.

(2-((3-(2-Fluoro-5-methylphenyl)-1-methyl-1H-pyrazol-5-yl)-amino)-4,6-dihydroxyphenyl)(isoindolin-2-yl)methanone (***9ap***). Amide bromide **8a** (77 mg, 0.150 mmol, 1 equiv) was coupled to **4ah** (33.9 mg, 0.165 mmol, 1.1 equiv) according to General Procedure **E1a**. The resulting product was deprotected according to General Procedure **E2a**. **9ap** (12.5 mg, 0.027 mmol) was obtained in 18% yield over two steps. ^{1}H NMR (500 MHz, DMSO-d_6): δ 9.60 (s, 1H), 9.29 (s, 1H), 7.72−7.66 (m, 1H), 7.37−7.30 (m, 2H), 7.30−7.23 (m, 2H), 7.19 (s, 1H), 7.14−7.05 (m, 2H), 6.33 (d, J = 3.9 Hz, 1H), 5.89 (d, J = 2.1 Hz, 1H), 5.63 (d, J = 2.1 Hz, 1H), 4.82−4.67 (m, 4H), 3.62 (s, 3H), 2.30 (s, 3H); ^{13}C NMR (126 MHz, DMSO-d_6): δ 166.32, 159.20, 156.44 (d, J = 244.4 Hz), 155.49, 143.78, 142.78, 141.37 (d, J = 2.1 Hz), 133.37 (d, J = 3.2 Hz), 129.35, 127.55 (d, J = 4.1 Hz), 127.21, 120.56 (d, J = 11.9 Hz), 115.75 (d, J = 22.3 Hz), 104.31, 99.55, 94.48, 92.90, 35.03, 20.22. UPLC/MS [M + H] = 459.256, t_R = 1.52 min.

(2-((3-(2-Fluoro-5-(trifluoromethyl)phenyl)-1-methyl-1H-pyrazol-5-yl)amino)-4,6-dihydroxyphenyl)(isoindolin-2-yl)methanone (***9aq***). Amide bromide **8a** (64 mg, 0.125 mmol, 1 equiv) was coupled to **4ai** (36 mg, 0.138 mmol, 1.1 equiv) according to General Procedure **E1b**. The resulting product was deprotected according to General Procedure **E2a**. **9aq** (36 mg, 0.071 mmol) was obtained in 57% yield over two steps. ^{1}H NMR (500 MHz, DMSO-d_6): δ 9.66 (s, 1H), 9.34 (s, 1H), 8.21−8.15 (m, 1H), 7.72−7.65 (m, 1H), 7.49−7.41 (m, 1H), 7.28 (q, J = 3.2 Hz, 3H), 7.25−7.17 (m, 2H), 6.42 (d, J = 4.1 Hz, 1H), 5.93 (d, J = 2.1 Hz, 1H), 5.68 (s, 1H), 4.72 (s, 4H), 3.67 (s, 3H); ^{13}C NMR (126 MHz, DMSO-d_6): δ 166.78, 161.24 (d, J = 254.5 Hz), 159.68, 156.06, 144.19, 142.61 (d, J = 2.3 Hz), 141.56, 137.13, 127.62, 126.55−125.77 (m), 125.39, 124.86−124.44 (m), 123.21 (d, J = 3.0 Hz), 122.48 (d, J = 13.2 Hz), 118.08 (d, J = 23.5 Hz), 105.03, 100.17 (d, J = 10.3 Hz), 95.20, 93.91, 49.04, 35.69. UPLC/MS [M + H] = 513.212, t_R = 1.63 min.

(2-((3-(2-Fluoro-5-(trifluoromethoxy)phenyl)-1-methyl-1H-pyrazol-5-yl)amino)-4,6-dihydroxyphenyl)(isoindolin-2-yl)methanone (***9ar***). Amide bromide **8a** (64 mg, 0.125 mmol, 1 equiv) was coupled to **4aj** (38 mg, 0.138 mmol, 1.1 equiv) according to General Procedure **E1b**. The resulting product was deprotected according to General Procedure **E2a**. **9ar** (33 mg, 0.063 mmol) was obtained in 50% yield over two steps. ^{1}H NMR (500 MHz, DMSO-d_6): δ 9.64 (d, J = 1.3 Hz, 1H), 9.32 (s, 1H), 7.82−7.76 (m, 1H), 7.40−7.19 (m, 7H), 6.40 (d, J = 4.1 Hz, 1H), 5.91 (d, J = 2.1 Hz, 1H), 5.65 (d, J = 2.0 Hz, 1H), 4.84−4.62 (m, 4H), 3.65 (s, 3H); ^{13}C NMR (126 MHz, DMSO-d_6): δ 166.31, 159.22, 157.27 (d, J = 248.5 Hz), 155.58, 144.54−144.35 (m), 143.74, 142.08 (d, J = 2.3 Hz), 141.25 (d, J = 2.2 Hz), 136.71, 127.18, 122.78, 122.65, 121.59 (d, J = 8.6 Hz), 121.09, 119.21 (d, J = 5.1 Hz), 119.05, 118.12 (d, J = 24.9 Hz), 104.53, 99.71 (d, J = 10.5 Hz), 94.70, 93.34, 35.23; ^{19}F NMR (470 MHz, DMSO-d_6) δ −57.20, −117.44 to −117.53 (m). UPLC/MS [M + H] = 529.529, t_R = 1.66 min.

(2-((3-(2,6-Difluorophenyl)-1-methyl-1H-pyrazol-5-yl)amino)-4,6-dihydroxyphenyl)(isoindolin-2-yl)methanone (***9as***). Amide bromide **8a** (45 mg, 0.087 mmol, 1 equiv) was coupled to **4ak** (20 mg, 0.096 mmol, 1.1 equiv) according to General Procedure **E1a**. The resulting product was deprotected according to General Procedure **E2a**. **9as** (20.6 mg, 0.045 mmol) was obtained in 52% yield over two steps. ^{1}H NMR (500 MHz, DMSO-d_6): δ 9.63 (s, 1H), 9.33 (s, 1H), 7.44−7.36 (m, 1H), 7.32 (s, 2H), 7.30−7.24 (m, 2H), 7.24−7.17 (m, 1H), 7.14 (t, J = 8.3 Hz, 2H), 6.27−6.23 (m, 1H), 5.89 (d, J = 2.1 Hz, 1H), 5.61 (d, J = 2.1 Hz, 1H), 4.87−4.56 (m, 4H), 3.62 (s, 3H); ^{13}C NMR (126 MHz, DMSO-d_6): δ 166.35, 159.73 (dd, J = 249.7, 7.3 Hz), 159.25, 155.53, 143.72, 140.91, 137.83, 129.40, 127.26, 112.02 (d, J = 25.9 Hz), 112.02 (d, J = 15.0 Hz), 111.43, 104.32, 101.85−100.61 (m), 94.52, 92.84, 35.13; ^{19}F NMR (470 MHz, DMSO-d_6) δ −112.05 to −112.16 (m). UPLC/MS [M + H] = 463.225, t_R = 1.36 min.

(2-((3-(4-Chloro-2-fluorophenyl)-1-methyl-1H-pyrazol-5-yl)-amino)-4,6-dihydroxyphenyl)(isoindolin-2-yl)methanone (***9at***). Amide bromide **8a** (64 mg, 0.125 mmol, 1 equiv) was coupled to **4al** (31 mg, 0.138 mmol, 1.1 equiv) according to General Procedure **E1b**. The resulting product was deprotected according to General Procedure **E2b**. **9at** (7 mg, 0.014 mmol) was obtained in 11% yield over two steps. ^{1}H NMR (500 MHz, DMSO-d_6): δ 9.61 (s, 1H), 9.30 (s, 1H), 7.89 (t, J = 8.5 Hz, 1H), 7.46−7.40 (m, 1H), 7.32−7.21 (m, 6H), 6.34 (d, J = 4.0 Hz, 1H), 5.89 (d, J = 2.1 Hz, 1H), 5.63 (d, J = 2.1 Hz, 1H), 4.87−4.52 (m, 4H), 3.63 (s, 3H); ^{13}C NMR (126 MHz, DMSO-d_6): δ 166.29, 159.20, 157.79 (d, J = 250.8 Hz), 155.53, 143.72, 141.72 (t, J = 2.5 Hz), 136.72, 132.15 (d, J = 10.5 Hz), 128.50 (d, J = 4.6 Hz), 127.18, 124.84 (d, J = 3.2 Hz), 122.80, 120.19 (d, J = 11.8 Hz), 116.65 (d, J = 26.1 Hz), 104.39, 99.42 (d, J = 9.7 Hz), 94.58, 93.11, 35.14; ^{19}F NMR (470 MHz, DMSO-d_6) δ −113.56 to −113.67 (m). UPLC/MS [M + H] = 479.259, t_R = 1.58 min.

(2-((3-(2-Chloro-4-fluorophenyl)-1-methyl-1H-pyrazol-5-yl)-amino)-4,6-dihydroxyphenyl)(isoindolin-2-yl)methanone (***9au***). Amide bromide **8a** (64 mg, 0.125 mmol, 1 equiv) was coupled to **4am** (31 mg, 0.138 mmol, 1.1 equiv) according to General Procedure **E1b**. The resulting product was deprotected according to General Procedure **E2b**. **9au** (18 mg, 0.037 mmol) was obtained in 30% yield over two steps. ^{1}H NMR (500 MHz, DMSO-d_6): δ 9.62 (s, 1H), 9.31 (s, 1H), 7.80−7.74 (m, 1H), 7.45 (dd, J = 8.9, 2.7 Hz, 1H), 7.32 (s, 2H), 7.29−7.20 (m, 4H), 6.45 (s, 1H), 5.90 (d, J = 2.1 Hz, 1H), 5.66 (d, J = 2.0 Hz, 1H), 4.85−4.64 (m, 4H), 3.62 (s, 3H); ^{13}C NMR (126 MHz, DMSO-d_6): δ 166.33, 160.98 (d, J = 247.9 Hz), 159.22, 155.53, 144.92, 143.74, 140.96, 136.58, 131.46 (d, J = 10.5 Hz), 131.29 (d, J = 8.7 Hz), 128.94 (d, J = 3.4 Hz), 127.22, 122.84, 117.17 (d, J = 24.9 Hz), 114.56 (d, J = 21.1 Hz), 104.33, 99.96, 94.54, 93.00, 35.04; ^{19}F NMR (470 MHz, DMSO-d_6) δ −113.06 to −113.20 (m). UPLC/MS [M + H] = 479.219, t_R = 1.52 min.

(2-((1-(tert-Butyl)-3-(2,3-dimethylphenyl)-1H-pyrazol-5-yl)-amino)-4,6-dihydroxyphenyl)(isoindolin-2-yl)methanone (***9av***).

https://dx.doi.org/10.1021/acs.jmedchem.0c01777
J. Med. Chem. 2021, 64, 1139−1169

Amide bromide **8a** (64 mg, 0.125 mmol, 1 equiv) was coupled to **4ao** (33 mg, 0.138 mmol, 1.1 equiv) according to General Procedure **E1b**. The resulting product was deprotected according to General Procedure **E2a**. **9av** (31 mg, 0.063 mmol) was obtained in 50% yield over two steps. ^{1}H NMR (500 MHz, DMSO-d_6): δ 9.68 (s, 1H), 9.30 (s, 1H), 7.37−7.32 (m, 2H), 7.32−7.25 (m, 3H), 7.16−7.05 (m, 2H), 6.99 (s, 1H), 6.24 (s, 1H), 5.86 (d, J = 2.1 Hz, 1H), 5.72 (d, J = 2.1 Hz, 1H), 4.89−4.75 (m, 4H), 2.34 (s, 3H), 2.27 (s, 3H), 1.55 (s, 9H); ^{13}C NMR (126 MHz, DMSO-d_6): δ 166.92, 159.44, 147.76, 145.08, 139.31, 136.86, 136.70, 133.91, 133.87, 128.68, 127.27, 126.89, 125.09, 122.85, 103.17, 103.03, 93.79, 92.11, 79.17, 59.17, 29.48, 20.43, 16.60. UPLC/MS [M + H] = 497.600, t_R = 1.80 min.

(2-((3-(5-Fluoro-2-methylphenyl)-1-isopropyl-1H-pyrazol-5-yl)-amino)-4,6-dihydroxyphenyl)(isoindolin-2-yl)methanone (***9aw***). Amide bromide **8a** (64 mg, 0.125 mmol, 1 equiv) was coupled to **4ap** (32 mg, 0.138 mmol, 1.1 equiv) according to General Procedure **E1b**. The resulting product was deprotected according to General Procedure **E2a**. **9aw** (40 mg, 0.083 mmol) was obtained in 66% yield over two steps. ^{1}H NMR (500 MHz, DMSO-d_6): δ 9.63 (s, 1H), 9.30 (s, 1H), 7.38−7.29 (m, 3H), 7.30−7.22 (m, 3H), 7.13 (s, 1H), 7.05−6.97 (m, 1H), 6.35 (s, 1H), 5.88 (d, J = 2.1 Hz, 1H), 5.63 (d, J = 2.1 Hz, 1H), 4.87−4.69 (m, 4H), 4.51−4.40 (m, J = 6.9 Hz, 1H), 2.44 (s, 3H), 1.35 (d, J = 6.5 Hz, 6H); ^{13}C NMR (126 MHz, DMSO-d_6): δ 166.48, 160.43 (d, J = 240.5 Hz), 159.26, 155.56, 147.71 (d, J = 2.4 Hz), 144.58, 139.50, 136.72, 135.06 (d, J = 7.9 Hz), 132.59 (d, J = 8.0 Hz), 130.93 (d, J = 2.9 Hz), 127.25, 122.85, 114.15 (d, J = 22.0 Hz), 113.51 (d, J = 20.7 Hz), 103.90, 100.20, 94.21, 92.57, 47.90, 22.20, 20.66; ^{19}F NMR (470 MHz, DMSO-d_6) δ −117.99 to −118.09 (m). UPLC/MS [M + H] = 487.545, t_R = 1.70 min.

(2-((1-(tert-Butyl)-3-(5-fluoro-2-methylphenyl)-1H-pyrazol-5-yl)-amino)-4,6-dihydroxyphenyl)(isoindolin-2-yl)methanone (***9ax***). Amide bromide **8a** (64 mg, 0.125 mmol, 1 equiv) was coupled to **4aq** (34 mg, 0.138 mmol, 1.1 equiv) according to General Procedure **E1b**. The resulting product was deprotected according to General Procedure **E2a**. **9ax** (35.5 mg, 0.067 mmol) was obtained in 54% yield over two steps. ^{1}H NMR (500 MHz, DMSO-d_6): δ 9.70 (s, 1H), 9.29 (s, 1H), 7.40−7.32 (m, 3H), 7.32−7.22 (m, 3H), 7.05−6.97 (m, 2H), 6.47 (s, 1H), 5.86 (d, J = 2.1 Hz, 1H), 5.70 (d, J = 2.1 Hz, 1H), 4.95−4.62 (m, 4H), 3.35 (s, 3H), 2.46 (s, 3H), 1.56 (s, 9H); ^{13}C NMR (126 MHz, DMSO-d_6): δ 166.90, 160.47 (d, J = 240.3 Hz), 159.45, 155.56, 146.05 (d, J = 2.4 Hz), 145.01, 139.78, 136.68, 134.88 (d, J = 7.7 Hz), 132.67 (d, J = 7.9 Hz), 130.90 (d, J = 2.9 Hz), 127.28, 122.85, 114.10 (d, J = 22.0 Hz), 113.48 (d, J = 20.8 Hz), 103.08, 102.94, 93.86, 92.18, 59.47, 29.38, 20.82; ^{19}F NMR (470 MHz, DMSO-d_6) δ −117.90 to −118.08 (m). UPLC/MS [M + H] = 501.569, t_R = 1.87 min.

(2-((1-Cyclopentyl-3-(5-fluoro-2-methylphenyl)-1H-pyrazol-5-yl)-amino)-4,6-dihydroxyphenyl)(isoindolin-2-yl)methanone (***9ay***). Amide bromide **8a** (64 mg, 0.125 mmol, 1 equiv) was coupled to **4ar** (36 mg, 0.138 mmol, 1.1 equiv) according to General Procedure **E1b**. The resulting product was deprotected according to General Procedure **E2a**. **9ay** (31 mg, 0.060 mmol) was obtained in 50% yield over two steps. ^{1}H NMR (500 MHz, DMSO-d_6): δ 9.64 (s, 1H), 9.31 (s, 1H), 7.39−7.30 (m, 3H), 7.30−7.22 (m, 3H), 7.15 (s, 1H), 7.04−6.97 (m, 1H), 6.36 (s, 1H), 5.88 (d, J = 2.1 Hz, 1H), 5.63 (d, J = 2.1 Hz, 1H), 4.87−4.69 (m, 4H), 4.61 (p, J = 7.1 Hz, 1H), 2.44 (s, 3H), 1.92 (s, 4H), 1.87−1.76 (m, 2H), 1.59−1.50 (m, 2H); ^{13}C NMR (126 MHz, DMSO-d_6): δ 166.50, 160.44 (d, J = 240.3 Hz), 159.25, 155.56, 147.70 (d, J = 2.3 Hz), 144.43, 140.18, 136.71, 134.96 (d, J = 7.7 Hz), 132.62 (d, J = 8.0 Hz), 130.92 (d, J = 2.8 Hz), 127.26, 122.84, 114.17 (d, J = 21.9 Hz), 113.51 (d, J = 20.7 Hz), 103.93, 100.05, 94.28, 92.72, 57.03, 32.28, 24.18, 20.72; ^{19}F NMR (470 MHz, DMSO-d_6) δ −117.94 to −118.06 (m). UPLC/MS [M + H] = 513.564, t_R = 1.83 min.

(2-((1-Cyclohexyl-3-(5-fluoro-2-methylphenyl)-1H-pyrazol-5-yl)-amino)-4,6-dihydroxyphenyl)(isoindolin-2-yl)methanone (***9az***). Amide bromide **8a** (64 mg, 0.125 mmol, 1 equiv) was coupled to **4as** (38 mg, 0.138 mmol, 1.1 equiv) according to General Procedure **E1b**. The resulting product was deprotected according to General Procedure **E2a**. **9az** (35 mg, 0.066 mmol) was obtained in 53% yield over two steps. ^{1}H NMR (500 MHz, DMSO-d_6): δ 9.60 (s, 1H), 9.28 (s, 1H), 7.36−7.29 (m, 3H), 7.30−7.21 (m, 3H), 7.11 (s, 1H), 7.00 (td, J = 8.4, 2.9 Hz, 1H), 6.36 (s, 1H), 5.87 (d, J = 2.1 Hz, 1H), 5.64 (d, J = 2.1 Hz, 1H), 4.87−4.70 (m, 4H), 4.07−4.00 (m, 1H), 2.43 (s, 3H), 1.90−1.70 (m, 6H), 1.64−1.55 (m, 1H), 1.25−1.12 (m, 3H); ^{13}C NMR (126 MHz, DMSO-d_6): δ 166.47, 160.42 (d, J = 240.3 Hz), 159.20, 155.52, 147.59 (d, J = 2.1 Hz), 144.50, 139.62, 136.65, 135.02 (d, J = 7.7 Hz), 132.57 (d, J = 7.9 Hz), 130.91 (d, J = 2.9 Hz), 127.25, 122.82, 114.13 (d, J = 22.0 Hz), 113.47 (d, J = 20.6 Hz), 103.99, 100.25, 94.25, 92.65, 55.33, 32.27, 25.05, 24.89, 20.69; ^{19}F NMR (470 MHz, DMSO-d_6) δ −118.01 to −118.16 (m). UPLC/MS [M + H] = 527.578, t_R = 1.90 min.

(2-((3-(2-Fluoro-3-methylphenyl)-1-isopropyl-1H-pyrazol-5-yl)-amino)-4,6-dihydroxyphenyl)(isoindolin-2-yl)methanone (***9ba***). Amide bromide **8a** (64 mg, 0.125 mmol, 1 equiv) was coupled to **4at** (32 mg, 0.138 mmol, 1.1 equiv) according to General Procedure **E1b**. The resulting product was deprotected according to General Procedure **E2a**. **9ba** (38 mg, 0.078 mmol) was obtained in 65% yield over two steps. ^{1}H NMR (500 MHz, DMSO-d_6): δ 9.62 (s, 1H), 9.29 (s, 1H), 7.79−7.71 (m, 1H), 7.36−7.30 (m, 2H), 7.30−7.23 (m, 2H), 7.21−7.15 (m, 1H), 7.14 (s, 1H), 7.09 (t, J = 7.6 Hz, 1H), 6.34 (d, J = 4.1 Hz, 1H), 5.87 (d, J = 2.1 Hz, 1H), 5.61 (d, J = 2.1 Hz, 1H), 4.85−4.68 (m, 4H), 4.52−4.40 (m, 1H), 2.25 (d, J = 2.1 Hz, 3H), 1.36 (d, J = 6.2 Hz, 6H); ^{13}C NMR (126 MHz, DMSO-d_6): δ 166.46, 159.25, 157.71 (d, J = 247.1 Hz), 155.56, 144.57, 142.99, 139.93 (d, J = 2.2 Hz), 136.72, 130.21 (d, J = 5.1 Hz), 127.26, 125.17 (d, J = 3.8 Hz), 124.86 (d, J = 17.6 Hz), 123.91 (d, J = 3.8 Hz), 122.87, 121.09 (d, J = 12.4 Hz), 104.00, 100.52 (d, J = 10.1 Hz), 94.26, 92.62, 48.02, 22.23, 14.35 (d, J = 4.8 Hz); ^{19}F NMR (470 MHz, DMSO-d_6) δ −120.64 to −121.59 (m). UPLC/MS [M + H] = 487.545, t_R = 1.70 min.

(2-((1-(tert-Butyl)-3-(2-fluoro-3-methylphenyl)-1H-pyrazol-5-yl)-amino)-4,6-dihydroxyphenyl)(isoindolin-2-yl)methanone (***9bb***). Amide bromide **8a** (77 mg, 0.150 mmol, 1 equiv) was coupled to **4au** (41 mg, 0.165 mmol, 1.1 equiv) according to General Procedure **E1b**. The resulting product was deprotected according to General Procedure **E2a**. **9bb** (41.8 mg, 0.084 mmol) was obtained in 56% yield over two steps. ^{1}H NMR (500 MHz, DMSO-d_6): δ 9.70 (s, 1H), 9.29 (s, 1H), 7.80−7.73 (m, 1H), 7.38−7.32 (m, 2H), 7.31−7.25 (m, 2H), 7.22−7.15 (m, 1H), 7.10 (t, J = 7.6 Hz, 1H), 7.02 (s, 1H), 6.43 (d, J = 4.2 Hz, 1H), 5.87 (d, J = 2.1 Hz, 1H), 5.68 (d, J = 2.1 Hz, 1H), 4.86−4.71 (m, 4H), 2.26 (d, J = 2.1 Hz, 3H), 1.57 (s, 9H); ^{13}C NMR (126 MHz, DMSO-d_6): δ 166.87, 159.42, 157.76 (d, J = 246.9 Hz), 155.56, 144.96, 141.26, 140.21 (d, J = 2.3 Hz), 136.68, 130.19 (d, J = 4.8 Hz), 127.27, 125.09 (d, J = 3.8 Hz), 124.84 (d, J = 17.5 Hz), 123.93 (d, J = 3.8 Hz), 122.85, 121.03 (d, J = 12.6 Hz), 103.29 (d, J = 10.1 Hz), 103.18, 93.94, 92.22, 59.59, 29.37, 14.32 (d, J = 4.7 Hz); ^{19}F NMR (470 MHz, DMSO-d_6) δ −121.11 to −121.25 (m). UPLC/MS [M + H] = 501.437, t_R = 1.88 min.

(2-((1-Cyclopentyl-3-(2-fluoro-3-methylphenyl)-1H-pyrazol-5-yl)-amino)-4,6-dihydroxyphenyl)(isoindolin-2-yl)methanone (***9bc***). Amide bromide **8a** (64 mg, 0.125 mmol, 1 equiv) was coupled to **4av** (36 mg, 0.138 mmol, 1.1 equiv) according to General Procedure **E1b**. The resulting product was deprotected according to General Procedure **E2a**. **9bc** (43 mg, 0.085 mmol) was obtained in 68% yield over two steps. ^{1}H NMR (500 MHz, DMSO-d_6): δ 9.63 (s, 1H), 9.30 (s, 1H), 7.77−7.70 (m, 1H), 7.36−7.30 (m, 2H), 7.26 (dd, J = 5.6, 3.2 Hz, 2H), 7.21−7.15 (m, 2H), 7.09 (t, J = 7.6 Hz, 1H), 6.35 (d, J = 4.1 Hz, 1H), 5.88 (d, J = 2.1 Hz, 1H), 5.62 (d, J = 2.1 Hz, 1H), 4.76 (s, 4H), 4.61 (p, J = 7.3 Hz, 1H), 2.25 (d, J = 2.1 Hz, 3H), 1.95−1.89 (m, 4H), 1.87−1.76 (m, 2H), 1.58−1.52 (m, 2H); ^{13}C NMR (126 MHz, DMSO-d_6): δ 166.50, 159.25, 157.72 (d, J = 247.0 Hz), 155.56, 144.44, 142.94, 140.62 (d, J = 2.3 Hz), 136.72, 130.23 (d, J = 5.0 Hz), 127.27, 125.17 (d, J = 3.9 Hz), 124.87 (d, J = 17.5 Hz), 123.94 (d, J = 3.8 Hz), 122.86, 121.06 (d, J = 12.4 Hz), 104.03, 100.43 (d, J = 10.0 Hz), 94.34, 92.75, 57.15, 32.22, 24.15, 14.35 (d, J = 4.7 Hz); ^{19}F NMR (470 MHz, DMSO-d_6) δ −119.76 to −122.97 (m). UPLC/MS [M + H] = 513.564, t_R = 1.80 min.

(2-((1-Cyclohexyl-3-(2-fluoro-3-methylphenyl)-1H-pyrazol-5-yl)-amino)-4,6-dihydroxyphenyl)(isoindolin-2-yl)methanone (***9bd***). Amide bromide **8a** (77 mg, 0.150 mmol, 1 equiv) was coupled to **4aw** (45 mg, 0.165 mmol, 1.1 equiv) according to General Procedure **E1b**. The resulting product was deprotected according to General

https://dx.doi.org/10.1021/acs.jmedchem.0c01777
J. Med. Chem. 2021, 64, 1139−1169

Procedure **E2a**. **9bd** (50.7 mg, 0.096 mmol) was obtained in 64% yield over two steps. ^{1}H NMR (500 MHz, DMSO-d_6): δ 9.60 (s, 1H), 9.28 (s, 1H), 7.77−7.70 (m, 1H), 7.35−7.30 (m, 2H), 7.29−7.22 (m, 2H), 7.20−7.13 (m, 1H), 7.13−7.05 (m, 2H), 6.35 (d, J = 4.1 Hz, 1H), 5.87 (d, J = 2.1 Hz, 1H), 5.62 (d, J = 2.0 Hz, 1H), 4.84−4.64 (m, 4H), 4.10−4.00 (m, 1H), 2.24 (d, J = 2.0 Hz, 3H), 1.79 (d, J = 28.9 Hz, 6H), 1.61−1.57 (m, 1H), 1.26−1.11 (m, 3H); ^{13}C NMR (126 MHz, DMSO-d_6): δ 166.50, 159.23, 157.71 (d, J = 247.1 Hz), 155.55, 144.52, 142.90, 140.04 (d, J = 2.1 Hz), 136.68, 130.19 (d, J = 4.8 Hz), 127.27, 125.15 (d, J = 3.8 Hz), 124.86 (d, J = 17.5 Hz), 123.90 (d, J = 3.8 Hz), 122.85, 121.09 (d, J = 12.4 Hz), 104.08, 100.60 (d, J = 10.1 Hz), 94.32, 92.70, 55.49, 32.30, 25.12, 24.93, 14.35 (d, J = 4.7 Hz); ^{19}F NMR (470 MHz, DMSO-d_6) δ −120.94 to −121.05 (m). UPLC/MS [M + H] = 527.589, t_R =1.90 min.

*(2-((3-(2,3-Difluorophenyl)-1-isopropyl-1H-pyrazol-5-yl)amino)-4,6-dihydroxyphenyl)(isoindolin-2-yl)methanone (**9be**).* Amide bromide **8a** (64 mg, 0.125 mmol, 1 equiv) was coupled to **4ax** (33 mg, 0.138 mmol, 1.1 equiv) according to General Procedure **E1b**. The resulting product was deprotected according to General Procedure **E2a**. **9be** (33 mg, 0.067 mmol) was obtained in 56% yield over two steps. ^{1}H NMR (500 MHz, DMSO-d_6): δ 9.65 (s, 1H), 9.31 (s, 1H), 7.75−7.68 (m, 1H), 7.41−7.09 (m, 7H), 6.37 (d, J = 3.7 Hz, 1H), 5.89 (d, J = 2.1 Hz, 1H), 5.61 (d, J = 2.0 Hz, 1H), 4.76−4.71 (m, 4H), 4.53−4.43 (m, 1H), 1.38−1.33 (m, 6H); ^{13}C NMR (126 MHz, DMSO-d_6): δ 166.40, 159.22, 155.62, 150.30 (d, J = 244.6 Hz), 147.06 (d, J = 248.9 Hz), 144.44, 140.40, 127.20, 124.63, 123.59, 122.80, 122.50, 115.63 (d, J = 16.6 Hz), 104.14, 100.40 (d, J = 8.7 Hz), 94.41, 92.85, 48.16, 22.16. UPLC/MS [M + H] = 491.531, t_R = 1.59 min.

*(2-((1-(tert-Butyl)-3-(2,3-difluorophenyl)-1H-pyrazol-5-yl)-amino)-4,6-dihydroxyphenyl)(isoindolin-2-yl)methanone (**9bf**).* Amide bromide **8a** (64 mg, 0.125 mmol, 1 equiv) was coupled to **4ay** (34.6 mg, 0.138 mmol, 1.1 equiv) according to General Procedure **E1b**. The resulting product was deprotected according to General Procedure **E2a**. **9bf** (33.4 mg, 0.066 mmol) was obtained in 53% yield over two steps. ^{1}H NMR (500 MHz, DMSO-d_6): δ 9.74 (s, 1H), 9.32 (s, 1H), 7.77−7.70 (m, 1H), 7.37−7.18 (m, 6H), 7.05 (s, 1H), 6.48 (d, J = 3.8 Hz, 1H), 5.88 (d, J = 2.1 Hz, 1H), 5.67 (d, J = 2.1 Hz, 1H), 4.82−4.79 (m, 4H), 1.57 (s, 9H); ^{13}C NMR (126 MHz, DMSO-d_6): δ 166.86, 159.44, 155.62, 150.40 (dd, J = 244.2, 12.7 Hz), 147.11 (dd, J = 249.6, 13.8 Hz), 144.89, 140.68 (d, J = 1.9 Hz), 140.21 (d, J = 3.4 Hz), 136.68, 127.30, 124.87−124.61 (m), 123.55 (d, J = 8.3 Hz), 122.87, 122.52 (t, J = 3.0 Hz), 115.71 (d, J = 17.1 Hz), 103.35, 103.29 (d, J = 1.9 Hz), 94.06, 92.34, 59.91, 29.34; ^{19}F NMR (470 MHz, DMSO-d_6) δ −138.74 to −139.72 (m), −142.92 to −143.90 (m). UPLC/MS [M + H] = 505.538, t_R = 1.83 min.

*(2-((1-(tert-Butyl)-3-(2,3-difluorophenyl)-1H-pyrazol-5-yl)-amino)-4,6-dihydroxyphenyl)(4-fluoroisoindolin-2-yl)methanone (**9bg**).* Amide bromide **8b** (67 mg, 0.125 mmol, 1 equiv) was coupled to **4ay** (35 mg, 0.138 mmol, 1.1 equiv) according to General Procedure **E1b**. The resulting product was deprotected according to General Procedure **E2a**. **9bg** (34 mg, 0.066 mmol) was obtained in 53% yield over two steps. ^{1}H NMR (500 MHz, DMSO-d_6): δ 9.77 (s, 1H), 9.33 (s, 1H), 7.77−7.70 (m, 1H), 7.38−7.27 (m, 2H), 7.26−7.17 (m, 2H), 7.14−7.04 (m, 2H), 6.47 (d, J = 3.7 Hz, 1H), 5.88 (d, J = 2.1 Hz, 1H), 5.67 (d, J = 2.1 Hz, 1H), 4.82 (m, 4H), 1.58 (s, 9H); ^{13}C NMR (126 MHz, DMSO-d_6): δ 166.80, 159.53, 155.66, 149.70 (d, J = 423.9 Hz), 144.98, 140.66, 140.18, 129.92, 124.69, 123.51 (d, J = 8.5 Hz), 122.46, 119.14, 115.66 (d, J = 17.2 Hz), 114.03, 113.68 (d, J = 19.1 Hz), 103.38, 102.94, 94.01, 92.45, 59.92, 29.32. UPLC/MS [M + H] = 523.576, t_R = 1.86 min.

*(2-((1-Cyclopentyl-3-(2,3-difluorophenyl)-1H-pyrazol-5-yl)-amino)-4,6-dihydroxyphenyl)(isoindolin-2-yl)methanone (**9bh**).* Amide bromide **8a** (64 mg, 0.125 mmol, 1 equiv) was coupled to **4az** (36 mg, 0.138 mmol, 1.1 equiv) according to General Procedure **E1b**. The resulting product was deprotected according to General Procedure **E2a**. **9bh** (44 mg, 0.085 mmol) was obtained in 68% yield over two steps. ^{1}H NMR (500 MHz, DMSO-d_6): δ 9.74 (s, 1H), 9.40 (s, 1H), 7.81 (t, J = 7.2 Hz, 1H), 7.46−7.25 (m, 7H), 6.48 (d, J = 3.7 Hz, 1H), 6.00 (d, J = 2.1 Hz, 1H), 5.72 (d, J = 2.0 Hz, 1H), 4.87−4.83 (m, 4H), 4.73 (p, J = 7.3 Hz, 1H), 2.04 (s, 4H), 1.96−1.88 (m, 2H), 1.70−1.61 (m, 2H); ^{13}C NMR (126 MHz, DMSO-d_6): δ 166.45, 159.24, 155.58, 150.22 (d, J = 248.2 Hz), 147.18 (d, J = 248.2 Hz), 144.33, 141.78, 141.07, 136.74, 127.22, 124.68, 123.55 (d, J = 8.6 Hz), 122.81, 122.52, 115.65 (d, J = 16.8 Hz), 104.18, 100.35 (d, J = 8.9 Hz), 94.49, 92.99, 57.27, 32.23, 24.14. UPLC/MS [M + H] = 517.533, t_R = 1.75 min.

*(2-((1-Cyclohexyl-3-(2,3-difluorophenyl)-1H-pyrazol-5-yl)-amino)-4,6-dihydroxyphenyl)(isoindolin-2-yl)methanone (**9bi**).* Amide bromide **8a** (64 mg, 0.125 mmol, 1 equiv) was coupled to **4bb** (38 mg, 0.138 mmol, 1.1 equiv) according to General Procedure **E1b**. The resulting product was deprotected according to General Procedure **E2a**. **9bi** (46 mg, 0.087 mmol) was obtained in 73% yield over two steps. ^{1}H NMR (500 MHz, DMSO-d_6): δ 9.64 (s, 1H), 9.30 (s, 1H), 7.74−7.66 (m, 1H), 7.34−7.09 (m, 7H), 6.37 (d, J = 3.8 Hz, 1H), 5.89 (d, J = 2.1 Hz, 1H), 5.63 (d, J = 2.1 Hz, 1H), 4.76−4.72 (m, 4H), 4.13−4.03 (m, 1H), 1.91−1.70 (m, 6H), 1.62−1.58 (m, 1H), 1.21−1.15 (m, 3H); ^{13}C NMR (126 MHz, DMSO-d_6): δ 166.87, 159.64, 156.03, 151.83, 146.30, 142.17, 140.97, 137.05, 127.65, 125.04, 123.99 (d, J = 8.6 Hz), 123.22, 122.93, 116.04 (d, J = 16.8 Hz), 104.68, 100.90 (d, J = 9.4 Hz), 94.92, 93.43, 56.01, 40.87, 25.51, 25.33. UPLC/MS [M + H] = 531.547, T_R = 1.85 min.

■ ASSOCIATED CONTENT

Supporting Information

The Supporting Information is available free of charge at https://pubs.acs.org/doi/10.1021/acs.jmedchem.0c01777.

Supporting Tables 1−8, Supporting Figures S1−S7 (PDF)

Confirmation of lysate EC_{50s} (Table 1); confirmation of fungal selectivity using purified NBDs (Table 2); HepG2 cytotoxicity dose−response data and statistics (Table 3); NIH 3T3 cytotoxicity dose−response data and statistics (Table 4); crystallographic data for apoprotein and NVP-AUY922-liganded structures (Table 5); crystallographic data for RAP-liganded structures (Table 6); features of selected Hsp90 NBD structures (Table 7); summary of computational docking results for the compounds in Table 4 (Table 8); correlation between lysate and purified NBD potencies in *C. neoformans* (Figure S1); correlation between lysate and purified NBD potencies in human (Figure S2); correlation between fold-selectivities calculated using lysates and purified NBDs (Figure S3); HepG2 cytotoxicity dose−response curves (Figure S4); NIH 3T3 cytotoxicity dose−response curves (Figure S5); ligand variability in the *C. neoformans* RAP complexes (Figure S6); and contact sites between ligands and structural elements of HSP90 (Figure S7) (PDF)

Molecular formula strings and associated biological data (CSV)

Coordinate files used to generate Figure 11B (PDB)

Coordinate files used to generate Figure 11C (PDB)

Coordinate files used to generate Figure 11D (PDB)

Coordinate files used to generate Figure 11E (PDB)

Coordinate files used to generate Figure 11F (PDB)

Coordinate files used to generate Figure 11G (PDB)

Accession Codes

Coordinates have been deposited in the PDB with the following accession numbers: apo (7K9R), NVP-AUY922 (7K9S), compound **19** (7K9U), compound **18** (7K9V), and compound **10** (7K9W). The authors will release coordinates and experimental data upon article publication.

https://dx.doi.org/10.1021/acs.jmedchem.0c01777
J. Med. Chem. 2021, 64, 1139−1169

AUTHOR INFORMATION

Corresponding Authors

Gilbert G. Privé − *Princess Margaret Cancer Centre, Toronto, Ontario M5G 1L7, Canada; Department of Medical Biophysics and Department of Biochemistry, University of Toronto, Toronto, Ontario M5G 1L7, Canada*; Email: Gil.Prive@uhnresearch.ca

Luke Whitesell − *Department of Molecular Genetics, University of Toronto, Toronto, Ontario M5G 1M1, Canada*; Email: luke.whitesell@utoronto.ca

Leah E. Cowen − *Department of Molecular Genetics, University of Toronto, Toronto, Ontario M5G 1M1, Canada*; orcid.org/0000-0001-5797-0110; Email: leah.cowen@utoronto.ca

Lauren E. Brown − *Department of Chemistry and Center for Molecular Discovery (BU-CMD), Boston University, Boston, Massachusetts 02215, United States*; orcid.org/0000-0001-9489-484X; Email: brownle@bu.edu

Authors

Paul T. Marcyk − *Department of Chemistry and Center for Molecular Discovery (BU-CMD), Boston University, Boston, Massachusetts 02215, United States*; orcid.org/0000-0001-5414-0293

Emmanuelle V. LeBlanc − *Department of Molecular Genetics, University of Toronto, Toronto, Ontario M5G 1M1, Canada*; orcid.org/0000-0003-4278-0984

Douglas A. Kuntz − *Princess Margaret Cancer Centre, Toronto, Ontario M5G 1L7, Canada*

Alice Xue − *Department of Molecular Genetics, University of Toronto, Toronto, Ontario M5G 1M1, Canada*

Francisco Ortiz − *Department of Biochemistry, UT Southwestern Medical Center, Dallas, Texas 75390-9038, United States*

Richard Trilles − *Department of Chemistry and Center for Molecular Discovery (BU-CMD), Boston University, Boston, Massachusetts 02215, United States*

Stephen Bengtson − *Department of Chemistry and Center for Molecular Discovery (BU-CMD), Boston University, Boston, Massachusetts 02215, United States*; orcid.org/0000-0002-9383-5159

Tristan M. G. Kenney − *Department of Medical Biophysics, University of Toronto, Toronto, Ontario M5G 1L7, Canada*; orcid.org/0000-0001-8242-4349

David S. Huang − *Department of Chemistry and Center for Molecular Discovery (BU-CMD), Boston University, Boston, Massachusetts 02215, United States*; orcid.org/0000-0003-0256-5307

Nicole Robbins − *Department of Molecular Genetics, University of Toronto, Toronto, Ontario M5G 1M1, Canada*

Noelle S. Williams − *Department of Biochemistry, UT Southwestern Medical Center, Dallas, Texas 75390-9038, United States*

Damian J. Krysan − *Departments of Pediatrics and Microbiology/Immunology, Carver College of Medicine, University of Iowa, Iowa City, Iowa 52242, United States*

Complete contact information is available at: https://pubs.acs.org/10.1021/acs.jmedchem.0c01777

Author Contributions

The manuscript was written through contributions of all authors. All authors have given approval to the final version of the manuscript.

Funding

NIH R01AI120958

Notes

The authors declare the following competing financial interest(s): L.E.C. is a cofounder, Chief Scientific Officer, and shareholder of Bright Angel Therapeutics, a platform company for the development of novel antifungal therapeutics. L.E.C. is a consultant for Boragen, a small molecule development company focused on leveraging the unique chemical properties of boron chemistry for crop protection and animal health. L.W. is a co-founder and shareholder of Bright Angel Therapeutics. L.E.B., D.S.H., P.T.M., L.E.C. and L.W. are named as inventors on a patent application pertaining to findings reported here.

ACKNOWLEDGMENTS

This work was supported by a grant from the National Institutes of Health (Grant R01AI120958 to L.E.C., L.E.B., and D.J.K.). L.E.C. holds a Canada Research Chair in Microbial Genomics & Infectious Disease and is Co-Director of the CIFAR Program, Fungal Kingdom: Threats & Opportunities. G.G.P. was supported by grants from NSERC and the Samuel Waxman Cancer Research Foundation.

ABBREVIATIONS USED

Hsp90, heat shock protein 90; Trap1, TNF receptor-associated protein 1; Grp94, 94 kDa glucose-regulated protein; NBD, nucleotide binding domain; ATP, adenosine triphosphate; Cl_{int}, intrinsic clearance; DIPEA, *N*,*N*-diisopropylethylamine; ELSD, evaporative light-scattering detector; FBS, fetal bovine serum; FP, fluorescence polarization; FS, fungal selectivity; HATU, hexafluorophosphate azabenzotriazole tetramethyl uronium; IS, internal standard; MRM, multiple reaction monitoring; TI, therapeutic index; UPLC, ultraperformance liquid chromatography; WHO, World Health Organization; YPD, yeast extract peptone dextrose

REFERENCES

(1) Brown, G. D.; Denning, D. W.; Gow, N. A.; Levitz, S. M.; Netea, M. G.; White, T. C. Hidden killers: human fungal infections. *Sci. Transl. Med.* **2012**, *4*, No. 165rv113.

(2) Fisher, M. C.; Hawkins, N. J.; Sanglard, D.; Gurr, S. J. Worldwide emergence of resistance to antifungal drugs challenges human health and food security. *Science* **2018**, *360*, 739−742.

(3) Brown, G. D.; Denning, D. W.; Levitz, S. M. Tackling human fungal infections. *Science* **2012**, *336*, 647.

(4) Pfaller, M. A.; Diekema, D. J. Epidemiology of invasive mycoses in North America. *Crit. Rev. Microbiol.* **2010**, *36*, 1−53.

(5) Köhler, J. R.; Hube, B.; Puccia, R.; Casadevall, A.; Perfect, J. R. Fungi that infect humans. *The Fungal Kingdom*; Wiley, 2017; Vol. *5*.

(6) Park, B. J.; Wannemuehler, K. A.; Marston, B. J.; Govender, N.; Pappas, P. G.; Chiller, T. M. Estimation of the current global burden of cryptococcal meningitis among persons living with HIV/AIDS. *AIDS* **2009**, *23*, 525−530.

(7) Rajasingham, R.; Smith, R. M.; Park, B. J.; Jarvis, J. N.; Govender, N. P.; Chiller, T. M.; Denning, D. W.; Loyse, A.; Boulware, D. R. Global burden of disease of HIV-associated cryptococcal meningitis: an updated analysis. *Lancet Infect. Dis.* **2017**, *17*, 873−881.

(8) Loyse, A.; Burry, J.; Cohn, J.; Ford, N.; Chiller, T.; Ribeiro, I.; Koulla-Shiro, S.; Mghamba, J.; Ramadhani, A.; Nyirenda, R.; Aliyu, S. H.; Wilson, D.; Le, T.; Oladele, R.; Lesikari, S.; Muzoora, C.; Kalata, N.; Temfack, E.; Mapoure, Y.; Sini, V.; Chanda, D.; Shimwela, M.; Lakhi, S.; Ngoma, J.; Gondwe-Chunda, L.; Perfect, C.; Shroufi, A.; Andrieux-Meyer, I.; Chan, A.; Schutz, C.; Hosseinipour, M.; Van der Horst, C.; Klausner, J. D.; Boulware, D. R.; Heyderman, R.; Lalloo, D.; Day, J.; Jarvis, J. N.; Rodrigues, M.; Jaffar, S.; Denning, D.; Migone, C.;

Doherty, M.; Lortholary, O.; Dromer, F.; Stack, M.; Molloy, S. F.; Bicanic, T.; van Oosterhout, J.; Mwaba, P.; Kanyama, C.; Kouanfack, C.; Mfinanga, S.; Govender, N.; Harrison, T. S. Leave no one behind: response to new evidence and guidelines for the management of cryptococcal meningitis in low-income and middle-income countries. *Lancet Infect. Dis.* **2019**, *19*, e143−e147.
(9) Maertens, J. A. History of the development of azole derivatives. *Clin. Microbiol. Infect.* **2004**, *10*, 1−10.
(10) Anderson, T. M.; Clay, M. C.; Cioffi, A. G.; Diaz, K. A.; Hisao, G. S.; Tuttle, M. D.; Nieuwkoop, A. J.; Comellas, G.; Maryum, N.; Wang, S.; Uno, B. E.; Wildeman, E. L.; Gonen, T.; Rienstra, C. M.; Burke, M. D. Amphotericin forms an extramembranous and fungicidal sterol sponge. *Nat. Chem. Biol.* **2014**, *10*, 400−406.
(11) Cowen, L. E.; Steinbach, W. J. Stress, drugs, and evolution: the role of cellular signaling in fungal drug resistance. *Eukaryotic Cell* **2008**, *7*, 747−764.
(12) Shapiro, R. S.; Robbins, N.; Cowen, L. E. Regulatory circuitry governing fungal development, drug resistance, and disease. *Microbiol. Mol. Biol. Rev.* **2011**, *75*, 213−267.
(13) Caplan, T.; Polvi, E. J.; Xie, J. L.; Buckhalter, S.; Leach, M. D.; Robbins, N.; Cowen, L. E. Functional genomic screening reveals core modulators of echinocandin stress responses in *Candida albicans*. *Cell Rep.* **2018**, *23*, 2292−2298.
(14) Robbins, N.; Caplan, T.; Cowen, L. E. Molecular evolution of antifungal drug resistance. *Annu. Rev. Microbiol.* **2017**, *71*, 753−775.
(15) Robbins, N.; Wright, G. D.; Cowen, L. E., Antifungal Drugs: the Current Armamentarium and Development of New Agents. In *The Fungal Kingdom*, Heitman, J.; Howlett, B.; Crous, P.; Stukenbrock, E.; James, T.; Gow, N., Eds. ASM Press: Washington DC., 2017; Vol. *4*, pp 903−922.
(16) O'Meara, T. R.; Veri, A. O.; Polvi, E. J.; Li, X.; Valaei, S. F.; Diezmann, S.; Cowen, L. E. Mapping the Hsp90 genetic network reveals ergosterol biosynthesis and phosphatidylinositol-4-kinase signaling as core circuitry governing cellular stress. *PLoS Genet.* **2016**, *12*, No. e1006142.
(17) Kim, S. H.; Iyer, K. R.; Pardeshi, L.; Munoz, J. F.; Robbins, N.; Cuomo, C. A.; Wong, K. H.; Cowen, L. E. Genetic analysis of *Candida auris* implicates Hsp90 in morphogenesis and azole tolerance and Cdr1 in azole resistance. *mBio* **2019**, *10*, e02529−02518.
(18) Veri, A. O.; Miao, Z.; Shapiro, R. S.; Tebbji, F.; O'Meara, T. R.; Kim, S. H.; Colazo, J.; Tan, K.; Vyas, V. K.; Whiteway, M.; Robbins, N.; Wong, K. H.; Cowen, L. E. Tuning Hsf1 levels drives distinct fungal morphogenetic programs with depletion impairing Hsp90 function and overexpression expanding the target space. *PLoS Genet.* **2018**, *14*, No. e1007270.
(19) O'Meara, T. R.; Robbins, N.; Cowen, L. E. The Hsp90 chaperone network modulates *Candida* virulence traits. *Trends Microbiol.* **2017**, *25*, 809−819.
(20) Leach, M. D.; Klipp, E.; Cowen, L. E.; Brown, A. J. Fungal Hsp90: a biological transistor that tunes cellular outputs to thermal inputs. *Nat. Rev. Microbiol.* **2012**, *10*, 693−704.
(21) Cowen, L. E.; Lindquist, S. Hsp90 potentiates the rapid evolution of new traits: drug resistance in diverse fungi. *Science* **2005**, *309*, 2185−2189.
(22) Singh, S. D.; Robbins, N.; Zaas, A. K.; Schell, W. A.; Perfect, J. R.; Cowen, L. E. Hsp90 governs echinocandin resistance in the pathogenic yeast *Candida albicans* via calcineurin. *PLoS Pathog.* **2009**, *5*, No. e1000532.
(23) Cowen, L. E.; Singh, S. D.; Kohler, J. R.; Collins, C.; Zaas, A. K.; Schell, W. A.; Aziz, H.; Mylonakis, E.; Perfect, J. R.; Whitesell, L.; Lindquist, S. Harnessing Hsp90 function as a powerful, broadly effective therapeutic strategy for fungal infectious disease. *Proc. Natl. Acad. Sci. U.S.A.* **2009**, *106*, 2818−2823.
(24) Chatterjee, S.; Tatu, U. Heat shock protein 90 localizes to the surface and augments virulence factors of *Cryptococcus neoformans*. *PLoS Negl. Trop. Dis.* **2017**, *11*, No. e0005836.
(25) de Aguiar Cordeiro, R.; Evangelista, A. J.; Serpa, R.; Marques, F. J.; de Melo, C. V.; de Oliveira, J. S.; Franco Jda, S.; de Alencar, L. P.; Bandeira Tde, J.; Brilhante, R. S.; Sidrim, J. J.; Rocha, M. F. , Inhibition of heat-shock protein 90 enhances the susceptibility to antifungals and reduces the virulence of *Cryptococcus neoformans*/*Cryptococcus gattii* species complex. *Microbiology* **2016**, *162*, 309−317.
(26) Li, L.; Wang, L.; You, Q. D.; Xu, X. L. Heat shock protein 90 inhibitors: An update on achievements, challenges, and future directions. *J. Med. Chem.* **2020**, *63*, 1798−1822.
(27) Jaeger, A. M.; Stopfer, L.; Lee, S.; Gaglia, G.; Sandel, D.; Santagata, S.; Lin, N. U.; Trepel, J. B.; White, F.; Jacks, T.; Lindquist, S.; Whitesell, L. Rebalancing protein homeostasis enhances tumor antigen presentation. *Clin. Cancer Res.* **2019**, *25*, 6392−6405.
(28) Jaeger, A. M.; Whitesell, L. HSP90: Enabler of cancer adaptation. *Annu. Rev. Cancer Biol.* **2019**, *3*, 275−297.
(29) Gewirth, D. T. Paralog specific Hsp90 inhibitors - a brief history and a bright future. *Curr. Top. Med. Chem.* **2016**, *16*, 2779−2791.
(30) Lee, C.; Park, H. K.; Jeong, H.; Lim, J.; Lee, A. J.; Cheon, K. Y.; Kim, C. S.; Thomas, A. P.; Bae, B.; Kim, N. D.; Kim, S. H.; Suh, P. G.; Ryu, J. H.; Kang, B. H. Development of a mitochondria-targeted Hsp90 inhibitor based on the crystal structures of human TRAP1. *J. Am. Chem. Soc.* **2015**, *137*, 4358−4367.
(31) Crowley, V. M.; Khandelwal, A.; Mishra, S.; Stothert, A. R.; Huard, D. J. E.; Zhao, J.; Muth, A.; Duerfeldt, A. S.; Kizziah, J. L.; Lieberman, R. L.; Dickey, C. A.; Blagg, B. S. J. Development of glucose regulated protein 94-selective inhibitors based on the BnIm and radamide scaffold. *J. Med. Chem.* **2016**, *59*, 3471−3488.
(32) Patel, P. D.; Yan, P.; Seidler, P. M.; Patel, H. J.; Sun, W.; Yang, C.; Que, N. S.; Taldone, T.; Finotti, P.; Stephani, R. A.; Gewirth, D. T.; Chiosis, G. Paralog-selective Hsp90 inhibitors define tumor-specific regulation of HER2. *Nat. Chem. Biol.* **2013**, *9*, 677−684.
(33) Que, N. L. S.; Crowley, V. M.; Duerfeldt, A. S.; Zhao, J.; Kent, C. N.; Blagg, B. S. J.; Gewirth, D. T. Structure based design of a Grp94-selective inhibitor: Exploiting a key residue in Grp94 to optimize paralog-selective binding. *J. Med. Chem.* **2018**, *61*, 2793−2805.
(34) Stothert, A. R.; Suntharalingam, A.; Huard, D. J.; Fontaine, S. N.; Crowley, V. M.; Mishra, S.; Blagg, B. S.; Lieberman, R. L.; Dickey, C. A. Exploiting the interaction between Grp94 and aggregated myocilin to treat glaucoma. *Hum. Mol. Genet.* **2014**, *23*, 6470.
(35) Stothert, A. R.; Suntharalingam, A.; Tang, X.; Crowley, V. M.; Mishra, S. J.; Webster, J. M.; Nordhues, B. A.; Huard, D. J. E.; Passaglia, C. L.; Lieberman, R. L.; Blagg, B. S. J.; Blair, L. J.; Koren, J.; Dickey, C. A. Isoform-selective Hsp90 inhibition rescues model of hereditary open-angle glaucoma. *Sci. Rep.* **2017**, *7*, No. 17951.
(36) Muth, A.; Crowley, V.; Khandelwal, A.; Mishra, S.; Zhao, J.; Hall, J.; Blagg, B. S. J. Development of radamide analogs as Grp94 inhibitors. *Bioorg. Med. Chem.* **2014**, *22*, 4083−4098.
(37) Khandelwal, A.; Crowley, V. M.; Blagg, B. S. J. Resorcinol-based Grp94-selective inhibitors. *ACS Med. Chem. Lett.* **2017**, *8*, 1013−1018.
(38) Khandelwal, A.; Kent, C. N.; Balch, M.; Peng, S.; Mishra, S. J.; Deng, J.; Day, V. W.; Liu, W.; Subramanian, C.; Cohen, M.; Holzbeierlein, J. M.; Matts, R.; Blagg, B. S. J. Structure-guided design of an Hsp90β N-terminal isoform-selective inhibitor. *Nat. Commun.* **2018**, *9*, No. 425.
(39) Ohkubo, S.; Kodama, Y.; Muraoka, H.; Hitotsumachi, H.; Yoshimura, C.; Kitade, M.; Hashimoto, A.; Ito, K.; Gomori, A.; Takahashi, K.; Shibata, Y.; Kanoh, A.; Yonekura, K. TAS-116, a highly selective inhibitor of heat shock protein 90α and β, demonstrates potent antitumor activity and minimal ocular toxicity in preclinical models. *Mol. Cancer Ther.* **2015**, *14*, 14−22.
(40) Ernst, J. T.; Neubert, T.; Liu, M.; Sperry, S.; Zuccola, H.; Turnbull, A.; Fleck, B.; Kargo, W.; Woody, L.; Chiang, P.; Tran, D.; Chen, W.; Snyder, P.; Alcacio, T.; Nezami, A.; Reynolds, J.; Alvi, K.; Goulet, L.; Stamos, D. Identification of novel HSP90α/β isoform selective inhibitors using structure-based drug design. Demonstration of potential utility in treating CNS disorders such as Huntington's Disease. *J. Med. Chem.* **2014**, *57*, 3382−3400.
(41) Ernst, J. T.; Liu, M.; Zuccola, H.; Neubert, T.; Beaumont, K.; Turnbull, A.; Kallel, A.; Vought, B.; Stamos, D. Correlation between chemotype-dependent binding conformations of HSP90α/β and isoform selectivity—Implications for the structure-based design of

https://dx.doi.org/10.1021/acs.jmedchem.0c01777
J. Med. Chem. 2021, 64, 1139−1169

HSP90α/β selective inhibitors for treating neurodegenerative diseases. *Bioorg. Med. Chem. Lett.* **2014**, *24*, 204−208.
(42) Whitesell, L.; Robbins, N.; Huang, D. S.; McLellan, C. A.; Shekhar-Guturja, T.; LeBlanc, E. V.; Nation, C. S.; Hui, R.; Hutchinson, A.; Collins, C.; Chatterjee, S.; Trilles, R.; Xie, J. L.; Krysan, D. J.; Lindquist, S.; Porco, J. A.; Tatu, U.; Brown, L. E.; Pizarro, J.; Cowen, L. E. Structural basis for species-selective targeting of Hsp90 in a pathogenic fungus. *Nat. Commun.* **2019**, *10*, No. 402.
(43) Woodhead, A. J.; Angove, H.; Carr, M. G.; Chessari, G.; Congreve, M.; Coyle, J. E.; Cosme, J.; Graham, B.; Day, P. J.; Downham, R.; Fazal, L.; Feltell, R.; Figueroa, E.; Frederickson, M.; Lewis, J.; McMenamin, R.; Murray, C. W.; O'Brien, M. A.; Parra, L.; Patel, S.; Phillips, T.; Rees, D. C.; Rich, S.; Smith, D. M.; Trewartha, G.; Vinkovic, M.; Williams, B.; Woolford, A. J. A. Discovery of (2,4-Dihydroxy-5-isopropylphenyl)- 5-(4-methylpiperazin-1-ylmethyl)-1,3-dihydroisoindol-2-yl methanone (AT13387), a novel inhibitor of the molecular chaperone Hsp90 by fragment based drug design. *J. Med. Chem.* **2010**, *53*, 5956−5969.
(44) Do, K.; Speranza, G.; Chang, L.-C.; Polley, E. C.; Bishop, R.; Zhu, W.; Trepel, J. B.; Lee, S.; Lee, M.-J.; Kinders, R. J.; Phillips, L.; Collins, J.; Lyons, J.; Jeong, W.; Antony, R.; Chen, A. P.; Neckers, L.; Doroshow, J. H.; Kummar, S. Phase I study of the heat shock protein 90 (Hsp90) inhibitor onalespib (AT13387) administered on a daily for 2 consecutive days per week dosing schedule in patients with advanced solid tumors. *Invest. New Drug.* **2015**, *33*, 921−930.
(45) Wagner, A. J.; Agulnik, M.; Heinrich, M. C.; Mahadevan, D.; Riedel, R. F.; von Mehren, M.; Trent, J.; Demetri, G. D.; Corless, C. L.; Yule, M.; Lyons, J. F.; Oganesian, A.; Keer, H. Dose-escalation study of a second-generation non-ansamycin HSP90 inhibitor, onalespib (AT13387), in combination with imatinib in patients with metastatic gastrointestinal stromal tumour. *Eur. J. Cancer* **2016**, *61*, 94−101.
(46) Canella, A.; Welker, A. M.; Yoo, J. Y.; Xu, J.; Abas, F. S.; Kesanakurti, D.; Nagarajan, P.; Beattie, C. E.; Sulman, E. P.; Liu, J.; Gumin, J.; Lang, F. F.; Gurcan, M. N.; Kaur, B.; Sampath, D.; Puduvalli, V. K. Efficacy of onalespib, a long-acting second-generation HSP90 inhibitor, as a single agent and in combination with temozolomide against malignant gliomas. *Clin. Cancer Res.* **2017**, *23*, 6215−6226.
(47) Stühmer, T.; Zöllinger, A.; Siegmund, D.; Chatterjee, M.; Grella, E.; Knop, S.; Kortüm, M.; Unzicker, C.; Jensen, M. R.; Quadt, C.; Chène, P.; Schoepfer, J.; García-Echeverría, C.; Einsele, H.; Wajant, H.; Bargou, R. C. Signalling profile and antitumour activity of the novel Hsp90 inhibitor NVP-AUY922 in multiple myeloma. *Leukemia* **2008**, *22*, 1604−1612.
(48) Jensen, M. R.; Schoepfer, J.; Radimerski, T.; Massey, A.; Guy, C. T.; Brueggen, J.; Quadt, C.; Buckler, A.; Cozens, R.; Drysdale, M. J.; Garcia-Echeverria, C.; Chène, P. NVP-AUY922: a small molecule HSP90 inhibitor with potent antitumor activity in preclinical breast cancer models. *Breast Cancer Res.* **2008**, *10*, No. R33.
(49) Doi, T.; Onozawa, Y.; Fuse, N.; Yoshino, T.; Yamazaki, K.; Watanabe, J.; Akimov, M.; Robson, M.; Boku, N.; Ohtsu, A. Phase I dose-escalation study of the HSP90 inhibitor AUY922 in Japanese patients with advanced solid tumors. *Cancer Chemother. Pharmacol.* **2014**, *74*, 629−636.
(50) Seggewiss-Bernhardt, R.; Bargou, R. C.; Goh, Y. T.; Stewart, A. K.; Spencer, A.; Alegre, A.; Bladé, J.; Ottmann, O. G.; Fernandez-Ibarra, C.; Lu, H.; Pain, S.; Akimov, M.; Iyer, S. P. Phase 1/1B trial of the heat shock protein 90 inhibitor NVP-AUY922 as monotherapy or in combination with bortezomib in patients with relapsed or refractory multiple myeloma. *Cancer* **2015**, *121*, 2185−2192.
(51) Renouf, D. J.; Hedley, D.; Krzyzanowska, M. K.; Schmuck, M.; Wang, L.; Moore, M. J. A phase II study of the HSP90 inhibitor AUY922 in chemotherapy refractory advanced pancreatic cancer. *Cancer Chemother. Pharmacol.* **2016**, *78*, 541−545.
(52) Bendell, J. C.; Bauer, T. M.; Lamar, R.; Joseph, M.; Penley, W.; Thompson, D. S.; Spigel, D. R.; Owera, R.; Lane, C. M.; Earwood, C.; Burris, H. A. A phase 2 study of the Hsp90 inhibitor AUY922 as treatment for patients with refractory gastrointestinal stromal tumors. *Cancer Invest.* **2016**, *34*, 265−270.
(53) Lin, T.-Y.; Bear, M.; Du, Z.; Foley, K. P.; Ying, W.; Barsoum, J.; London, C. The novel HSP90 inhibitor STA-9090 exhibits activity against Kit-dependent and -independent malignant mast cell tumors. *Exp. Hematol.* **2008**, *36*, 1266−1277.
(54) Ying, W. W.; Du, Z. J.; Sun, L. J.; Foley, K. P.; Proia, D. A.; Blackman, R. K.; Zhou, D.; Inoue, T.; Tatsuta, N.; Sang, J.; Ye, S. X.; Acquaviva, J.; Ogawa, L. S.; Wada, Y.; Barsoum, J.; Koya, K. Ganetespib, a unique triazolone-containing Hsp90 inhibitor, exhibits potent antitumor activity and a superior safety profile for cancer therapy. *Mol. Cancer Ther.* **2012**, *11*, 475−484.
(55) Lock, R. B.; Carol, H.; Maris, J. M.; Kang, M. H.; Reynolds, C. P.; Kolb, E. A.; Gorlick, R.; Keir, S. T.; Billups, C. A.; Kurmasheva, R. T.; Houghton, P. J.; Smith, M. A. Initial testing (stage 1) of ganetespib, an Hsp90 inhibitor, by the pediatric preclinical testing program. *Pediatr. Blood Cancer* **2013**, *60*, E42−E45.
(56) Jhaveri, K.; Chandarlapaty, S.; Lake, D.; Gilewski, T.; Robson, M.; Goldfarb, S.; Drullinsky, P.; Sugarman, S.; Wasserheit-Leiblich, C.; Fasano, J.; Moynahan, M. E.; D'Andrea, G.; Lim, K.; Reddington, L.; Haque, S.; Patil, S.; Bauman, L.; Vukovic, V.; El-Hariry, I.; Hudis, C.; Modi, S. A phase II open-label study of ganetespib, a novel heat shock protein 90 inhibitor for patients with metastatic breast cancer. *Clin. Breast Cancer* **2014**, *14*, 154−160.
(57) Jhaveri, K.; Wang, R.; Teplinsky, E.; Chandarlapaty, S.; Solit, D.; Cadoo, K.; Speyer, J.; D'Andrea, G.; Adams, S.; Patil, S.; Haque, S.; O'Neill, T.; Friedman, K.; Esteva, F. J.; Hudis, C.; Modi, S. A phase I trial of ganetespib in combination with paclitaxel and trastuzumab in patients with human epidermal growth factor receptor-2 (HER2)-positive metastatic breast cancer. *Breast Cancer Res.* **2017**, *19*, No. 89.
(58) Thakur, M. K.; Heilbrun, L. K.; Sheng, S.; Stein, M.; Liu, G.; Antonarakis, E. S.; Vaishampayan, U.; Dzinic, S. H.; Li, X.; Freeman, S.; Smith, D.; Heath, E. I. A phase II trial of ganetespib, a heat shock protein 90 Hsp90) inhibitor, in patients with docetaxel-pretreated metastatic castrate-resistant prostate cancer (CRPC)-a prostate cancer clinical trials consortium (PCCTC) study. *Invest. New Drug.* **2016**, *34*, 112−118.
(59) Goyal, L.; Wadlow, R. C.; Blaszkowsky, L. S.; Wolpin, B. M.; Abrams, T. A.; McCleary, N. J.; Sheehan, S.; Sundaram, E.; Karol, M. D.; Chen, J.; Zhu, A. X. A phase I and pharmacokinetic study of ganetespib (STA-9090) in advanced hepatocellular carcinoma. *Invest. New Drug.* **2015**, *33*, 128−137.
(60) Socinski, M. A.; Goldman, J.; El-Hariry, I.; Koczywas, M.; Vukovic, V.; Horn, L.; Paschold, E.; Salgia, R.; West, H.; Sequist, L. V.; Bonomi, P.; Brahmer, J.; Chen, L.-C.; Sandler, A.; Belani, C. P.; Webb, T.; Harper, H.; Huberman, M.; Ramalingam, S.; Wong, K.-K.; Teofilovici, F.; Guo, W.; Shapiro, G. I. A multicenter phase II study of ganetespib monotherapy in patients with genotypically defined advanced non−small cell lung cancer. *Clin. Cancer Res.* **2013**, *19*, 3068−3077.
(61) Goldman, J. W.; Raju, R. N.; Gordon, G. A.; El-Hariry, I.; Teofilivici, F.; Vukovic, V. M.; Bradley, R.; Karol, M. D.; Chen, Y.; Guo, W.; Inoue, T.; Rosen, L. S. A first in human, safety, pharmacokinetics, and clinical activity phase I study of once weekly administration of the Hsp90 inhibitor ganetespib (STA-9090) in patients with solid malignancies. *BMC Cancer* **2013**, *13*, No. 152.
(62) Huang, D. S.; LeBlanc, E. V.; Shekhar-Guturja, T.; Robbins, N.; Krysan, D. J.; Pizarro, J.; Whitesell, L.; Cowen, L. E.; Brown, L. E. Design and synthesis of fungal-selective resorcylate aminopyrazole Hsp90 inhibitors. *J. Med. Chem.* **2020**, *63*, 2139−2180.
(63) Martinez, L. R.; Casadevall, A. Susceptibility of *Cryptococcus neoformans* biofilms to antifungal agents in vitro. *Antimicrob. Agents Chemother.* **2006**, *50*, 1021−1033.
(64) Casadevall, A.; Nosanchuk, J. D.; Williamson, P.; Rodrigues, M. L. Vesicular transport across the fungal cell wall. *Trends Microbiol.* **2009**, *17*, 158−162.
(65) Zaragoza, O. Multiple disguises for the same party: The concepts of morphogenesis and phenotypic variations in *Cryptococcus neoformans*. *Front. Microbiol.* **2011**, *2*, 181.
(66) O'Meara, T. R.; Alspaugh, J. A. The *Cryptococcus neoformans* capsule: a sword and a shield. *Clin. Microbiol. Rev.* **2012**, *25*, 387−408.

https://dx.doi.org/10.1021/acs.jmedchem.0c01777
J. Med. Chem. 2021, 64, 1139−1169

(67) Cannon, R. D.; Lamping, E.; Holmes, A. R.; Niimi, K.; Baret, P. V.; Keniya, M. V.; Tanabe, K.; Niimi, M.; Goffeau, A.; Monk, B. C. Efflux-mediated antifungal drug resistance. *Clin. Microbiol. Rev.* **2009**, *22*, 291−321.
(68) Rossi, A. M.; Taylor, C. W. Analysis of protein-ligand interactions by fluorescence polarization. *Nat. Protoc.* **2011**, *6*, 365−387.
(69) McNaney, C. A.; Drexler, D. M.; Hnatyshyn, S. Y.; Zvyaga, T. A.; Knipe, J. O.; Belcastro, J. V.; Sanders, M. An automated liquid chromatography-mass spectrometry process to determine metabolic stability half-life and intrinsic clearance of drug candidates by substrate depletion. *Assay Drug Dev. Technol.* **2008**, *6*, 121−129.
(70) Butts, A.; DiDone, L.; Koselny, K.; Baxter, B. K.; Chabrier-Rosello, Y.; Wellington, M.; Krysan, D. J. A repurposing approach identifies off-patent drugs with fungicidal cryptococcal activity, a common structural chemotype, and pharmacological properties relevant to the treatment of cryptococcosis. *Eukaryotic Cell* **2013**, *12*, 278−287.
(71) Brough, P. A.; Aherne, W.; Barril, X.; Borgognoni, J.; Boxall, K.; Cansfield, J. E.; Cheung, K.-M. J.; Collins, I.; Davies, N. G. M.; Drysdale, M. J.; Dymock, B.; Eccles, S. A.; Finch, H.; Fink, A.; Hayes, A.; Howes, R.; Hubbard, R. E.; James, K.; Jordan, A. M.; Lockie, A.; Martins, V.; Massey, A.; Matthews, T. P.; McDonald, E.; Northfield, C. J.; Pearl, L. H.; Prodromou, C.; Ray, S.; Raynaud, F. I.; Roughley, S. D.; Sharp, S. Y.; Surgenor, A.; Walmsley, D. L.; Webb, P.; Wood, M.; Workman, P.; Wrightt, L. 4,5-diarylisoxazole HSP90 chaperone inhibitors: Potential therapeutic agents for the treatment of cancer. *J. Med. Chem.* **2008**, *51*, 196−218.
(72) Taldone, T.; Chiosis, G. Purine-scaffold Hsp90 inhibitors. *Curr. Top. Med. Chem.* **2009**, *9*, 1436−1446.
(73) Stebbins, C. E.; Russo, A. A.; Schneider, C.; Rosen, N.; Hartl, F. U.; Pavletich, N. P. Crystal structure of an Hsp90−geldanamycin complex: targeting of a protein chaperone by an antitumor agent. *Cell* **1997**, *89*, 239−250.
(74) Keefe, L. J.; Sondek, J.; Shortle, D.; Lattman, E. E. The alpha aneurism: a structural motif revealed in an insertion mutant of staphylococcal nuclease. *Proc. Natl. Acad. Sci. U.S.A.* **1993**, *90*, 3275−3279.
(75) Wright, L.; Barril, X.; Dymock, B.; Sheridan, L.; Surgenor, A.; Beswick, M.; Drysdale, M.; Collier, A.; Massey, A.; Davies, N.; Fink, A.; Fromont, C.; Aherne, W.; Boxall, K.; Sharp, S.; Workman, P.; Hubbard, R. E. Structure−activity relationships in purine-based inhibitor binding to HSP90 isoforms. *Chem. Biol.* **2004**, *11*, 775−785.
(76) Friesner, R. A.; Banks, J. L.; Murphy, R. B.; Halgren, T. A.; Klicic, J. J.; Mainz, D. T.; Repasky, M. P.; Knoll, E. H.; Shelley, M.; Perry, J. K.; Shaw, D. E.; Francis, P.; Shenkin, P. S. Glide: a new approach for rapid, accurate docking and scoring. 1. Method and assessment of docking accuracy. *J. Med. Chem.* **2004**, *47*, 1739−1749.
(77) Halgren, T. A.; Murphy, R. B.; Friesner, R. A.; Beard, H. S.; Frye, L. L.; Pollard, W. T.; Banks, J. L. Glide: a new approach for rapid, accurate docking and scoring. 2. Enrichment factors in database screening. *J. Med. Chem.* **2004**, *47*, 1750−1759.
(78) Zurcher, M.; Diederich, F. Structure-based drug design: exploring the proper filling of apolar pockets at enzyme active sites. *J. Org. Chem.* **2008**, *73*, 4345−4361.
(79) Bissantz, C.; Kuhn, B.; Stahl, M. A medicinal chemist's guide to molecular interactions. *J. Med. Chem.* **2010**, *53*, 5061−5084.
(80) Granger, D. L.; Perfect, J. R.; Durack, D. T. Virulence of *Cryptococcus neoformans*. Regulation of capsule synthesis by carbon dioxide. *J. Clin. Invest.* **1985**, *76*, 508−516.
(81) LaFayette, S. L.; Collins, C.; Zaas, A. K.; Schell, W. A.; Betancourt-Quiroz, M.; Gunatilaka, A. A.; Perfect, J. R.; Cowen, L. E. PKC signaling regulates drug resistance of the fungal pathogen *Candida albicans* via circuitry comprised of Mkc1, calcineurin, and Hsp90. *PLoS Pathog.* **2010**, *6*, No. e1001069.
(82) Houston, J. B. Utility of in vitro drug metabolism data in predicting in vivo metabolic clearance. *Biochem. Pharmacol.* **1994**, *47*, 1469−1479.
(83) Davies, B.; Morris, T. Physiological parameters in laboratory animals and humans. *Pharm. Res.* **1993**, *10*, 1093−1095.
(84) Barter, Z. E.; Bayliss, M. K.; Beaune, P. H.; Boobis, A. R.; Carlile, D. J.; Edwards, R. J.; Houston, J. B.; Lake, B. G.; Lipscomb, J. C.; Pelkonen, O. R.; Tucker, G. T.; Rostami-Hodjegan, A. Scaling factors for the extrapolation of in vivo metabolic drug clearance from in vitro data: reaching a consensus on values of human microsomal protein and hepatocellularity per gram of liver. *Curr. Drug Metab.* **2007**, *8*, 33−45.
(85) Iwatsubo, T.; Suzuki, H.; Sugiyama, Y. Prediction of species differences (rats, dogs, humans) in the in vivo metabolic clearance of YM796 by the liver from in vitro data. *J. Pharmacol. Exp. Ther. A* **1997**, *283*, 462−469.
(86) Kabsch, W. XDS. *Acta Crystallogr., Sect. D: Biol. Crystallogr.* **2010**, *66*, 125−132.
(87) Winn, M. D.; Ballard, C. C.; Cowtan, K. D.; Dodson, E. J.; Emsley, P.; Evans, P. R.; Keegan, R. M.; Krissinel, E. B.; Leslie, A. G.; McCoy, A.; McNicholas, S. J.; Murshudov, G. N.; Pannu, N. S.; Potterton, E. A.; Powell, H. R.; Read, R. J.; Vagin, A.; Wilson, K. S. Overview of the CCP4 suite and current developments. *Acta Crystallogr., Sect. D: Biol. Crystallogr.* **2011**, *67*, 235−242.
(88) Emsley, P.; Lohkamp, B.; Scott, W. G.; Cowtan, K. Features and development of Coot. *Acta Crystallogr., Sect. D: Biol. Crystallogr.* **2010**, *66*, 486−501.
(89) Liebschner, D.; Afonine, P. V.; Baker, M. L.; Bunkoczi, G.; Chen, V. B.; Croll, T. I.; Hintze, B.; Hung, L. W.; Jain, S.; McCoy, A. J.; Moriarty, N. W.; Oeffner, R. D.; Poon, B. K.; Prisant, M. G.; Read, R. J.; Richardson, J. S.; Richardson, D. C.; Sammito, M. D.; Sobolev, O. V.; Stockwell, D. H.; Terwilliger, T. C.; Urzhumtsev, A. G.; Videau, L. L.; Williams, C. J.; Adams, P. D. Macromolecular structure determination using X-rays, neutrons and electrons: recent developments in Phenix. *Acta Crystallogr., Sect. D: Struct. Biol.* **2019**, *75*, 861−877.
(90) Morin, A.; Eisenbraun, B.; Key, J.; Sanschagrin, P. C.; Timony, M. A.; Ottaviano, M.; Sliz, P. Collaboration gets the most out of software. *eLife* **2013**, *2*, No. e01456.

https://dx.doi.org/10.1021/acs.jmedchem.0c01777
J. Med. Chem. 2021, 64, 1139−1169